

**DEVELOPMENT OF NANOPARTICLE-MODIFIED SENSOR
PLATFORM FOR CANCER MARKER DETECTION**

by

ZEYNEP ALTINTAŞ

Submitted to the Graduate School of Engineering and Natural Sciences

in partial fulfilment of

the requirements for the degree of

Doctor of Philosophy

Sabanci University

February 2012

**DEVELOPMENT OF NANOPARTICLE-MODIFIED SENSOR
PLATFORM FOR CANCER MARKER DETECTION**

APPROVED BY:

Assoc. Prof. Dr. Uğur Sezerman

(Dissertation Advisor)



Prof. Dr. Yaşar Gürbüz

(Dissertation Co-advisor)



Prof. Dr. Hakan Bermek



Prof. Dr. Selim Çetiner



Assist. Prof. Dr. Alpay Taralp



DATE OF APPROVAL: 29.02.2012

© ZEYNEP ALTINTAS 2012

All Rights Reserved

ABSTRACT

The detection and quantification of cancer biomarkers in human blood is crucial to diagnose patients in the early stage of a disease. The recent advances in biosensor technology can improve detection by reducing the application time and cost without an invasive approach. The development of such detection system is a major thrust of the rapidly growing biotechnology industry. It involves a multidisciplinary research effort including chemical engineering, microelectronics and biology.

This study focused on the development of nanomaterial-modified sensing platform to enhance the sensitivity for cancer marker detection. An electrochemical-based capacitive biosensor was aimed to develop using two alternative nanomaterial modification including gold nanoparticles (Au-NPs) and magnetic beads (MBs) in cancer detection for the first time. Surface Plasmon resonance (SPR) and quartz crystal microbalance (QCM)-based sensors were initially employed to verify the bioassays and the surface chemistries. The successful achievement of these research works was transferred into an electrochemical based-capacitive biosensor to increase the sensitivity and reliability of the assays for the quantification of the biological markers. The optimized sensor methods were conducted in the capacitive sensor using standard methodologies and the detection limit was increased 6 fold without a signal amplification tool. However, the quantification of some biomarkers is difficult since they have trace threshold level in human blood and/or small size. Moreover, real patient samples include various biological molecules beside the target analyte and this makes the detection difficult due to the non-specific responses and requires the signal amplification. Due to these reasons, a novel nanoparticle modified capacitive sensor was developed and used for synchronous multiple marker detection for the first time. The developed sensor increased the sensitivity up to 600 fold (5 pg.mL^{-1}) when compared with standard sensor assays. The results have provided alternative and effective quantification approaches to the current tools; and also a promising future for precise detection of the cancer types using multiple marker assays. The developed and improved methodologies/sensors in this thesis can also be applied for the other diseases that have biomarkers in human body.

ÖZET

İnsan kanındaki kanser biyomarkırlarının algılanması ve miktarlarının ölçülmesi hastalara erken tanı konulması için hayati önem taşımaktadır. Biyosensör teknolojisindeki en son gelişmeler invaziv olmayan yöntemlerle, uygulama zamanını ve maliyeti de düşürerek tanıyı güçlendirmektedir. Böyle bir teşhis sisteminin geliştirilmesi, hızla gelişen biyoteknoloji endüstrisinin bir ihtiyacı olup kimya mühendisliği, mikro elektronik ve biyoloji alanlarını kapsayan çok disiplinli bir araştırma gerektirmektedir.

Bu çalışma kanser markır ölçümünde hassasiyeti artırmak amacıyla nanomalzemelerle modifiye edilmiş sensör platform geliştirmeye odaklanmıştır. Elektrokimyasal kapasitif biyosensör altın nanopartiküller ve magnetik boncuklar olmak üzere iki alternatif nanomalzeme kullanılarak geliştirilip kanser markırlarının teşhisinde ilk defa kullanılmıştır. Başlangıç olarak, biyolojik metodlar ve yüzey kimyaları surface plasmon rezonans (SPR) ve quartz crystal microbalance (QCM) sensörler kullanılarak doğrulanmıştır. Bu araştırmalardan elde edilen başarılı sonuçlar, metodların biyolojik markır ölçümündeki hassasiyetini ve güvenilirliğini artırmak amacıyla elektrokimyasal temelli kapasitif sensöre transfer edilmiştir. SPR ve QCM’de optimize edilmiş metodlar herhangi bir sinyal artırıcı araç kullanmadan kapasitif sensöre uygulandığında markır ölçüm hassasiyetinde 6 katlık bir artış elde edilmiştir. Ancak, insan kanındaki bazı markırların teşhisi, kanser seviyelerinin iz miktarda oluşu ve/veya boyutlarının küçük oluşu nedeniyle zordur. Gerçek hasta örnekleri kanser teşhisinde kullanılacak hedef markırın yanısıra çeşitli biyolojik molekülleri içerir ve bu durum spesifik olmayan ölçüm sonuçlarına sebep olduğundan biyosensörlerin verdiği sinyal arttırılarak iz miktardaki markır seviyelerinin ölçülmesi gerekmektedir. Bu sebeplerle, bu tezde nanopartiküllerle modifiye edilmiş yeni bir kapasitif sensör geliştirilmiş ve eş zamanlı-çoklu marker teşhisi amacıyla ilk defa kullanılmıştır. Geliştirilen sensor standart kapasitif sensörle kıyaslandığında hassasiyeti 600 kata (5 pg. mL^{-1}) kadar arttırmıştır. Elde edilen bulgular varolan metodlara alternatif ve etkili ölçüm yöntemleri sunmakta, ve ayrıca çoklu markır teşhisi kullanılarak kanser tiplerinin kesin ayrımında ümit vadecici bir gelecek oluşturmaktadır. Bu tezde geliştirilen ve iyileştirilen metodlar/ sensörler insan vücudunda biyomarkırı olan diğer hastalıkların tanısında da uygulanabilir.

To my people,

past, present and future ...

Shoot for the moon. Even if you miss, you will land among the stars.

Les Brown

ACKNOWLEDGEMENTS

I would like to thank my supervisors, Prof. Dr. Uğur Sezerman and Prof. Dr. Yaşar Gürbüz for their all encouragement during the development of the ideas in this thesis. I am very thankful to the jury members of my thesis; Assoc. Prof. Dr. Uğur Sezerman, Prof. Dr. Selim Çetiner (Biological Sciences and Bioengineering), Prof. Dr. Yaşar Gürbüz (Electronics Engineering), Prof. Dr. Hakan Bermek (Molecular Biology and Genetics Department of İTÜ) and Assist. Prof. Dr. Alpay Taralp (Material Science and Engineering) for their valuable comments and suggestions on the thesis.

Thank you my friends in Microsystem Design Group for sharing hard and fun times; Mehmet Doğan, Hüseyin Kayhan, Melik Yazıcı and Emre Heves and to all other colleagues in the group.

I would like to thank Prof. Dr. Sam Tothill, Cranfield University, (UK) for valuable support, enthusiasm and insightful conversations during my PhD period in UK.

Finally, thank you my worthy friends Mücahit, Meshude, İbrahim; and my family for always believing in me and support my decisions.

Zeynep Altıntaş

February 2012, Istanbul

TABLE OF CONTENTS

ABSTRACT.....	IV
LIST OF FIGURES	XII
LIST OF TABLES.....	XVIII
LIST OF ABBREVIATIONS.....	XIX
1 INTRODUCTION.....	1
1.1 The Need for Cancer Diagnosis	1
1.2 Biomarkers for Early Detection of Lung Cancer	4
1.3 Biosensor Technology in Diagnostics.....	6
1.3.1 Optical biosensors.....	8
1.3.2 Piezoelectric biosensors	9
1.3.3 Electrochemical capacitive biosensors	10
1.4 Use of Biosensors for Lung Cancer Detection and Problems.....	11
1.5 Solutions to Problems and Proposed Study	12
1.6 Organization of the Thesis	13
2 CEA MARKER DETECTION THROUGH QCM AND SPR-BASED SENSORS...	15
2.1 Materials and Instrumentation.....	16
2.2 Sensor Chip Cleaning and SAM Coating.....	17
2.2.1 CEA assay using QCMA-1 sensor.....	18

2.3	Results and Discussion for QCMA-1 Assays	19
2.4	SPR-Based Immunosensor for the Detection of CEA	24
2.4.1	Materials and reagents	24
2.4.2	Instrumentations.....	24
2.4.3	Sensor chip cleaning and MUDA coating	25
2.4.4	Control surface selection.....	25
2.4.5	Immobilisation of antibodies	25
2.4.6	CEA detection.....	26
2.5	Results and Discussions	27
2.5.1	Assay optimisation.....	27
2.5.2	Sandwich and RAM-capture assays characterisation	31
3	CAPACITIVE SENSOR PLATFORM FOR CANCER DETECTION AND QUANTIFICATION.....	35
3.1	Capacitive Detection of EGFR.....	39
3.1.1	Material and methods.....	40
3.1.1.1	Materials and reagents.....	40
3.1.1.2	Fabrication of the sensor platform	40
3.1.1.3	Sensor chip cleaning and MPA coating	40
3.1.1.4	Immobilization of antibodies	41
3.1.1.5	hEGFR protein detection.....	41
3.1.1.6	Detection of hEGFR in human serum sample.....	42
3.1.2	Results and discussions.....	42
3.1.2.1	FT-IR analysis of SAM-coated and EDC-NHS activated GID surfaces	43

3.1.2.2	Surface topology by atomic force microscopy (AFM) of the sensor surface	45
3.1.2.3	Determination of hEGFR using Network Analyzer.....	47
3.1.2.4	Kinetics of hEGFR binding on the sensor surface.....	49
3.1.2.5	Detection of hEGFR in real human serum samples.....	50
4	DEVELOPMENT OF NANOPARTICLE-MODIFIED CAPACITIVE SENSOR PLATFORM.....	52
4.1	Gold Nanoparticle Modified Sensor Platform	52
4.1.1	Materials and methods	54
4.1.1.1	Preperation of Au-NP modified sensor platform	54
4.1.1.2	Antibody immobilization	54
4.1.1.3	Protein detection.....	55
4.1.2	Results and discussions.....	55
4.1.2.1	FT-IR and AFM analysis	55
4.1.2.2	Determination of IL-6 antigen	57
4.2	DEVELOPMENT OF MAGNETIC BEAD MODIFIED CAPACITIVE SENSOR PLATFORM.....	62
4.2.1	Behavior of magnetic beads on the platform	64
4.2.2	Methodology.....	69
4.2.2.1	The protocol of the applied bioassay using magnetic beads:.....	69
4.2.2.2	Preparation of secondary antibody immobilized-magnetic beads	69
4.2.3	Results.....	71
4.2.3.1	Antigen binding on the surface	71
4.2.3.2	Modified MB application on the surface	73
4.3	MULTIPLE MARKER ASSAY FOR PRECISE DISEASE DETECTION	75

4.3.1	Materials and reagents	76
4.3.2	Antibody immobilization (anti-CEA, anti-hEGFR and anti-CA15-3)	76
4.3.3	Detection of multiple cancer markers	77
4.3.4	Results and discussion	77
CHAPTER 5		88
5	SUMMARY, CONCLUSION AND FUTURE PROSPECTS	88
5.1	Novelty and Quality of the Work.....	89
5.2	Future Prospects	90
6	REFERENCES.....	92

LIST OF FIGURES

Figure 1-1 The incidence and mortality rates of most common cancers.	2
Figure 1-2 Age-standardised incidence rates in lung cancer, by sex. The x axis shows the ages and rate per 100,000 population. (www.cancerresearchuk.org)	2
Figure 1-3 The most frequent ten cancers in Turkey (2005). [1].....	3
Figure 1-4 Schematic representation of the SPR detection principle.	9
Figure 1-5 The principle of the bioassay with capacitive biosensor. [55]	11
Figure 2-1. Fully automated QCMA-1 instrument and its sensor chips.....	17
Figure 2-2 Biacore 3000 instrument and bare gold sensor chip.	17
Figure 2-3 Emitech K 1050X plasma asher. (EM Technologies Ltd., Kent, UK).....	18
Figure 2-4. Immobilisation of RAM (blue) and anti-CEA (red) antibodies on the control and active sensing spots of QCMA-1 sensor chip at 25 °C.....	20
Figure 2-5 The detection of 60 ng.mL ⁻¹ CEA in QCMA-1 device. A 60 ng.mL ⁻¹ CEA was injected to the active and control surfaces. Anti-CEA provided the active sensor surface while mouse IgG was the control. In the graph red line represents CEA binding on anti-CEA whereas blue line shows non-specific CEA binding on the control surface (mouse IgG).....	21
Figure 2-6 Sandwich assay with anti-CEA+HRP secondary antibody. First binding shows the direct assay using a 40 ng.mL ⁻¹ of CEA, the surfaces were then regenerated with 100 mM HCl. Later sandwich assay was performed with the injection of 20 ng.mL ⁻¹ CEA marker and a 5 µg.mL ⁻¹ of anti-CEA+HRP antibody. The blue line shows the control surface whereas the red line is the active sensor surface.....	21

Figure 2-7. Capture assay results in QCMA-1 instrument in the concentration range of 400-6.25 ng.mL⁻¹ (from left to right). Each CEA sample included 5µg.mL⁻¹ detection antibody.....23

Figure 2-8. Sandwich assay results in QCMA-1 instrument in the concentration range of 400-6.25 ng.mL⁻¹ (from left to right). Each CEA sample included 5 µg.mL⁻¹ detection antibody. The surface was coated by immobilising of anti-CEA primary antibody prior to the binding assay.....23

Figure 2-9 Confirmative assay for the control surface selection with PBS buffer. The non-specific binding of BSA to each antibody surface (first binding), the non-specific binding of CEA antigen in PBS or BSA solution (second and third bindings), the non-specific binding of the mixed sample included detection antibody and CEA antigen (last binding). The immobilized surfaces: anti-PSA (a), anti-troponin (b), mouse IgG (c).28

Figure 2-10 Direct assay sensorgram with a 300 ng.mL⁻¹ concentration of CEA biomarker using the SPR sensor. CEA antigen binding on Abcam’s anti-CEA immobilized (a) and Sigma’s anti-CEA immobilized (b, c, d) sensor surfaces.....29

Figure 2-11 Schematic representation of homogenous RAM-capture (a) and sandwich assay (b).30

Figure 2-12 Optimization of the incubation time. After first 2 hours of the incubation the recorded response change was gradually decreased.31

Figure 2-13 Immobilisation of anti-CEA coating antibody (red), rabbit anti-mouse (green) and mouse IgG (blue) antibodies on the sensor chip surface.....32

Figure 2-14 Sensorgram of the CEA assay through sandwich (a) and capture (b) methods in the concentration range of 3- 400 ng.mL⁻¹. The lowest line represents the control in each assay and the RU change gradually increased from bottom to the top according to the increased CEA concentration.....33

Figure 2-15 The overall results of sandwich assay. (All shown data is control subtracted).....34

Figure 2-16 The overall results of RAM-capture assay (All shown data is control subtracted).....	34
Figure 3-1 Schematic representation of the IDEs and parallel plates that mentioned above.	36
Figure 3-2 Microscopic image of gold interdigitated transducer electrode array.....	43
Figure 3-3 FT-IR spectra of SAM coated (a) and EDC-NHS activated (b) sensor surfaces.	44
Figure 3-4 AFM analysis of blank and antibody immobilized surfaces. Height images (a, b), particle distribution on the surface (c, d) and surface roughness (e, f) of blank and antibody immobilized sensor platforms.....	46
Figure 3-5 Changes in the capacitance depending on the different concentrations of hEGFR antigen in the frequency range of 700-850 MHz.....	48
Figure 3-6 Logarithmic regression and correlation coefficient of the results obtained at 800 MHz frequency.	48
Figure 3-7 Kinetic analysis for the bioassay in dose and frequency dependent manner. ..	49
Figure 3-8 Test of hEGFR protein in real human serum in the concentration range of 0-10 ng.mL ⁻¹	51
Figure 4-1 The principle of the bioassay on Au-NP modified capacitive sensing platform.	53
Figure 4-2 Confirmation of SAM formation with thiourea employing FT-IR prior to Au-NP modification.	56
Figure 4-3 Confirmation of Au-NP modification on the sensor using AFM tool. Surface roughness of Au-NP modified (a) and non-modified (b) sensor platforms. Particle distribution on the Au-NP modified (c) and non-modified (d) sensor surfaces. (Red arrows show the distance between two particles).....	57

Figure 4-4 Capacitive responses of SAM-coated and Au-NP modified sensor surfaces for 5 electrode.....	58
Figure 4-5 Capacitive detection of IL-6 marker with standard errors in the frequency range of 600-1000 MHz.....	59
Figure 4-6 All investigated concentration range of IL-6 at selected 6 frequency points to determine the optimal frequency range for the bioassay.	60
Figure 4-7 Logarithmic regression analysis for the bioassay at a constant frequency point (800 MHz).....	61
Figure 4-8 Experimental steps of atrazine detection using immunomagnetic electrochemical sensor.....	64
Figure 4-9 Schematic representation of gold interdigitated fingers of an IDE.....	66
Figure 4-10 Bare-MB measurements according to the tested concentrations of MBs by Network Analyzer in a wide (50MHz-4 GHz) and zoomed (600-1000 MHz) frequency ranges.	67
Figure 4-11 Capacitance measurements of 1%MB on SAM-coated sensor surface in a broad (a) and particular frequency ranges (b).....	68
Figure 4-12 The principle of the applied bioassay using magnetic particles. (Adapted). [111].....	70
Figure 4-13 CRP antigen detection in the concentration range of 0-500 pg.mL ⁻¹ at all frequency.....	72
Figure 4-14 Capacitive detection of CRP antigen in the concentration range of 0-500 pg.mL ⁻¹ at a constant frequency.....	73
Figure 4-15 Capacitance change after secondary antibody-coated MB application on the antigen bound surfaces in all frequency range.....	74

Figure 4-16 Capacitance change after secondary antibody-coated MB application on the antigen bound surfaces in the frequency range of 600-1000 MHz (a) and the difference between the control surface and the lowest antigen bound surface after MB application (b).....75

Figure 4-17 Schematic representation of capacitive biosensor chips (a) and bioassays applied with the particle modifications (b). (b part of the figure was adapted). [111]76

Figure 4-18 Capacitive detection of CEA, hEGFR and CA15-3 cancer markers with Au-NP modified capacitive sensor in the frequency range of 500-900 MHz. CEA and hEGFR detection in the concentration range of 5-1000 pg.mL^{-1} (a and b). CA15-3 marker detection in the concentration range from 1 U.mL^{-1} to 100 U.mL^{-1} (c).....79

Figure 4-19 Multiple marker detection at a constant frequency (800 MHz) with Au-NP modified sensor platform. The concentration range of CEA and EGFR is 5-1000 pg.mL^{-1} while it is 1-100 U.mL^{-1} for CA15-3 protein marker.....80

Figure 4-20 Regression analysis of the bioassays conducted with Au-NP modified sensor platform at a constant frequency. The specificity of the assays was tested using PBS buffer (0 pg.mL^{-1} marker) and a non-specific protein (10 ng.mL^{-1} BSA).81

Figure 4-21 Capacitance change on the sensor due to the antigen binding at the effective frequency range prior to the magnetic bead modification. CEA and hEGFR marker detection in the concentration range of 5-1000 pg.mL^{-1} (a, b). CA15-3 detection in the concentration range of 1-100 U.mL^{-1} (c).83

Figure 4-22 Signal enhancement with magnetic particles for the detection of CEA marker in the concentration range of 5-1000 pg.mL^{-1} at the effective frequency range. Comparison of the sample responses with the negative controls after magnetic bead application (a). The results of constant magnetic bead solution application on the different CEA concentrations in the concentration range of 5-1000 pg.mL^{-1} (b). Specificity test of the bioassays using the lowest amount of CEA sample and the negative controls (c).85

Figure 4-23 Signal enhancement with magnetic bead modification on the capacitive sensor platform for hEGFR and CA15-3 cancer markers at the effective frequency range. Capacitance change due to the magnetic bead application after antigen binding step of

hEGFR bioassay with/out the negative controls (a, b). Capacitance change due to the magnetic bead application after antigen binding step of CA15-3 bioassay with/out the negative controls (c, d).....86

LIST OF TABLES

Table 1-1: Currently available tools for cancer diagnostics.	4
Table 1-2. The list of protein markers of lung cancer.....	5
Table 1-3. The list of genetic markers of lung cancer.	6
Table 1-4. Some common biosensing materials	7
Table 1-5. A variety of biosystem-transducer combinations in terms of transducer, measurement mode and potential application.....	7
Table 1-7 Summary of disease markers used in this thesis with their normal and disease levels.	13
Table 2-1 Results of kinetic calculations for CEA marker detection with standard and optimised assay formats.....	29
Table 3-1 Calculations of dissociation constants (K_d) and maximum responses (R_{max}) in the selected frequency points in the concentration range of 0.5-64 ng mL ⁻¹ antigen.	50
Table 4-1 Kinetic data analysis at selected frequency points to determine the affinity between the target antigen-antibody pair (IL-6-anti-IL-6).	61
Table 4-2 Comparison of IL-6 detection for standard and Au-NP modified capacitive sensor platforms.....	61
Table 4-3 Immunomagnetic electrochemical assays using different transducers and enzymatic labels.....	63
Table 4-4 Comparison of all investigated sensor platforms in this PhD thesis.	87
Table 5-1 Comparison of different sensor platforms for the marker detection with each others and our results in this thesis.	90

LIST OF ABBREVIATIONS

µg-Microgram

µl-Microliter

µM-Micromolar

Au-NP-Gold nanoparticle

Bcl-2- B cell lymphoma-2 gene

BSA-Bovine serum albumin

CA 15-3-Cancer antigen 15-3

CA-125-Cancer antigen 125

CA-19- Cytokeratin nineteen fragment

CAT- Computerized axial tomography

CEA- Carcinoembryonic antigen

CHRNA3- Neuronal acetylcholine receptor subunit alpha-3

CT- Computed tomography

CYFRA 21-1-Cytokeratin fragment

DNA-Deoxyribonucleic acid

EDC - 1-ethyl-3-(3-dimethylaminopropyl)-carbodiimide

ELISA-Enzyme-linked immunosorbent assay

FHIT- Fragile histidine triad gene

HCl-Hydrogen chloride

HER2- Human epidermal growth factor receptor 2

hGPX1-Glutathione peroxidase1 gene

HRP – Horse radish peroxidase

Hz-Hertz

IDEs-Interdigitated electrodes

IgG-Immunoglobulin G
kD- Kilo Dalton
KLK5-Kallikrein 5 gene
KLK6- Kallikrein 6 gene
KLK7- Kallikrein 7 gene
MB- Magnetic bead
mg - Milligram
ml - Millilitre
MRI- Magnetic resonance imaging
mRNA - Messenger RNA
MUDA - Mercaptoundecanoic acid
NA-Neutravidin
NaOH-Sodium hydroxide
ng – Nanogram
NHS - N-hydroxysuccinimide
NSCLC-Non-small cell lung cancer
NSE-Neuron specific enolase
PAMAM - polyamidoamine
PBS – phosphate buffer saline
PCNA-Proliferating cell nuclear antigen
PCR-Polymerase chain reaction
PET-Positron emission tomography
pg-Picogram
PSA-Prostate specific antigen
QCM – Quartz crystal microbalance

RAM-Rabbit anti-mouse

RASSF1A-Ras association domain family 1A gene

RNA- Ribonucleic acid

RRM1-ribonucleotide reductase M1 gene

RUNX3- Runt-related transcription factor 3

SAM-Self assembly monolayer

SCC- Squamous cell carcinoma

SCLC- Small cell lung cancer

SEP15-Selenoprotein 15 gene

SEPP1-Selenoprotein P1 gene

SNP-Single nucleotide polymorphism

SPR-Surface Plasmon resonance

TPA-Tissue polypeptide antigen

TSM - Thickness-shear mode

UK-United Kingdom

U-Unite

US-Unites States

CHAPTER 1

1 INTRODUCTION

1.1 The Need for Cancer Diagnosis

Cancer is a large group of different diseases that occur due to the unregulated cell growth. It may affect people of all ages and certain types of it arises more according to the gender, age or geographical location at globe. 13% of all human deaths worldwide occurred due to the cancer in 2007. The incidence and mortality rates of the cancer show a significant difference depending on the cancer type. For example, the commonest cancer types include breast, lung, prostate and colon carcinomas; however, the rate of mortality is quite low for breast and prostate cancers when compared with lung cancer. Moreover, the mortality and incidence rates of lung cancer show similarity and this increases the importance of early diagnosis for the disease. It is the second most common cancer in men and the third in women with about 22% of all cancer incidences arise from lung cancer (www.cancerresearchuk.org). The disease displays the highest mortality rate, 1.3 million people per year worldwide, compared to the other common cancers (Figure 1-1 and Figure 1-2). According to 2005 US statistics 107,416 men and 89,271 women were diagnosed with lung cancer, however the vast majority of the patients died from lung cancer; 90,139 of men and 69,078 of women (U.S. Cancer Statistics Working Group; Department of Health and Human Services, Centers for Disease Control and Prevention, and National Cancer Institute; 2009).

In Turkey the cancer incidence rates increased between 2002 and 2005 according to Ministry of Health Department of Cancer Control database. Incidence rates rose from 133.78 per 100 thousand in 2002 to 173.85 per 100 thousand in 2005. Lung cancer has the highest incidence rate in our country and followed by four other frequent cancer types including prostate (24.33), skin (18.91), breast (17.96), stomach (9.92) cancer with an incidence of per 100 thousand as shown in Figure 1-3 [1] .

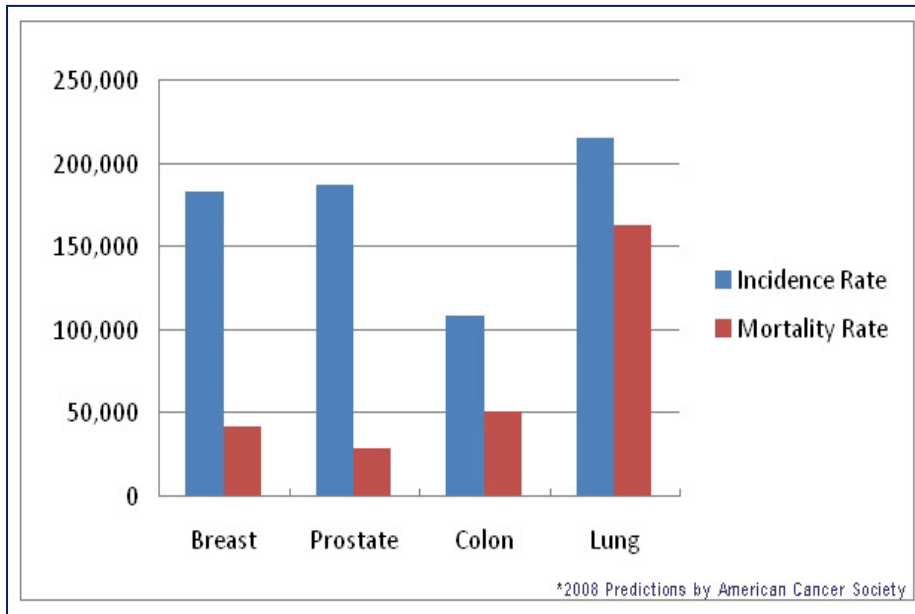


Figure 1-1 The incidence and mortality rates of most common cancers.
(American Cancer Society, 2008)

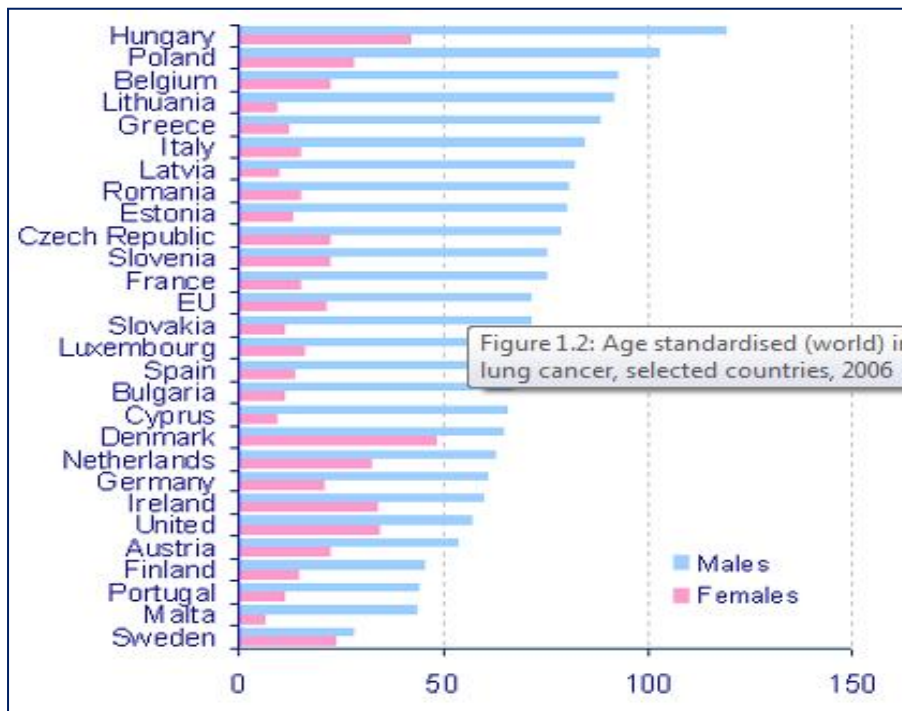


Figure 1-2 Age-standardised incidence rates in lung cancer, by sex. The x axis shows the ages and rate per 100,000 population. (www.cancerresearchuk.org)

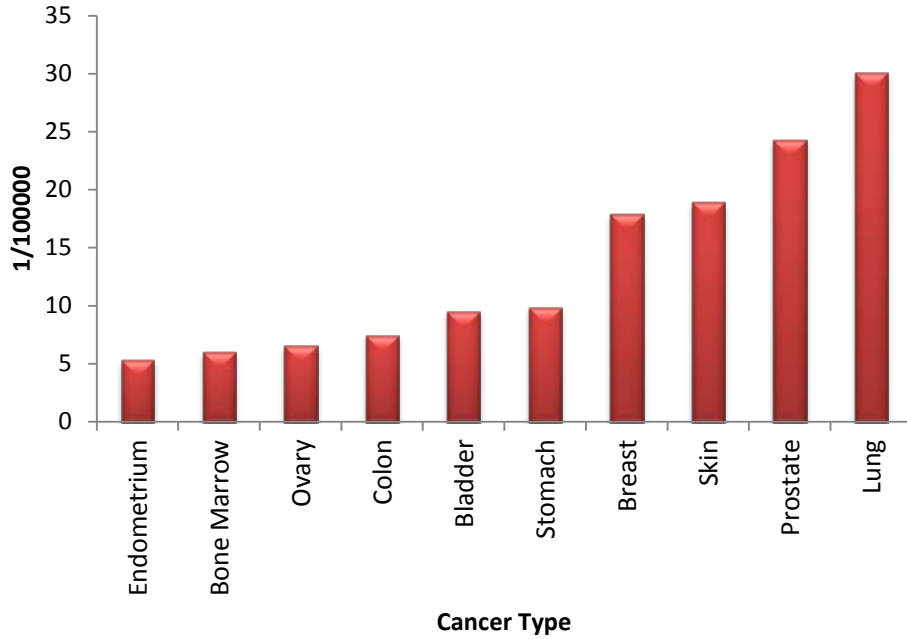


Figure 1-3 The most frequent ten cancers in Turkey (2005). [1]

The treatment of the disease is a long and difficult process and the survival scarcely attains to 5 years. The most crucial point for the best result is to diagnose the disease at an early stage. For this aim, there are many methods to apply that are chest x-ray, computerized tomography, magnetic resonance imaging, positron emission tomography, sputum cytology and biopsy although some of them are not suitable to all people due to the other pathologies that the patient has (National Cancer Institute). Moreover, the patients can often experience a great pain and complication because of some diagnostic tools such as biopsy.

Table 1-1 shows the currently available methods for cancer diagnostics with their advantages and disadvantages. Since the current diagnostic tools are also time consuming, a new sensitive and rapid method is necessary for lung cancer detection. With this approach, sensor technology has provided a promising future for the detection of many important diseases through rapid, sensitive and easy applications. Getting high specific and sensitive results by this technology for the biomarkers from blood samples may provide both early and easy detection without painful and non-invasive techniques.

Table 1-1: Currently available tools for cancer diagnostics.

Diagnostic method	Advantage	Disadvantage	Reference
Chest X-ray	Quite reliable	Use of radiation, false negative response, high cost	[2-3]
Computerized tomography (CT)	Quite reliable	High cost, false negative scans, use of radiation	[4-5]
Magnetic resonance imaging (MRI)	Quite reliable	Use of magnetic field, high cost, not suitable for all patients that have other complications	[6-7]
Pozitron emission tomography	Quite reliable	Need for radioactive substance and sophisticated instrument, not suitable for all patients that have other complications, high cost	[8] [9]
Sputum cytology	Easy and non-invasive	Degradation of biomarkers due to the enzymes in sputum, false positive results	[10-11]
Biopsy	Fast and easy	Inflammation, painful, invasive	[12-13]

1.2 Biomarkers for Early Detection of Lung Cancer

The current blood tests for lung cancer biomarkers base on ELISA type assay and gene expression profiling with PCR techniques. Although these methods are promising for early detection, they need professional experience, more time and grant. Therefore, developing a new technology which provides rapid and highly sensitive detection for diseases has been an inevitable aim for scientists. Investigations on biosensors have been rapidly increase in last decade to achieve this aim for early, non-invasive and effective detection of the important diseases including different kind of cancers, cardiovascular diseases and diabetes. There are many protein and genetic markers of lung cancer that can be used for detection as seen in Table 1-2 and Table 1-3.

Table 1-2. The list of protein markers of lung cancer

Lung cancer protein marker	References
Neuroendocrine markers, p53 and HER2	[14-15]
CEA and CYFRA 21-1	[16-17]
CA 15-3, CA 19-9, TPA	[17-18]
NSE	[15, 19]
TAG-72.3, CA 125, SCC	[18]
hnRNP-A2/B1	[20]
PCNA and CD34	[21]
c-erbB2	[22]
FHIT, CTNNB1, and MUC1	[23]
Cyclin D1	[24]

Table 1-3. The list of genetic markers of lung cancer.

Lung cancer genetic marker	References
<i>P53</i> , <i>FHIT</i> genes	[25]
<i>p19^{ras}</i> gene	[26]
Blood-based CHRNA3 SNP	[27]
Telomere related genes	[28]
miRNAs	[29]
<i>Bcl-2</i>	[21]
<i>K-ras</i>	[30-32]
Methylation of <i>p16^{INK4a}</i>	[33-34]
<i>cdc25B</i> gene	[35]
<i>KLF6</i> gene	[36]
Polymorphisms in the caspase7 gene	[37]
Polymorfisms in the survivin gene	[38]
<i>p16</i> gene	[39-41]
<i>KLK5</i> and <i>KLK7</i> genes	[42]
Polymorphisms of the <i>RRM1</i> gene	[43]
<i>RASSF1A</i> and <i>RUNX3</i> genes	[44]
<i>SEPP1</i> , <i>SEP15</i> and <i>hGPX1</i> genes	[45]
Circulating DNA and RNA	[46-47]

1.3 Biosensor Technology in Diagnostics

A biosensor is a device that has two main components including a receptor and a detector. The receptor is responsible for the selectivity of the sensor such an enzyme, antibodies while the transducer translates the changes that can be chemical or physical by recognizing the analyte and relaying it through an electrical signal [48-49]. The detector is also called as a transducer that is not selective, for instance it can be an oxygen electrode, a pH-electrode or piezoelectric crystal. The biological sensing element

selectively recognizes a particular biological molecule through a reaction, specific adsorption, or other process as physical/chemical and the transducer converts the results of this recognition into a usable signal that can be quantified. Some common biosensor materials and various biosystem-transducer combinations take place in Table 1-4 and Table 1-5, respectively.

Table 1-4. Some common biosensing materials

Analytes	Examples
Respiratory gases	O ₂ , CO ₂
Toxic gases	H ₂ S, Cl ₂ , CO, NH ₃
Ions	H ⁺ , Li ⁺ , K ⁺ , Na ⁺ , Ca ⁺ , phosphates
Metabolites	Glucose, urea
Trace metabolites	Hormones, steroids, drugs
Toxic vapors	Benzene, toluene
Protein and nucleic acids	DNA, RNA
Antigen and antibodies	Human Ig, anti-human Ig
Microorganism	Viruses, bacteria, parasites

Table 1-5. A variety of biosystem-transducer combinations in terms of transducer, measurement mode and potential application.

Transducer System	Measurement Mode	Typical Applications
Ion-selective electrode	Potentiometric	Ions in media, enzyme electrodes
Gas-sensing electrodes	Potentiometric	Gases, enzyme, organelle, cell or tissue electrodes
Field-effect transistors	Potentiometric	Ions, gases, enzyme substrates immunological analytes
Optoelectronic and fiber -optic devices	Optical	pH, enzymes, immunological analytes
Thermistors	Calorimetric	Enzyme, organelle, gases, pollutants, antibiotics, vitamins
Enzyme electrodes	Amperometric	Enzymes, immunological systems
Conductimeter	Conductance	Enzyme substrates
Piezoelectric crystals	Acoustic (mass)	Volatile gases and vapors, antibodies

Because of increment of cancer cases in last decade, biosensing technologies have been used for cancer detection and the most crucial aim about biosensors is attaining non-invasive and effective early diagnosis through developing sensor platforms [50]. In this project QCM, SPR and IDE-capacitive biosensors were used and developed to investigate the biomarkers of lung cancer for early detection. SPR and QCM-based sensors have been widely used and reliable tools in biosensing technology. Due to this, these biosensors were used for verification of the bioassays and surface chemistries. Electrochemical-based capacitive sensor was then aimed to use and develop for cancer quantification since it provides cost effective, easily applicable and more sensitive measurements in broader dynamic ranges of biomarkers. The sensor types employed throughout the thesis were briefly mentioned below.

1.3.1 Optical biosensors

The basis of optical sensors established on surface plasmon and today the different types of the optical sensors are available. These have been investigated and used depending on the aim of the studies. The optical biosensors include optrode-based fiber optic biosensors, evanescent wave fiber optic biosensors, flow immunosensor, time-resolved fluorescence, the resonant mirror optical biosensor, interferometric biosensors and surface plasmon resonance biosensors (SPR).

The SPR sensor responds to refractive index near the sensor surface and with binding of certain substances such an enzyme to the surface lead to changes in reflectivity (Figure 1-4). In SPR sensors, a surface plasmon is excited at the interface between a metal film and a dielectric medium, changes in the refractive index of are to be measured. A change in the refractive index of the dielectric medium (also called as superstrate) produces a change in the propagation constant of the surface plasmon. The sensor has been used to detect both small analytes as nerve agents and large analytes as a protein [51].

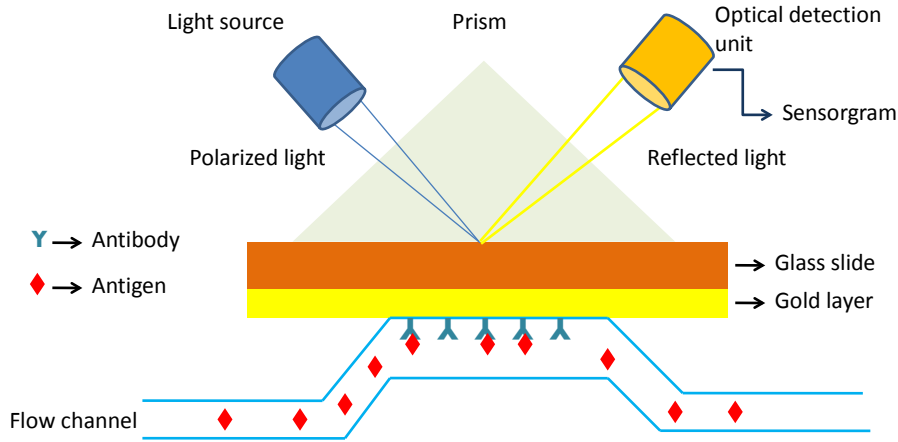


Figure 1-4 Schematic representation of the SPR detection principle.

1.3.2 Piezoelectric biosensors

A QCM is a piezoelectric mass-sensing device that measures the change in frequency of a quartz crystal resonator as a mass per unit area. In the QCM sensor, analyte detection is based on adsorbate recognition where selective binding leads to a mass change that can be identified by a corresponding change in the acoustic parameters of piezoelectric quartz crystal. With applying electricity to the crystal the piezoelectric effect occurs in crystals and the crystal lattice is deformed [52]. In 1959, Sauerbrey firstly demonstrated the basic theory of signal dependence on adsorbed mass in which he exhibited that the frequency change of a quartz crystal TSM resonator was a linear function of the mass per area m_s , or absolute mass Δm :

$$\Delta f_m = -\frac{f_0^2}{F_q \rho_q} m_s = -\frac{f_0^2}{F_q \rho_q} \frac{\Delta m_s}{A_{el}}$$

In the formula f_0 is the resonance frequency of the unperturbed quartz resonator, F_q the frequency constant of the crystal, ρ_q the quartz density and A_{el} the electrode area. This equation is only valid for thin, solid layers which are deposited on the resonator. After Sauerbrey, the following studies were done to develop the equation for viscous and lossy liquids. Kazanawa, in 1997, expanded the model with this aim and attained the equation

below that demonstrates the frequency shift for liquid-loaded sensor surface. Here, the liquid is described by its density ρ_l and viscosity η_l .

$$\Delta f = -f_q^{3/2} \sqrt{\frac{\rho_l \eta_l}{\pi \rho_q \mu_q}}$$

In the formula μ_q is the shear module in the x-direction and ρ_q is the density of the crystal. The equations are used as the below representation for a two-layer system:

$$\Delta f = \Delta f_m + \Delta f_l = -f_0^2 \left(\frac{\Delta m_s}{F_q \rho_q A_{el}} + \sqrt{\frac{\eta_l \rho_l}{f_0 \pi \mu_q \rho_q}} \right)$$

[53]

Many types of crystals show the piezoelectric effect; however, due to the mechanical, electrical and chemical properties of the quartz it is the most commonly used crystal type in analytical applications. QCM can be used in a wide variety of applications including the detection of small molecular weight ligands, carbohydrates, proteins, nucleic acids, viruses, bacteria, cells and lipidic-polymeric interfaces [53].

1.3.3 Electrochemical capacitive biosensors

Capacitive biosensor is a type of electrochemical sensor to detect different kinds of molecules including proteins, antigen, DNA, antibody and heavy metal ions. Many diseases such as cardiovascular diseases and cancers have been investigated with capacitive biosensor to achieve early and simpler diagnosis [54]. The capacitive biosensor is an extremely sensitive device that has detection limits under 10^{-15} molar. Though the most commonly studied biosensors are optical ones, the detection limits of the electrochemical sensors are anticipated to better with simpler instrumentation that is not required the special qualifications for applications [55].

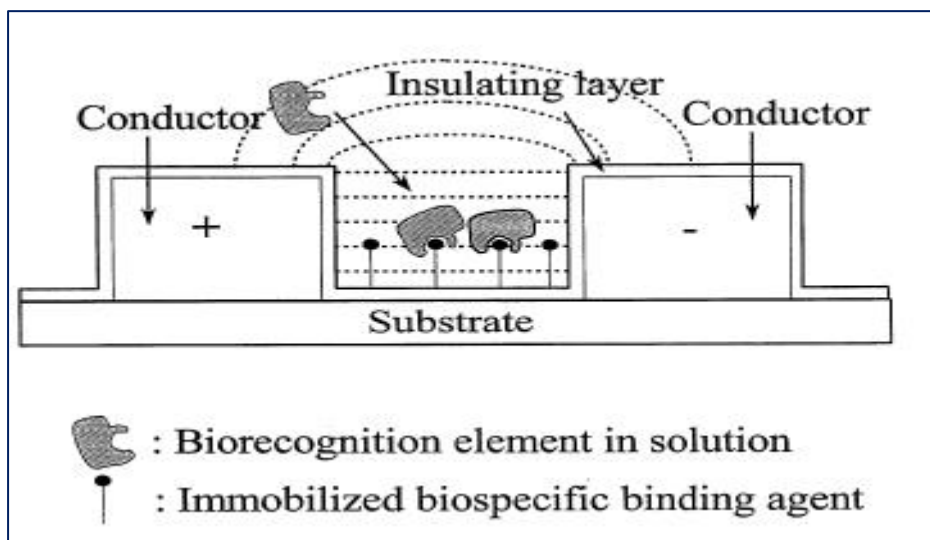


Figure 1-5 The principle of the bioassay with capacitive biosensor. [55]

The first articles about the applications of the electrochemical sensors for liquids were published in late 1980s. In these publications, the principle of the measurement depended on the changes in dielectric properties, dimension, shape and charge distribution while antibody-antigen complex occurred on the electrode surface. In the event of a conformational change of a surface protein through binding of an analyte, this can be detected by capacitance measurements. The capacitance measurement can be realized through two approaches in an experiment including the measurement of the change in the capacitance between two metal conductors in near proximity to one another with the recognition element immobilized between them (IDEs) and measuring the capacitance potentiostatically at an electrode/solution interface with the recognition components on the working electrode surface.

1.4 Use of Biosensors for Lung Cancer Detection and Problems

Although the disease has available and widely investigated markers as reviewed in Table 1-2 and Table 1-3, the lung cancer has scarcely been studied with biosensing technology. There are some important limitations related to integration of the disease detection with the use of

biosensors. For example, SPR and QCM-based sensors are more common and reliable platforms for the aim of biosensing when compared to the other sensor types. However, these sensors require more reagents for the testing and the detection limits are generally high while some markers have trace threshold levels for cancer indication such as pg.mL^{-1} levels. Moreover, the parameters have to be optimized for lung cancer markers including surface chemistry, incubation type/time for each application during the detection processes. On the other hand, electrochemical based-capacitive sensors show a promising approach and compensate the problems of other sensor types described above. This platform provides an easier instrumentation without a need for special qualifications and cost-effective methodologies although appropriate surface modifications, assay optimizations and signal enhancement may be required in many cases.

1.5 Solutions to Problems and Proposed Study

Due to the reasons described above, biosensors were investigated/developed to provide an alternative/cost-effective and non-invasive approach for the early detection of lung cancer that has highest mortality rate because of the limitations on current diagnostic tools. With this aim, SPR and QCM biosensors were initially employed to obtain a convenient methodology for lung cancer biomarkers. An optimized immunoassay was developed for CEA marker detection and this study was published in an international journal as one of the first papers in the literature for lung cancer detection using sensor technology. In this research, threshold level of CEA marker was successfully detected without performing any signal enhancement method. The developed methodology was then transferred into an electrochemical based-capacitive sensor platform to reach lower detection limits. The detection limit was increased up to 6 fold in capacitive sensor and hEGFR marker of lung cancer was successfully investigated. However, the platform was required to improve sensitivity since some disease markers have too smaller size and/or lower threshold levels to define the occurrence or the stage of the disease. Moreover, there is a need for specific immobilization material to detect biological molecules or cells by biosensors and the affinity between the immobilization material and the targeted marker can be low for many times.

Here, we aimed to improve our capacitive sensor platform to achieve the quantification of trace biomarker levels at high specificity using nanomaterials and this approach has provided an excellent output when compared with previous investigations. The gold and magnetic particle-modified capacitive sensors increased the sensitivity and

stability of the sensing platform ~25 fold even for lower concentration of the markers and led to 600 fold decrease in the detection limit.

The importance of this work is the development of the nanoparticle modified-capacitive platforms for the first time and used for lung cancer detection. Here, both Au-NPs and MBs were successfully implemented to the non-faradaic interdigitated capacitive sensor and 600-fold increment was achieved in the detection limit for the tests of lung cancer biomarkers. The investigated protein markers during the PhD thesis were seen in Table 1-6 with their normal and disease levels. Multiple marker detection for the precise detection employing the capacitive sensing platform was the other novelty of this study. The improved methodologies and the obtained results provide a very prospective alternative approach for the early diagnosis of the cancer cases without an invasive and painful tool such as biopsy. The achievements of the study can also be compared with the other non-invasive methods including SPR, QCM and capacitive sensors in the literature. When we compared our work within itself, it is clear that the particle-modified sensor platforms have provided a significant superiority over the other sensors (SPR and QCM) and non-modified capacitive sensor platform.

Table 1-6 Summary of disease markers used in this thesis with their normal and disease levels.

Protein Marker	Disease	Normal levels	Disease levels	Reference
CEA	Cancer	5 ng.ml ⁻¹	5 ng.ml ⁻¹ <	[56]
hEGFR	Cancer	64 ng.ml ⁻¹	64 ng.ml ⁻¹ >	[57]
CA15-3	Cancer	30 U.ml ⁻¹	50 U.ml ⁻¹ <	[58]
IL-6	Cancer&CVD	4 pg.ml ⁻¹	138 pg.ml ⁻¹	[59]
CRP	Cancer&CVD	0.22 mg.dml ⁻¹	> 1 mg.dl ⁻¹	[59]

1.6 Organization of the Thesis

This thesis contains five chapters that explain the assay and surface chemistry developments/optimizations with SPR and QCM-based sensors; transferring these

methodologies into an electrochemical-based capacitive sensor platform; the development of capacitive sensing platform using nanomaterials for signal amplification; multiple marker detection using the particle-modified capacitive sensor platforms for the precise detection of the cancer cases; and finally conclusions.

A brief outline of each chapter is seen below;

- **Chapter 2** describes the assay development and optimizations for the detection of lung cancer markers using CEA protein as the model analyte through SPR and QCM-based sensors.
- **Chapter 3** mentions the successful integration of the developed methodologies in SPR and QCM sensors for the electrochemical-based non-faradaic capacitive sensor; and the improved sensitivity for the detection of cancer markers using the cost-effective and miniature system.
- **Chapter 4** presents the nanoparticle modified-capacitive sensor platforms using Au-NPs and MBs for more sensitive, reliable and stable sensing approach; comparison of them; and also multiple marker detection for lung cancer cases using three different markers of the disease (CEA, hEGFR and CA15-3).
- **Chapter 5** gives a summary of the thesis, indicates the novelty and importance of the achievements, compares the results of various sensor systems used through the thesis with literature and each others, and end up with the future prospects.

CHAPTER 2

2 CEA MARKER DETECTION THROUGH QCM AND SPR-BASED SENSORS

Carcinoembryonic antigen (CEA) has been widely studied in clinical analysis as a tumour biomarker. It is a cell adhesion glycoprotein belongs to the immunoglobulin super family [60]. The protein was first identified from human colon cancer tissue extracts in 1965 by Phild Gold and Samuel O. Freedman [61]. It is produced during foetal development and the production of it terminates before birth. In healthy individuals the normal level of CEA is between 3-5 ng.mL⁻¹ and this level may increase up to 10 ng.mL⁻¹ due to other benign diseases [62]. The protein scarcely exists in the blood of healthy people except cigarette-smokers. However, its concentration shows a significant increase in some conditions including lung cancer, colorectal carcinoma, pancreatic carcinoma and breast carcinoma [63]. Hence, it can be used as a biomarker for diagnosis and prognosis of cancer. CEA levels over 20 ng. mL⁻¹ are usually associated with patients with cancer in metastatic state [64]. It is one of the most investigated tumour markers in certain cancers [65], with several clinical and research-based applications [16]. However, due to the absence of both rapid and sensitive diagnostic tool, CEA related cancers cannot be detected at an early stage which is vital for successful treatment. Therefore, biosensor technologies can play a crucial role in achieving this aim [50, 66]. Though enzyme-linked immunoassay (ELISA) has been generally used for both clinical and research field, the QCM or SPR-based biosensors have provided label-free and real-time detection systems [67]. Due to this, the detection of CEA was investigated through QCM (QCMA-1, Sierra Sensors) and SPR-based (Biacore 3000, GE Healthcare) biosensor platforms and the verified methods were then transferred into the capacitive sensor platform.

2.1 Materials and Instrumentation

Phosphate buffered saline (PBS, 0.01 M phosphate buffer, 0.0027 M potassium chloride and 0.137 M sodium chloride, pH 7.4), bovine serum albumin (BSA), N-hydroxysuccinimide (NHS), 11-mercaptopundecanoic acid (MUDA) and ethanolamine were bought from Sigma Aldrich (Poole, UK). 1-ethyl-3-(3dimethylaminopropyl)-carbodiimide (EDC) was purchased from Pierce-Thermo Scientific (Cramlington, UK). Mouse monoclonal antibody to carcino embryonic antigen (CEA) and anti-CEA coated with horse radish peroxidase (HRP) were purchased from Abcam (Cambridge, UK). Human CEA protein, Mouse IgG and Rat-anti mouse IgG was bought from Stratech Scientific Ltd (Newmarket, UK). CEA and its monoclonal antibody were also purchased from Sigma (Dorset, UK). QCM-1 and Biacore 3000 biosensors were supplied by Sierra Sensors GmbH (Hamburg, Germany) and Biacore GE Healthcare (Uppsala, Sweden), respectively. The sensor chips of the QCM-1 and Biacore 3000 were provided by their companies.

A fully automated QCMA-1 and Biacore 3000 instruments and their sensor chips were selected as the biosensor platforms to develop and detect CEA antigen. QCMA-1 device has two separate sensing spot whereas Biacore 3000 possess four spots. QCM-1 is a kind of piezoelectric mass-sensing device that works by sending an electrical signal through a gold-plated quartz crystal which leads to a vibration at some resonant frequency and the experiment results are obtained as frequency changes due to alterations in mass on the surface of the sensor chip (Figure 2-1). In the assays, one sensing spot of each sensor was employed as control surface whilst the others were used as active surfaces. The working temperature of the assays was 25 °C in both sensors and the flow rate was 50 $\mu\text{l}\cdot\text{min}^{-1}$ and 10 $\mu\text{l}\cdot\text{min}^{-1}$ for QCMA-1 (Figure 2-1) and Biacore 3000 (Figure 2-2), respectively. Bare gold sensor chips were cleaned by nitrogen plasma, coated with MUDA and then stored in the refrigerator until their use.

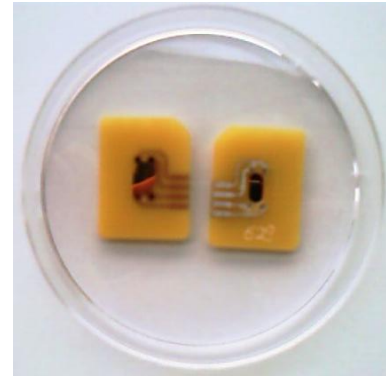
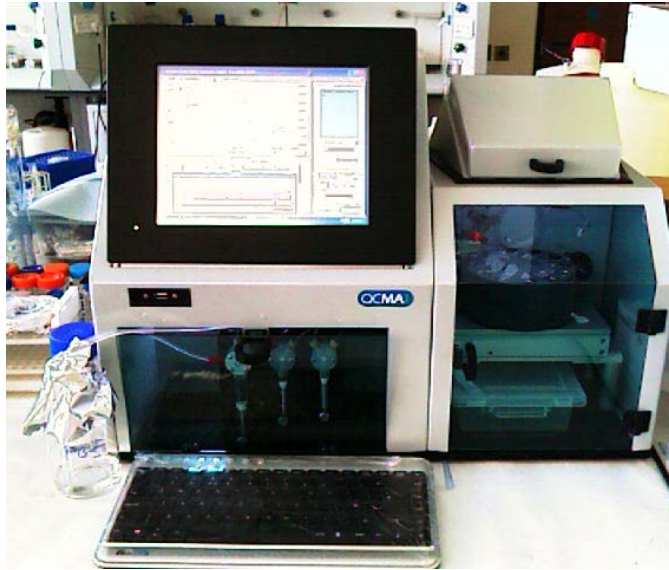


Figure 2-1. Fully automated QCMA-1 instrument and its sensor chips.

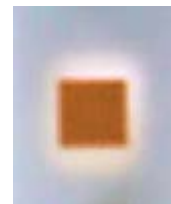


Figure 2-2 Biacore 3000 instrument and bare gold sensor chip.

2.2 Sensor Chip Cleaning and SAM Coating

Used or new chips were cleaned with a procedure including plasma cleaning and ethanol washing prior to MUDA coating. The chips were kept in ethanol for some minutes, then washed with ethanol and dried with nitrogen stream gently. PC analyser (Figure 2-3) was then employed to clean the chip surfaces. There are two different types

of plasma cleaning with oxygen or nitrogen gasses. For the cleaning of sensor chips nitrogen plasma was preferred to employ in this study; however, if bare gold sensor chip is previously coated with a polymer or any microorganism detection is studied on the surface from the different resources, the O₂ plasma should be preferred due to stronger nature of oxygen plasma. The setup of the analyser was arranged according to the optimised conditions.

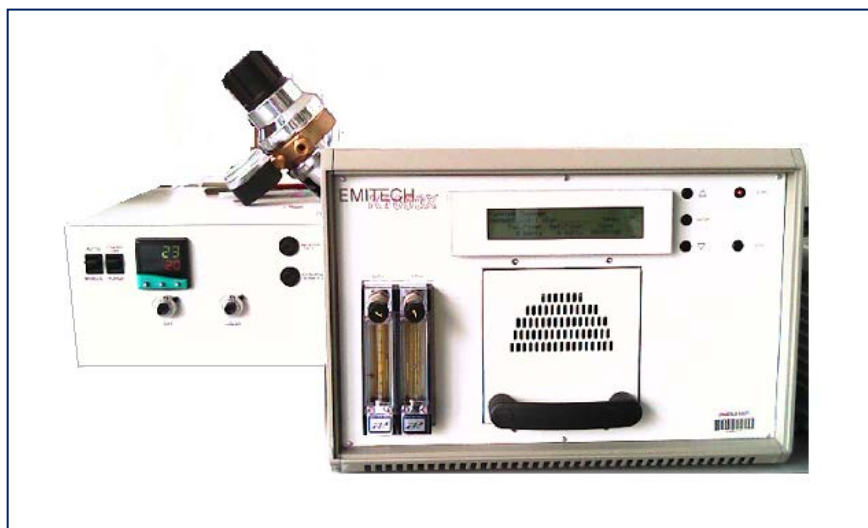


Figure 2-3 Emitech K 1050X plasma asher. (EM Technologies Ltd., Kent, UK)

After plasma cleaning all items were washed with dH₂O and ethanol, respectively. The chips were kept in ethanol from washing step to preparing MUDA solution. 2 mM MUDA was prepared within spectrophotometric grade ethanol for coating the surface of sensor chips to form self assembly monolayer (SAM) on the surface. This surface consists of the carboxyl group that EDC/NHS can bind to activate carbon groups on the surface. The chips were kept in MUDA solution and the petri dish was covered with aluminium foil to obtain dark condition during overnight incubation at ambient temperature. MUDA coated chips were then washed with ethanol, kept in ethanol for 3 minutes, washed with dH₂O and dried with N₂ stream, respectively. These chips were employed right away or kept in refrigerator at +4 °C until their use.

2.2.1 CEA assay using QCMA-1 sensor

With docking QCMA-1 sensor chips to the instrument, the assays were started via the prime option using previously degassed 1xPBS (Dulbecco's modified phosphate buffered

saline) as running buffer until the immobilisation of antibodies on the surface was finished. The chips were then calibrated and a baseline was acquired during 10 minutes to understand the situation of the chips before bioassays. To get rid of air bubbles in the flow channels was very crucial at this process, because the air bubbles usually cause to lose the assay at the beginning of the experiment or misunderstand the result when doing analysis due to unexpected signals or drift on the real-time graphs.

Immobilisation stage of the assay was started by injection of 1:1 mixture of 400 mM EDC and 100 mM NHS, prepared in deionised water. This solution was immediately mixed prior to use and simultaneously injected to the sensor surfaces during 3 min for activating the surface. A 30 $\mu\text{g. mL}^{-1}$ rabbit anti-mouse (RAM) or mouse IgG antibodies was then injected to one sensing spot to obtain a control surface whereas same concentration of anti-CEA antibody (produced in mouse) was injected to the other spot of QCMA-1 device as active sensor surface. Both control and target antibodies were prepared in 10 mM sodium acetate buffer (pH 5.5) and injected for 3 min with 50 $\mu\text{L. min}^{-1}$ flow rate. The sensor surfaces were then blocked with the injection of a 50 $\mu\text{g. mL}^{-1}$ BSA solution for 3 min that diluted in PBS buffer and finally 1M ethanolamine (pH 8.5) injection was employed during 3 min to cap non-reacted NHS esters on the surfaces. The produced frequency changes of the sensor surfaces were recorded for immobilised antibodies during 2 minutes after the injection of each was completed. After antibody immobilisation, the assays were carried on with CEA antigen binding stage. A variety concentration of CEA marker was endeavoured to detect. Each concentration of the biomarker was injected to the sensor surfaces for 3 min.

2.3 Results and Discussion for QCMA-1 Assays

The most important opportunity of QCMA-1 instrument is that it provides a real-time experiment approach for users. Due to this, the problems or the tenor of the process may be easily understood while the bioassay occurs. The instrument generally has a characteristic graph for particular assay types. For QCMA-1 assay, the sensor chips were initially coated with MUDA solution to obtain a self assembly monolayer on the surface for antibody immobilisation. The coated chip then docked to the sensor, the sensor was primed with PBS buffer and 10 minute buffer flow was applied to get a stabile baseline. The process was carried on with antibody immobilisation using conventional EDC-NHS chemistry.

Rabbit anti-mouse antibody immobilised sensors produced an average frequency change of 600 ± 20 Hz (n=3), mouse IgG immobilised sensors produced 727 ± 35 Hz (n=3) and anti-CEA immobilised sensors produced 642 ± 40 Hz (n=3) under 25°C (Figure 2-4).

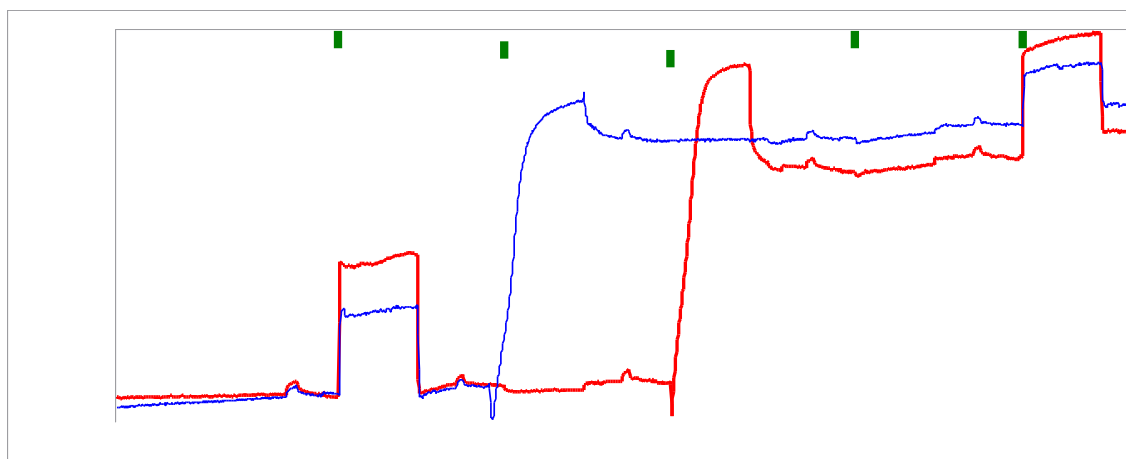


Figure 2-4. Immobilisation of RAM (blue) and anti-CEA (red) antibodies on the control and active sensing spots of QCMA-1 sensor chip at 25 °C.

60 ng.mL^{-1} CEA was detected by direct assay and the bioassay was repeated for four times. Figure 2-5 shows the binding of 60 ng.mL^{-1} CEA to the active (anti-CEA, red line) and control surfaces (mouse IgG, blue line). The sensor surfaces were regenerated with 100 mM HCl solution after each binding reaction. Sandwich assay was then conducted by QCMA-1 sensor; however, the binding between the antigen and the secondary antibody could not be observed with standard assay as seen in Figure 2-6.

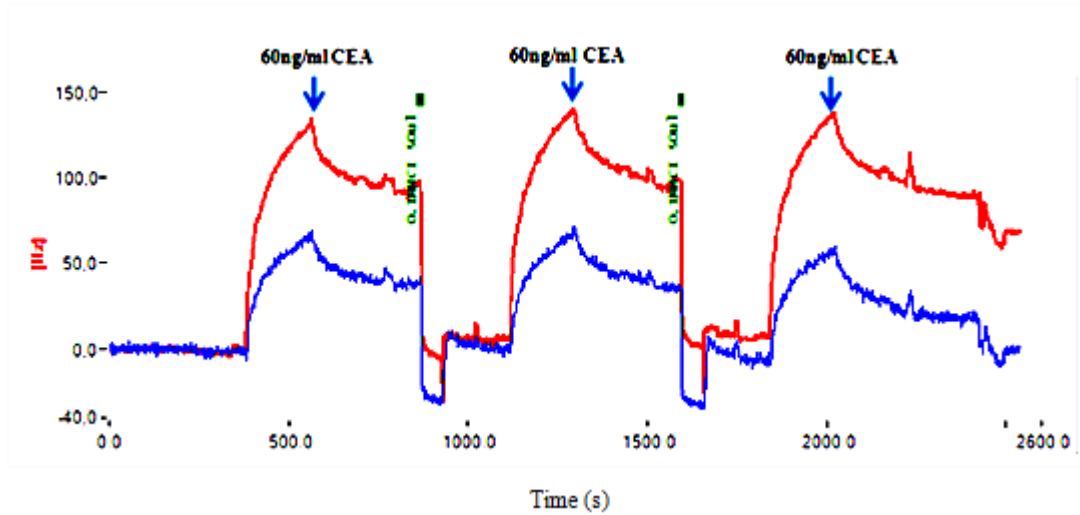


Figure 2-5 The detection of $60 \text{ ng}\cdot\text{mL}^{-1}$ CEA in QCMA-1 device. A $60 \text{ ng}\cdot\text{mL}^{-1}$ CEA was injected to the active and control surfaces. Anti-CEA provided the active sensor surface while mouse IgG was the control. In the graph red line represents CEA binding on anti-CEA whereas blue line shows non-specific CEA binding on the control surface (mouse IgG).

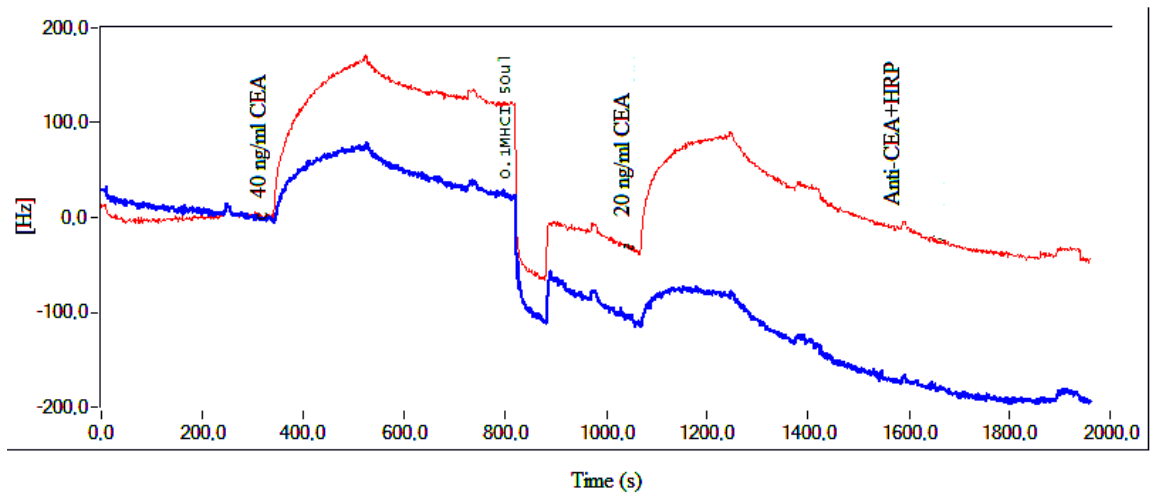


Figure 2-6 Sandwich assay with anti-CEA+HRP secondary antibody. First binding shows the direct assay using a $40 \text{ ng}\cdot\text{mL}^{-1}$ of CEA, the surfaces were then regenerated with 100 mM HCl. Later sandwich assay was performed with the injection of $20 \text{ ng}\cdot\text{mL}^{-1}$ CEA marker and a $5 \mu\text{g}\cdot\text{mL}^{-1}$ of anti-CEA+HRP antibody. The blue line shows the control surface whereas the red line is the active sensor surface.

To achieve the detection of CEA at lower concentration with higher frequency change, detection antibody and CEA antigen were incubated during 2 hours prior to measurement. RAM and anti-CEA antibody (Abcam) were immobilised to the sensor surfaces as previously described and the incubated samples were then simultaneously injected to the surfaces for capture and sandwich assays. The studied concentration range of CEA was 6.25-400 ng.mL⁻¹ and the amount of detection antibody in the incubated samples was 5 µg.mL⁻¹. Incubation was performed under ambient temperature on a shaker for 2 hours. Capture assay was applied employing RAM immobilised sensor surface whilst sandwich assay was performed on anti-CEA immobilised surface. The immobilisation anti-CEA antibody was the product of Abcam Company whereas detection anti-CEA antibody from Sigma Company. The injection time of each sample was 3 min and the sensor chip surface was regenerated after each binding reaction by 100 mM HCl solution. A 5 µg.mL⁻¹ of the detection antibody was measured as a control prior to CEA included samples and 30 Hz frequency change was observed between the lowest concentration of CEA sample and the control. Figure 2-7 and Figure 2-8 shows the control subtracted data for capture and sandwich assays, respectively. As seen in these figures, the produced frequency change by the sensor surfaces gradually decreased between 400-50 ng.mL⁻¹ concentration of CEA antigen; however, the frequency change shows an increase after this point. This was most probably a result of competition between detection antibody and CEA in the lower concentration of the antigen for incubated samples and this behaviour was observed for both assay types.

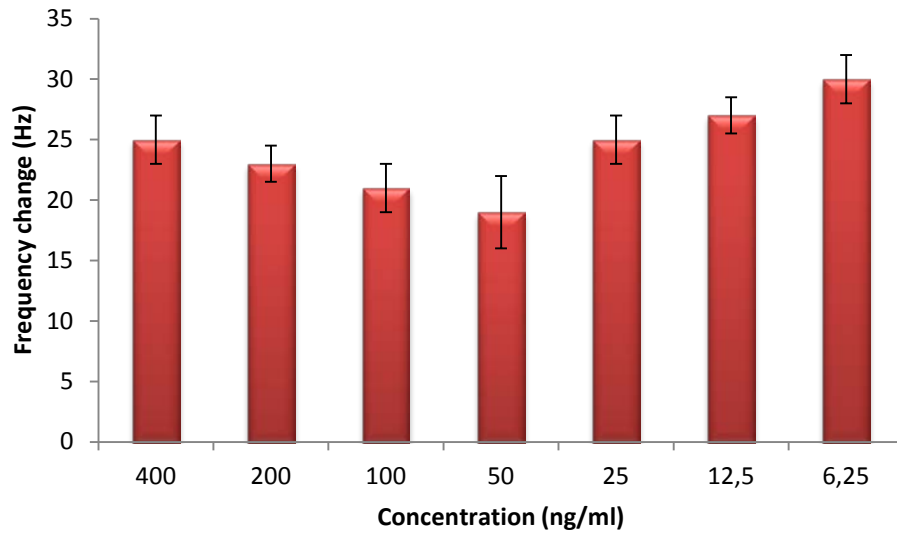


Figure 2-7. Capture assay results in QCMA-1 instrument in the concentration range of 400-6.25 ng.mL⁻¹ (from left to right). Each CEA sample included 5 μg.mL⁻¹ detection antibody.

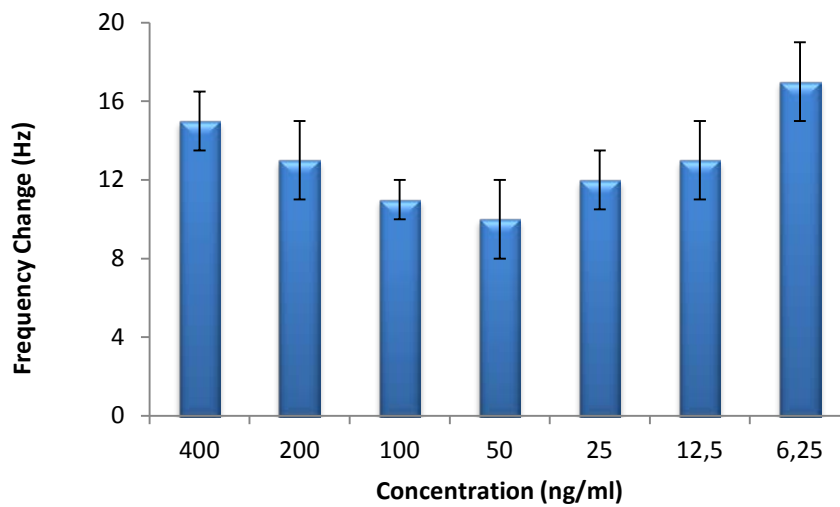


Figure 2-8. Sandwich assay results in QCMA-1 instrument in the concentration range of 400-6.25 ng.mL⁻¹ (from left to right). Each CEA sample included 5 μg.mL⁻¹ detection antibody. The surface was coated by immobilising of anti-CEA primary antibody prior to the binding assay.

Here, a QCM-based biosensor was used and the different assay types were conducted. CEA marker was tried to detect in a broad dynamic range and the aim was achieved using homogenous sandwich and capture assays in the concentration range of 6.25-400 ng.mL⁻¹.

However, the sensor assay required further optimization to obtain more stable and reliable results according to the concentration of the marker. Due to this, the sensor assays were developed in a SPR-based biosensor using CEA marker of lung cancer as model analyte.

2.4 SPR-BASED IMMUNOSENSOR FOR THE DETECTION OF CEA

Here, an immunoassay for CEA was developed and optimised on the SPR gold sensor surface to achieve high sensitivity for a real-time disease detection. Different homogeneous assay formats were investigated including capture and sandwich immunoassays. By using this label-free real-time biosensor a low detection limit for CEA which represents the critical CEA level in non-smoker individuals was achieved. The detection technique shows a promising future technology for the diagnosis of cancer at inchoate stage without the use of invasive surgical procedures.

2.4.1 Materials and reagents

Phosphate buffered saline (PBS, 0.01 M phosphate buffer, 0.0027 M potassium chloride and 0.137 M sodium chloride, pH 7.4), bovine serum albumin (BSA), N-hydroxysuccinimide (NHS), ethanolamine, Human CEA (cat no. C4835) and its monoclonal antibody (C2331) were purchased from Sigma Aldrich (Poole, UK). 1-ethyl-3-(3 dimethylaminopropyl)-carbodiimide (EDC) was purchased from Pierce-Thermo Scientific (Cramlington, UK). Mouse monoclonal antibody to carcinoembryonic antigen (CEA) (cat no. ab10037) and Mouse Monoclonal (1C11) to cardiac Troponin T: ab8295 was purchased from Abcam (Cambridge, UK), monoclonal PSA detection antibody (cat no: MCA2561) obtained from AbD Serotec (Kidlington, UK). Mouse IgG (cat no. 015-000-003) and rabbit anti-mouse IgG (RAM) was bought from Stratech Scientific Ltd./Jackson ImmunoResearch (Newmarket, UK). In the developed sandwich and RAM-capture assays, Sigma anti-CEA antibody (C2331) was used as the detection antibody to perform the assay. All other chemicals were of analytical grade.

2.4.2 Instrumentations

A fully automated SPR-based Biacore 3000 biosensor and the bare gold sensor chips were supplied by Biacore GE Healthcare (Uppsala, Sweden). The sensor possesses four sensing spots that provide four separate areas for different assay simultaneously. In the current study two sensing spots were employed for sandwich and indirect assay formats

while the third spot provided the control surface. The operating temperature of the assays was 25 °C and the flow rate of the buffer was 10 $\mu\text{l}\cdot\text{min}^{-1}$ throughout the assay.

2.4.3 Sensor chip cleaning and MUDA coating

Bare gold sensor chips were first cleaned using nitrogen plasma for one minute and then coated with self assembled monolayer (SAM) by immersing the sensors in 2 mM solution of 11-mercaptoundecanoic acid (MUDA) overnight followed by rinsing with ethanol and Milli-Q water and then dried under nitrogen. The SPR sensor chips were then stored at 4 °C until used.

2.4.4 Control surface selection

For the selection of the best control sensor surface, three different antibodies (mouse IgG, anti-PSA and anti-troponin produced in mouse) were examined. Since the samples were prepared using 5 $\mu\text{g}\cdot\text{mL}^{-1}$ BSA in all experiments, 300 $\text{ng}\cdot\text{mL}^{-1}$ CEA was diluted in BSA and the non-specific binding of this solution to each control surface was measured. A high concentration of CEA antigen was used in this confirmation study and the non-specific binding of the antigen to each control surface was recorded during the SPR assay.

2.4.5 Immobilisation of antibodies

The SAM coated sensor chip was first docked to the Biacore instrument and primed with running buffer (10 mM PBS, pH 7.4, 0.0027 M potassium chloride, 0.137 M sodium chloride) at a flow rate of 10 $\mu\text{l}\cdot\text{min}^{-1}$. Monoclonal mouse anti-CEA antibody was then immobilised via one flow path of the instrument for the sandwich assay whereas rabbit anti-mouse and mouse IgG antibodies (control antibody) were immobilized to the second and third sensor array of the chip, to conduct the capture assay and obtain control surface, respectively. The immobilisation stage of the immunoassay was obtained using conventional amine coupling chemistry. The running buffer in this stage was degassed phosphate buffered saline (PBS). During the immobilisation step firstly the sensor chip surfaces were activated with a mixture of 400 mM EDC and 100 mM NHS (1:1). Both reagents were prepared in deionised water and immediately mixed before use. EDC-NHS was injected onto the four sensor surfaces simultaneously for 3 min (30 μl) to activate the sensor chip surface. Then, 30 $\mu\text{g}\cdot\text{mL}^{-1}$ coating antibodies (anti-CEA antibodies, rabbit anti-mouse and mouse IgG) prepared in 10 mM sodium acetate buffer (pH: 5.5) were

immobilized to the sensor surfaces. After antibody immobilisation, the sensor surfaces were blocked with $30 \mu\text{g.mL}^{-1}$ BSA in PBS buffer for 3 min (30 μl). Finally, 1 M ethanolamine (pH: 8.5) was used to cap the non-reacted NHS esters exist on the sensor surface for 3 min (30 μl). The RU changes were recorded two minutes after the protein injection was completed.

2.4.6 CEA detection

First assays were performed using direct assay approach without incubation. To increase the signal amplification the homogeneous assay was then applied as sandwich and capture methods with an incubation step added before the assay taking place in the instrument. Different incubation methods were examined, including water bath at 37°C and with/without shaker at room temperature applied prior to the assay. The CEA and detection antibody were incubated in the 1.5 ml Eppendorf tube for each concentration of the antigen. The detection antibody concentration was chosen as always higher than CEA to prevent any free CEA in the solution that can interfere with the binding results. The incubation conditions were then optimized as time, temperature and detection/capture antibody concentration. The best results were achieved through applying incubation at room temperature for 2 hours using a shaker. PBS buffer was used as the running buffer during the CEA marker detection and $5 \mu\text{g.mL}^{-1}$ BSA in PBS was used to prepare the CEA samples. For the sandwich assay, two different mouse anti-CEA antibodies (a coating and detection antibodies) were used while rabbit anti-mouse (RAM) was preferred as coating antibody for the capture assay. RAM-capture assay is an indirect assay here in which RAM was used to capture either mouse anti-CEA antibody or CEA bound mouse anti-CEA antibody. The sensor signal difference due to the mass difference of free or antigen (CEA) bound anti-CEA antibody was investigated to obtain the results. The anti-CEA captured on RAM causes an SPR signal, however the SPR signal is higher (due to higher mass) when antigen bound anti-CEA antibody is captured on RAM immobilised surface. By subtracting the two responses the affect of antigen to the assay can be calculated. Before samples injection, $5 \mu\text{g.mL}^{-1}$ BSA and anti-CEA detection antibody were injected to all sensor surfaces as negative controls in the experiments. Each CEA sample and negative controls were injected onto the sensor surface for 3 minutes and RU changes were recorded. After each binding step the sensor chip surface was regenerated by injecting 100 mM HCl (1 min, 10 μl) and additional 20 mM NaOH (1

min, 10 μ l) where these were found to give the best sensor surface regeneration without hindering the affinity of the immobilised antibody. All the data points presented are the averages of the triplet measurements unless otherwise stated. The limit of detection (LOD) was calculated as the signal obtained from the CEA concentration that is equivalent to the 3 times the standard deviation of the signals obtained from the blank standards.

2.5 Results and Discussions

In this study an SPR based assay for the detection of human CEA tumour marker was developed and optimised using different immunoassay formats constructed on the surface of a Biacore bare gold sensor chip including a standard capture, rabbit anti-mouse (RAM) capture and sandwich assays.

2.5.1 Assay optimisation

Bare gold SPR sensor chips were employed in this work as the sensor platform for the CEA detection. Each chip consists of four sensing arrays. The modification of the chips using self-assembled monolayer's (SAM) was carried out on the sensor surface. The SAM coated sensor chip was first docked to the Biacore instrument and primed with running buffer using a flow rate of 10 μ l.min⁻¹. To eliminate non-specific binding to the control sensor array surface, control surface selection study was conducted. Three different antibodies (mouse IgG, anti-PSA and anti-troponin) were investigated and used in this study. The antibodies were immobilized to the three different sensor arrays on the Biacore chip using different flow channels of the sensor respectively with conventional EDC-NHS chemistry [68]. A 3 minutes injection of the antibodies was sufficient to achieve the signal with concentration of 30 μ g.mL⁻¹ antibody saturation. A 300 ng.mL⁻¹ CEA solution in PBS buffer containing 5 μ g.mL⁻¹ BSA was then injected to all immobilised control surfaces on the sensor array. In addition to the CEA, a 5 μ g.mL⁻¹ BSA solution was also examined in a separate experiment in order to measure the non-specific binding caused by this solution alone. The recorded RU change for non-specific BSA binding was 1 \pm 1 RU for anti-PSA and anti-troponin immobilized surface while it was 1 \pm 0.5 for mouse IgG. Moreover, non-specific binding of the CEA antigen against each surface was observed at zero level and therefore mouse IgG was selected as the control surface for further experiments (Figure 2-9).

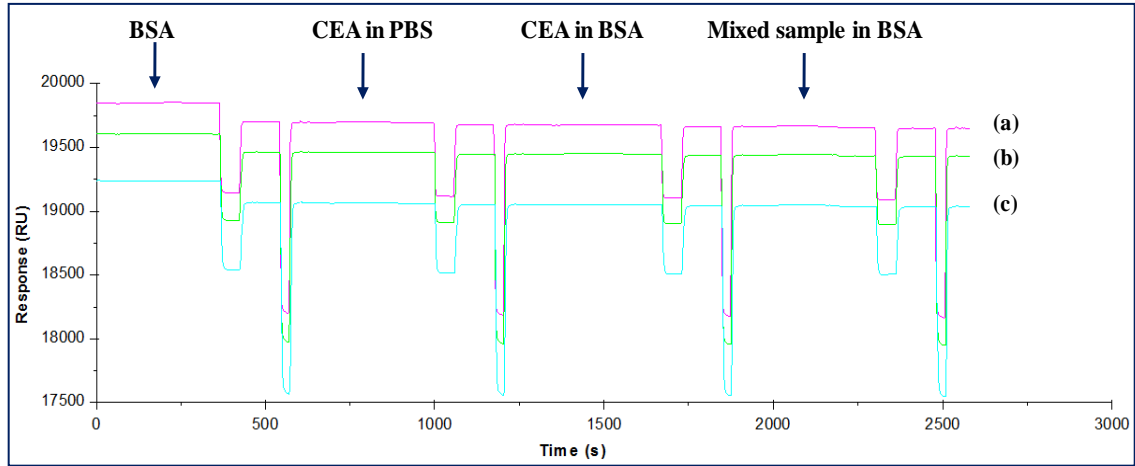


Figure 2-9 Confirmative assay for the control surface selection with PBS buffer. The non-specific binding of BSA to each antibody surface (first binding), the non-specific binding of CEA antigen in PBS or BSA solution (second and third bindings), the non-specific binding of the mixed sample included detection antibody and CEA antigen (last binding).

The immobilized surfaces: anti-PSA (a), anti-troponin (b), mouse IgG (c).

A standard direct assay format in which the coating anti-CEA antibody was immobilized onto the active sensor surface and mouse IgG immobilised to the control surface was then developed. CEA antigen was then injected on the sensor surface in the concentration range of 100-400 ng.mL^{-1} . Though a clear difference was observed between the active sensor surface and the control surface, the obtained results were low despite the high concentration of CEA used in the test (Figure 2-10). The recorded response changes were 258 ± 19 RU using the standard direct assay for the binding of 300 ng.mL^{-1} CEA. These preliminary tests with high concentrations of CEA showed that the direct detection of CEA biomarker using the SPR sensor may not be suitable for the measurement of low CEA concentrations. This was confirmed when the optimised direct assay conditions were then applied for the detection of lower CEA concentrations (down to 100 ng.mL^{-1}) achieving a low and irreproducible signal.

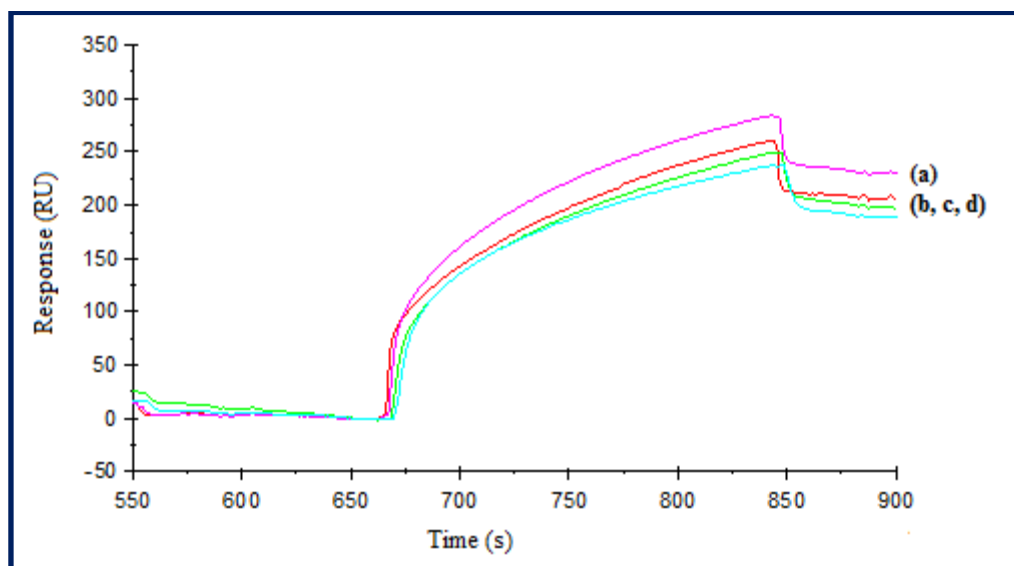


Figure 2-10 Direct assay sensorgram with a 300 ng.mL^{-1} concentration of CEA biomarker using the SPR sensor. CEA antigen binding on Abcam's anti-CEA immobilized (a) and Sigma's anti-CEA immobilized (b, c, d) sensor surfaces.

Kinetic data analysis was performed for this assay results and the data was fitted to 1:1 Langmuir binding model to determine the binding association and dissociation rates [69]. With this binding model, K_A , K_D , R_{max} values were calculated as $1.13 \times 10^8 \text{ M}^{-1}\text{s}^{-1}$, $8.8 \times 10^{-9} \text{ M}$ and 215 RU for the concentration of 300 ng.mL^{-1} CEA (using Abcam antibodies in a direct affinity assay) (Table 2-1). Due to the weak responses with the direct assay, other assay formats were then investigated.

Table 2-1 Results of kinetic calculations for CEA marker detection with standard and optimised assay formats.

Parameters/Assay type	Standard assays	Optimised RAM-capture assay	Optimised Sandwich assay
k_a (1/Ms)	8.17×10^4	1×10^3	6.88×10^5
k_d (1/s)	7.29×10^{-4}	1.46×10^{-6}	2.09×10^{-5}
R_{max}	215 RU	428 RU	734 RU
K_D (M)	8.8×10^{-9}	1.46×10^{-9}	3.04×10^{-11}
K_A (1/M)	1.13×10^8	9.97×10^4	3.29×10^{10}

A sandwich and RAM-capture assays were then developed under optimised conditions that gave much higher response when compared to the standard capture assay. Langmuir binding model was also performed for the optimised assays in the linear dynamic range of 3-400 ng.mL⁻¹ of CEA and the results are reported in

Table 2-1. The developed assays provided higher responses than the standard direct assay format using Rabbit anti-mouse and Abcam anti-CEA antibody as the surface capture antibodies and in both assays the anti-CEA antibody (Sigma) was employed as the detection antibody. To enhance the sensor signal and improve the sensitivity of the assay further an incubation step was introduced where the detection anti-CEA antibody (from Sigma) was incubated first with CEA antigen in buffer before the sample was applied to the sensor surface. To optimise this step various incubation procedures were examined including temperature (37 °C, or 22 °C and with/out shaking conditions). Optimal results were achieved when a 22 °C with a shaker incubator was used. The principle of the applied homogenous assays (RAM-capture and sandwich assays) are shown in Figure 2-11.

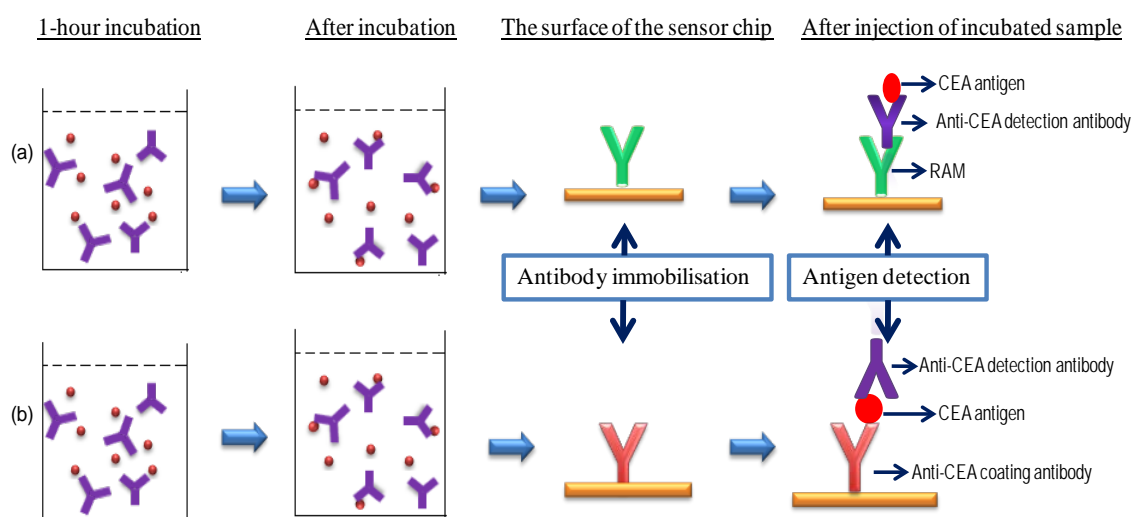


Figure 2-11 Schematic representation of homogenous RAM-capture (a) and sandwich assay (b).

The concentration of the anti-CEA detection antibody used in the assay was also optimised. Various concentrations of detection antibody in the range of 1-5 µg.mL⁻¹ were examined using CEA sample concentration range of 50-400 ng.mL⁻¹. Optimal results

were achieved when $5 \mu\text{g.mL}^{-1}$ detection antibody was used. Higher concentrations of anti-CEA detection antibody were also tested but did not give higher responses. The time of incubation between the detection antibody and the CEA before injecting on the sensor surface was then optimised under these conditions to achieve maximum sensitivity. The RU responses were measured throughout 5 hours and the highest RU changes were recorded in the first 2 hours of incubation; however, the obtained RU changes for each CEA concentration showed gradual decrease after 2 hours as depicted in Figure 2-12.

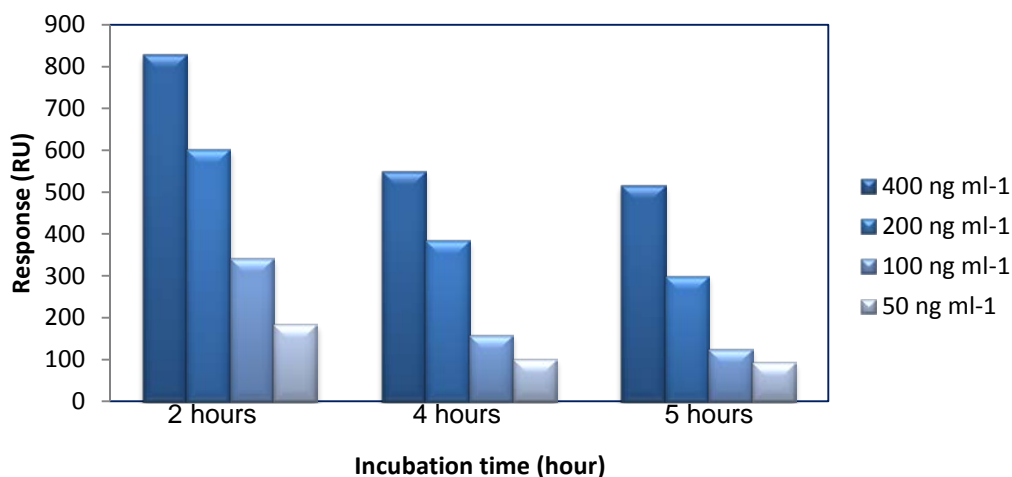


Figure 2-12 Optimization of the incubation time. After first 2 hours of the incubation the recorded response change was gradually decreased.

However, it must be noted that these samples did not contain preservatives or protein stabilisers. After obtaining these results the assays were performed using 1 or 2-hour incubation to observe the difference; however, the recorded RU changes were similar in both incubation periods. Therefore, 1 hour incubation was preferred to perform the assay at ambient temperature on a shaker in order to minimise the total assay time. This incubation step was performed prior to the measurement of CEA binding on the Biacore 3000 biosensor.

2.5.2 Sandwich and RAM-capture assays characterisation

In the development of the immunoassay on the sensor chip, three different antibodies were used and these included; monoclonal mouse anti-CEA antibody (from Abcam), rabbit anti-mouse and mouse IgG. The antibodies were immobilised through the separate flow paths of the three arrays on the sensor platform. Anti-CEA monoclonal antibodies and rabbit anti-mouse antibodies were used as the coating antibody for the sandwich and

RAM-capture assays respectively, whereas mouse IgG provided the control surface. The immobilization signal of each antibody was measured during a 3 minutes duration and the evaluated RU changes for the immobilization reaction were recorded as 3500 ± 95 for anti-CEA (Abcam), 3000 ± 120 for rabbit anti-mouse and 2800 ± 37.6 for mouse IgG antibodies respectively (Figure 2-13). A 3 minutes injection of antibodies was sufficient for the signal to reach equilibrium; therefore, the immobilisation time was kept at 3 minutes for the assay. Although the RU changes for the immobilized antibodies showed similarity to each other they were different antibodies produced by different companies.

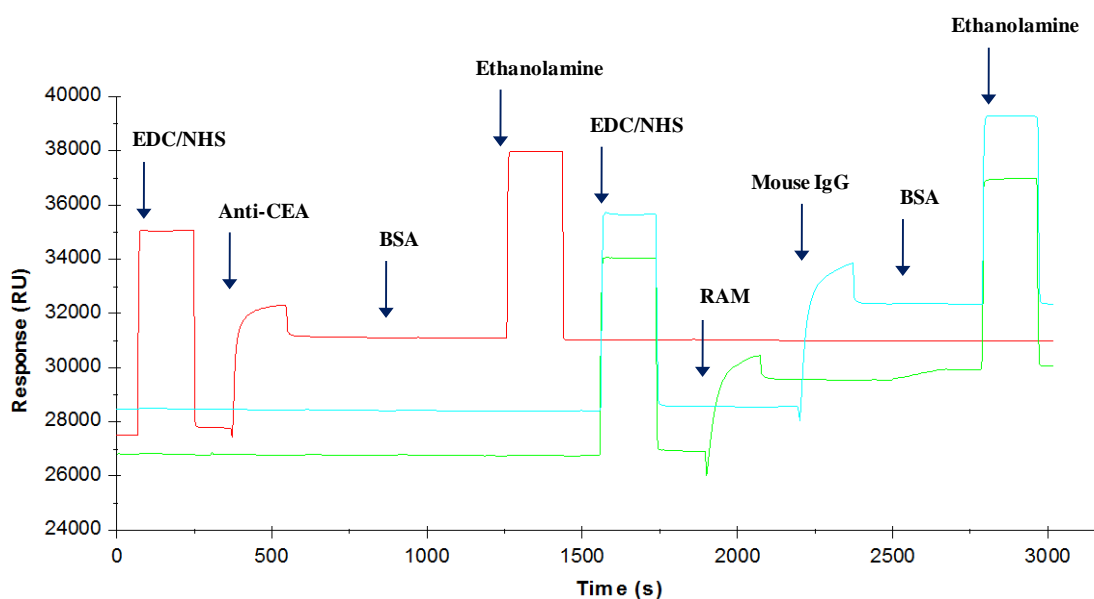


Figure 2-13 Immobilisation of anti-CEA coating antibody (red), rabbit anti-mouse (green) and mouse IgG (blue) antibodies on the sensor chip surface.

In the sandwich assay method, the CEA antigen in the sample was first incubated with the anti-CEA detection antibody (Sigma, $5 \mu\text{g.mL}^{-1}$) for 1 hour at $22 \text{ }^\circ\text{C}$ and then was injected on the anti-CEA coated sensor surface. Whereas for the indirect capture assay the anti-CEA detection antibody coupled with CEA antigen (Ab-Ag complex) was injected on the Rabbit anti Mouse (RAM) and mouse IgG coated sensor arrays for the RAM-capture and control assays respectively. Each incubated sample was prepared in $5 \mu\text{g.mL}^{-1}$ BSA and the non-specific binding of both $5 \mu\text{g.mL}^{-1}$ anti-CEA detection antibody and $5 \mu\text{g.mL}^{-1}$ BSA were recorded before each experiment. The non-specific binding of $5 \mu\text{g.mL}^{-1}$ anti-CEA detection on the anti-CEA coating antibodies was recorded as 5.1 ± 5.2

while non-specific binding of the $5 \mu\text{g.mL}^{-1}$ BSA on all surface caused only 3 ± 2 RU change.

The selected concentration range of CEA samples for the detection was $3\text{-}400 \text{ ng.mL}^{-1}$ and this concentration range was studied through two different assay types. The recorded RU changes were from 30 to 802 RU in the concentration range of $3\text{-}400 \text{ ng.mL}^{-1}$ CEA and $5 \mu\text{g.mL}^{-1}$ detection antibody control caused only 3.5 ± 2.7 RU change in the sandwich assay. On the other hand, the obtained results were between 13- 430 RU change in the same concentration range of CEA antigen for the RAM- capture assay. Moreover, the non-specific binding of CEA on the control surface was measured as only 3.5 ± 2.7 RU change. Figure 2-14 represents the sensorgrams of the sandwich assays and RAM-capture assay respectively.

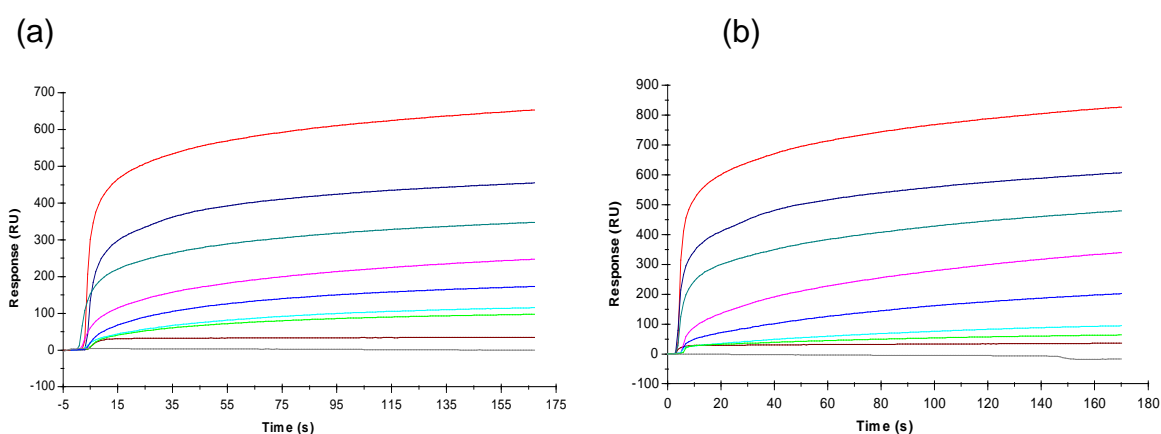


Figure 2-14 Sensorgram of the CEA assay through sandwich (a) and capture (b) methods in the concentration range of $3\text{-}400 \text{ ng.mL}^{-1}$. The lowest line represents the control in each assay and the RU change gradually increased from bottom to the top according to the increased CEA concentration.

A clear difference was observed between the control and active surfaces through both assay types. All data were control subtracted. However, the recorded RU changes were found to be higher in the sandwich assay (Figure 2-15) when compared to the RAM-capture assay (Figure 2-16) according to the CEA concentration tested. As it is seen in the figures the obtained correlation coefficient of the sandwich and RAM-capture assays were 1.00 and 0.99 respectively with the 3 ng.mL^{-1} detection limit for both assays.

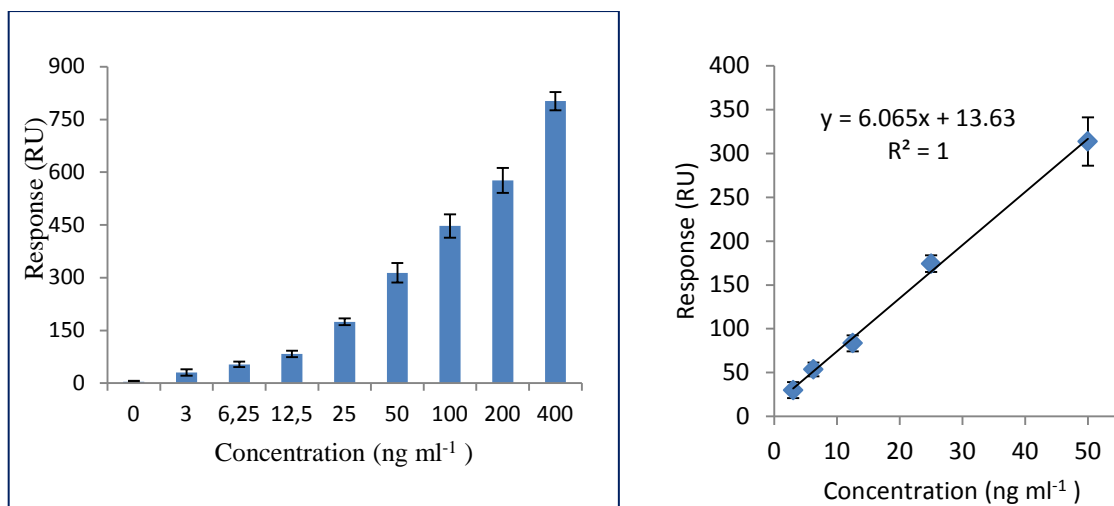


Figure 2-15 The overall results of sandwich assay. (All shown data is control subtracted).

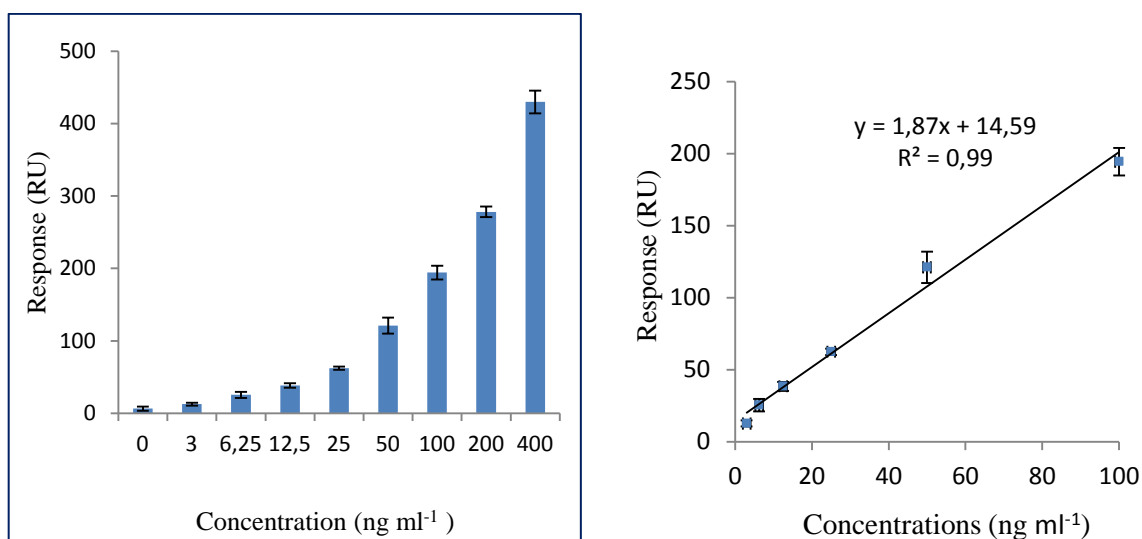


Figure 2-16 The overall results of RAM-capture assay (All shown data is control subtracted).

. Here, we have achieved a detection limit of 3 ng.mL⁻¹ CEA concentration with a simple assay design without the use of assay amplifiers such as nanoparticles which we can implement to enhance the sensitivity further. The follow up work concentrated on transferring/developing the methodologies for an electrochemical-based capacitive sensor to reach lower detection limits with a cost effective, miniaturize sensing platform.

CHAPTER 3

3 CAPACITIVE SENSOR PLATFORM FOR CANCER DETECTION AND QUANTIFICATION

Capacitive sensors can be divided into two groups as faradaic and non-faradaic sensors depending on the transient current flow. In a faradaic process charge is transferred across an interface whereas transient currents can flow without addition of a redox charge transfer in nonfaradaic processes. Therefore, redox species are alternately oxidized and reduced by the transfer of an electron to and from the metal electrode in faradaic capacitive sensors. Due to this, these kind of capacitive sensors require the addition of a redox-active species and DC bias conditions. On the other hand, additional reagent is not required in non-faradaic sensor and this behaviour makes them more amenable to point-of-care applications [70]. Since we have used non-faradaic capacitive sensors in our research group, the main focus was on the development of interdigitated capacitive sensors in this PhD thesis.

One of the most crucial points in capacitive biosensors is to immobilize the biorecognition layer that has to be sufficiently insulated in order to keep ions on the layer to avoid short circuiting of the system that causes a recession or lack of the signal. Though different types of semiconductors materials exist, silicon is the most popular one to develop capacitive biosensors because of its advantages which are being both obtainable under quotable conditions and biocompatible. In the course of an experiment the change in capacitance can be measured as a dielectric constant change or the layer thickness change immobilized on the transducer.

The principle of the measurement depended on the changes in dielectric properties, dimension, shape and charge distribution while antibody-antigen or probe-DNA/RNA complexes occurred on the electrode surface. In the event of a conformational change of a surface protein through binding of an analyte, this can be detected by capacitance measurements. The capacitance measurement can be realized through two approaches in an experiment including the measurement of the change in the capacitance between two metal conductors in near proximity to one another with the recognition element

immobilized between them (IDEs) and measuring the capacitance potentiostatically at an electrode/solution interface with the recognition components on the working electrode surface. For interdigitated electrodes the capacitance is defined with equation 3.1

$$C = \epsilon\epsilon_0 A/d \quad (\text{Equation 3-1})$$

where, ϵ is the dielectric constant of the medium between the plates, ϵ_0 (8.85419 Pf/m) is the constant of permittivity of free space, A is the area of the plates and d is the distance between the plates. According to equation, if a change occurs in the dielectric properties in the supplies between the plates, it leads to a change in the capacitance. The equation also shows that the capacitance and its sensitivity increase when the distance of two conductors decrease.

When protein assays are conducted in the capacitive sensor platforms, the antibodies have low dielectric constant with respect to water, thus a change in the dielectric properties occurs between the electrodes that lead to a variation in the capacitance. Interdigitated fingers (Figure 3-1) have been used to obtain a larger sensor surface and with some modifications on IDEs they provide the direct detection of many substances including acetylcholine, toxin, oxygen bubbles, toxin, HIV and human IgG antibodies. In this case, the capacitance between the IDEs can be described by the equation of $C=2n \epsilon\epsilon_0 A/d$ where n is the number of electrodes and factor 2 shows each electrode forming two capacitors.

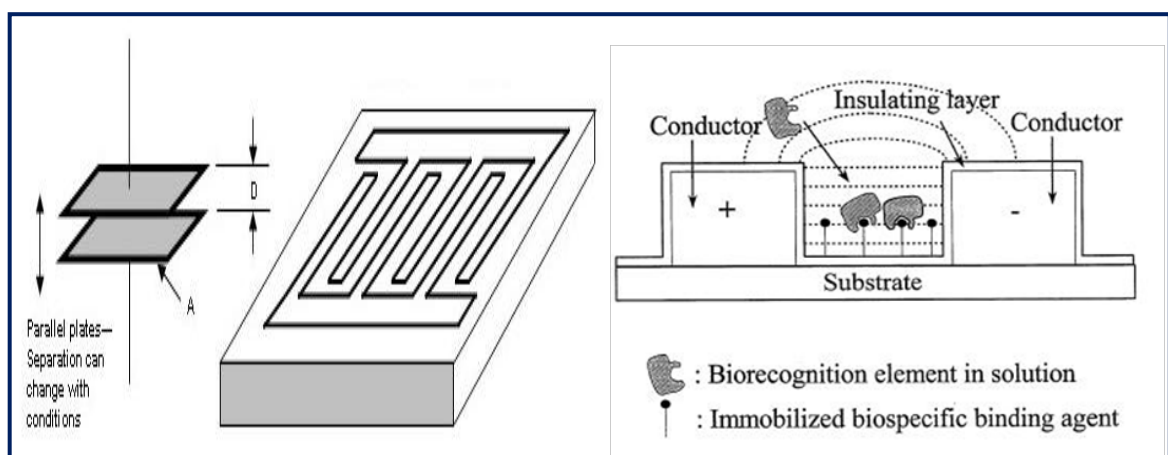


Figure 3-1 Schematic representation of the IDEs and parallel plates that mentioned above.

Non-faradaic capacitive sensors are also affected by dipole-dipole interactions, relaxation time of biological molecules and charge distribution throughout the sensor layer. A complex protein includes hydrophobic and hydrophilic regions, and the protein folds in a soluble media depending on this behaviour. When the protein fold, the hydrophilic regions that include non-polar amino acids constitute the core of the protein whereas the polar regions interact with water. There are positively and negatively charged amino acids in the protein structure that constitute ionisable side chains. The simplest molecular dipole is composed of a pair of opposite electrical charges with magnitude of $+q$ and $-q$ and separated by a vector distance (r). The molecular dipole moment (m) is defined by the equation $m=qr$. Each type of polar or polarizable substance displays a characteristic response to the imposed electric field. When a protein is immobilized on a solid surface and allowed to bind its analyte, a protein–analyte complex is formed. The change in conformation brought on by this interaction leads to an increase in molecular size of a protein–analyte complex. This increase in size of a protein–analyte complex leads to a relatively large permanent dipole moment. The relaxation time and polarizability constants can thus be evaluated.

Moreover, proteins have N–C bond in the peptide units that shows a partial double bond character and gives a coplanar nature to $C\alpha NHCOC\alpha$ structure. The C=O bond has also polar nature that brings a permanent dipole moment in the peptide bond. Due to the permanent dipole moment of each peptide unit in a protein, polypeptide chains take the form of strings of connected dipoles. The increase dipole moment directly relates with impedance, thus with capacitance. As seen in the following equation, the increased dipole moment leads to the decrease in the impedance; therefore, increase in the capacitance due to the reverse interaction between the impedance and the capacitance. Dipole moment is affected by the charge distribution of biological molecules, the media used and pH. It also relates to polarization. The impedance equivalent network circuit bases on Cole-Cole model of IDE sensor. In the equations R_∞ is the high frequency impedance, R_0 is the low frequency impedance, m is the polarizability constant, and τ is the relaxation time constant.

$$Z(\omega) = Z(o)\left\{1 - m \left[1 - \frac{1}{1+(j\omega\tau)}\right]\right\} \quad \text{(Equation 3-2) [71]}$$

$$R_0 = Z(o) \quad \text{(Equation 3-3)}$$

$$R_{\infty} = Z(o)[1 - m] \quad (\text{Equation 3-4})$$

In the capacitive sensor platform, the polarizability constant value of only antibody was found lower than the antibody-antigen complex. The rotational motion of the target antibody-antigen complex can be related to the increase in polarizability constant. The dielectric dispersion $\Delta\epsilon' = (\epsilon'_s - \epsilon'_{\infty})$ of the antigen injected sample was found higher than the control and the changes in the value of $\Delta\epsilon'$ related to change in shape and volume of proteins investigated in the study. This may be due to increased conductivity which accompanied by a decrease in the values of dielectric constant [71].

The dielectric constants of many liquids and solids depend markedly on the frequency of measurement. The dependence is in general found to be a decrease from a static value ϵ_0 at low frequencies to a smaller limiting value ϵ_{∞} at higher frequencies. In the transition region of anomalous dispersion there is an "absorption conductivity" and the situation may be described in terms of a complex dielectric constant $\epsilon^* = \epsilon' - i \epsilon''$. The classical theory of the effect for polar liquids is due to Debye [72]. In this theory the difference between the values ϵ_0 and ϵ_{∞} , is attributed to dipole polarization. The orientation of polar molecules in an alternating-current field is opposed by the effects of thermal agitation and molecular interactions. Debye represents the second effect by a picture of viscous damping, the molecules being regarded as spheres in a continuous medium having the macroscopic viscosity. The theoretical analysis in this case leads to equation 3.5.

$$\epsilon^* - \epsilon_{\infty} = (\epsilon_0 - \epsilon_{\infty})/(1 + i\omega\tau_0) \quad (\text{Equation 3-5})$$

can be written as

$$\epsilon' - \epsilon_{\infty} = (\epsilon_0 - \epsilon_{\infty})/(1 + \omega\tau_0)^2 \quad (\text{Equation 3-6})$$

$$\epsilon'' = (\epsilon_0 - \epsilon_{\infty})\omega\tau_0/[1 + \omega\tau_0)^2] \quad (\text{Equation 3-7})$$

where $\omega = 2\pi$ frequency and the parameter τ_0 is a characteristic constant which may be called the relaxation time. Dispersion and absorption can also occur in nonhomogeneous dielectrics. The possibility of absorption in a double-layer dielectric if the ratios of conductivities and dielectric constants of the two layers are not equal [73]. Since the target antigen-antibody complex has more molecular size than the antibody alone, the increase in relaxation time is correlated to the increase in the size of a protein molecule.

In this PhD thesis, an electrochemical-based non-faradaic capacitive sensor was employed and developed for cancer detection. With this aim, hEGFR marker of lung cancer was initially worked without using any signal amplification methods and the nanoparticle modified sensor platforms were then conducted to achieve lower detection limits with high sensitivity and stability.

3.1 CAPACITIVE DETECTION OF EGFR

Human-Epidermal Growth Factor Receptor is a transmembrane glycoprotein, which has an extracellular ligand-binding domain and an intracellular domain that possess intrinsic tyrosine kinase activity. When a ligand binds to hEGFR, receptor dimerization leads to both activation of tyrosine kinase domain and recruitment and phosphorylation of intracellular substrates, driving normal cell growth and differentiation. Many molecular events may lead to the persistent activation of the kinase activity, consequently triggering a broader spectrum of downstream signal transduction pathways. It is documented that hEGFR is closely related to cancer and overexpressed in some cancer types including lung carcinomas [74-80]. The overexpression of the receptor in various series of non-small cell lung carcinomas (NSCLC) ranges from 43% to 89% [81]. The normal range of hEGFR in a healthy individual is 64 ng.mL^{-1} and the level of the marker plays crucial role in cancer diagnosis and progression. The lower level of the marker ($< 64 \text{ ng.mL}^{-1}$) is especially correlated with breast cancer [57], [82-86]. Therefore, the detection of hEGFR can play a significant role in early detection of the cancer.

In this work, for the first time, hEGFR was investigated for detection using a GID capacitor sensor. A direct detection of hEGFR was demonstrated using hEGFR-antibody as the capturing ligand which was covalently immobilized on GID region of capacitors. When the immobilized antibody formed a complex with hEGFR-antigen, this interaction led to the change in thickness of the dielectric layer on GID surface, and induced changes in capacitance that directly related to the antigen concentration. The novelty of this research is being (1) label-free method, (2) capacitive detection based on the change in surface charges induced by binding of antigen on the antibody immobilized sensor surface, and (3) detection of hEGFR marker in real human serum. The method described here is based on a direct detection of hEGFR in its native forms without using any signal

amplification method or mediator chemicals. Capacitive detection of hEGFR was successfully achieved using standard assays in much lower concentration than the normal levels ($\sim 64 \text{ ng.mL}^{-1}$) and the capacitive sensor was then aimed to develop employing nanomaterials for signal amplification in the case of trace biomarker amounts (see Chapter 4).

3.1.1 Material and Methods

3.1.1.1 Materials and reagents

Phosphate buffered saline (PBS) and 2X HEPES buffer were purchased from PAN BIOTECH GmbH and Fluka, respectively. Ethanolamine (99%), bovine serum albumin (BSA), sheep monoclonal antibody to human epidermal growth factor receptor (anti-hEGFR) and human epidermal growth factor receptor (hEGFR), N-(3-dimethylaminopropyl)-N-ethylcarbodiimide hydrochloride (EDC) and N-hydroxysuccinimide (N-hydroxy-2,5-pyrrolidinedione, NHS) were purchased from Sigma Aldrich (USA). HPLC grade 3-Mercaptopropionic acid (MPA, 99%) was purchased from Fluka. Human serum was bought from PANTM Biotech GmbH (Germany). Doubly distilled water was used throughout the experiments.

3.1.1.2 Fabrication of the sensor platform

GID array electrodes were patterned on SiO₂ surface using image reversal technique. In this process, the metal layers were patterned using the dual tone photoresist AZ5214E. A 2- μm thick AZ5214E photo resist was patterned with the help of a mask for a lift-off process. Following this step, a very thin titanium layer of $\sim 20 \text{ nm}$ size was layered to improve the adhesion of gold on the SiO₂ film by DC sputter deposition, and about $\sim 180 \text{ nm}$ thick gold layer was deposited. The lift-off process was performed in pure acetone as a solvent. The length of each electrode was $800 \mu\text{m}$ and a width of $40 \mu\text{m}$ with a distance between two electrodes was $40 \mu\text{m}$. As a result, each GID array on a capacitor contained 24 GID fingers.

3.1.1.3 Sensor chip cleaning and MPA coating

The fabricated sensor chip was washed several times with ethanol and rinsed with sterile dH₂O. The cleaned surface was dried by nitrogen gun. The blank measurements

were taken by Network Analyzer prior to any surface/bio-chemical treatment/application on the surface. The sensor surface was then coated with self-assembled monolayer (SAM) by immersing the sensor in 10 mM solution of 3-mercaptopropionic acid (MPA) during overnight incubation followed by rinsing with ethanol and Milli-Q water and then dried using nitrogen gas. The formation of SAM layer on the surface was confirmed by FT-IR. The surface topology, roughness and the distribution of the particles on blank surface was observed using an Atomic Force Microscope (AFM, Nanoscope).

3.1.1.4 Immobilization of antibodies

The SAM coated GID electrode surface of capacitors were activated using a mixture of 100 mM EDC and 50 mM NHS (1:1). Both reagents were prepared in sterile-deionised water and immediately mixed before the use. EDC-NHS was carefully applied on to each GID electrodes in 5 μL volumes and incubated for 4 h in a Petri dish. After the EDC-NHS activation, the sensor wafer was washed with PBS buffer and then dried with a nitrogen gun. Each GID capacitor was immobilized by incubating 2.5 μL of 50 $\mu\text{g}\cdot\text{mL}^{-1}$ anti-hEGFR antibody in PBS buffer for 1 h. (To determine the optimal antibody concentration in our sensor platform, a preliminary test was performed using different concentrations of the antibody and 50 $\mu\text{g}\cdot\text{mL}^{-1}$ was then selected according to the results.) The sensor wafer was then washed with PBS and dried prior to the blocking step with ethanolamine. The non-reacted groups on the sensor surface were blocked by adding 5 μL of 100 mM ethanolamine on each GID electrode and incubated for 2 h. The antibody immobilized sensors were further subjected to blocking with 2.5 μL of 50 $\mu\text{g}\cdot\text{mL}^{-1}$ bovine serum albumin (BSA). The sensor was then rinsed with PBS and sterile dH_2O , and dried with nitrogen gun prior to the measurements for antibody immobilization using a Network Analyzer. The analyzer was calibrated and triplicate measurements were then taken for each GID electrode for error analysis. FT-IR of the antibody immobilized surface was performed for confirmation and AFM images were taken to compare with blank surface.

3.1.1.5 hEGFR protein detection

A series of hEGFR concentrations (0.5-256 $\text{ng}\cdot\text{mL}^{-1}$) were prepared in 1X HEPES buffer and the same buffer was used as a blank control. Each concentration of the biomarker was tested on three independent GID capacitors for error analysis. The hEGFR

samples prepared in the buffer were incubated for 2 h for the antigen detection step and the sensor was then carefully rinsed with PBS followed by dH₂O to remove traces of salts on the sensor surface. The sensor was quickly dried with nitrogen gas and each GID capacitor was measured for the detection of hEGFR marker. The specificity of the interaction between the target antibody (anti-hEGFR) and antigen (hEGFR) was checked by applying 50 ng.mL⁻¹ of non-specific BSA protein on the anti-hEGFR immobilized (GID) electrodes instead of the target protein marker. The average values of the change in capacitance were plotted and the standard deviations of the triplicate experiments were shown as error bars.

3.1.1.6 Detection of hEGFR in human serum sample

The human serum sample was spiked with different concentrations of hEGFR protein (0-10 ng.mL⁻¹). The hEGFR concentrations were prepared in 100% human serum (Type AB, Male donar, PANTM Biotech GmbH). For negative control, BSA protein was spiked in human serum in a final concentration of 50 ng.mL⁻¹ and incubated on the antibody immobilized surface to validate the specificity of the binding between target antibody-antigen pair. All samples were incubated on the sensor surface for 2 h. After the antigen binding process during 2 h, the sensors were washed for three times with PBS buffer followed by quick wash with distilled water to remove traces of salt and other molecules. Finally, the sensor was dried before taking the measurements. Each concentration of the marker was incubated on three independent GID capacitors for error analysis and the measurements were taken using a Network Analyzer.

3.1.2 Results and Discussions

In this study, we report on a bioassay using an electrochemical-based capacitive sensor platform for the detection of hEGFR, whose level is a potential indicator to assess whether a patient is at a risk of breast or lung cancers. Although hEGFR receptor has a crucial importance for the diagnosis of cancer, both investigations and applications have been limited with current diagnostic and monitoring techniques that are time-consuming, invasive or require high-cost. To our knowledge, EGFR has been not investigated with sensor technologies yet. There is only one published study that mentioned the anti-EGFR antibody modification with colloidal gold nanoparticles to detect the living whole cells. The researchers used surface plasmon resonance (SPR) scattering technique to measure

the cell viability that is completely different approach when compared with our work [87]. Aaron et al. applied the similar methodology with various nanoparticles and optical imaging to measure the cell viability using EGFR [88]. Choi et al. performed ELISA test to detect hEGFR for gastric carcinoma patients and could measure 0.6 nmol of EGFR [89]. When we compared the detection limit of ELISA with our test we could achieve to detect 2.94 fmol that is much lower with respect to the ELISA test. (0.5 ng.mL^{-1} was converted to the mole to do exact comparison and it is equal to 2.94 fmol for 170 kDa protein). Moreover, the ELISA technique does not provide higher sensitivity and it needs much more reagent with special qualifications.

Here, a real time, label-free and non-invasive method was adapted through a highly sensitive and specific capacitive sensor array to detect the cancer marker hEGFR for the first time (Figure 3-2).

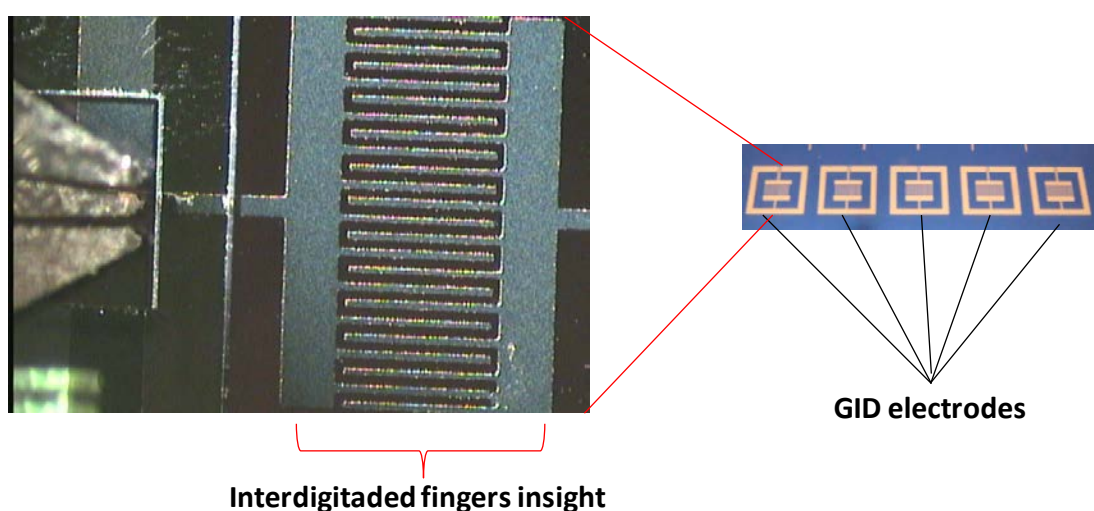


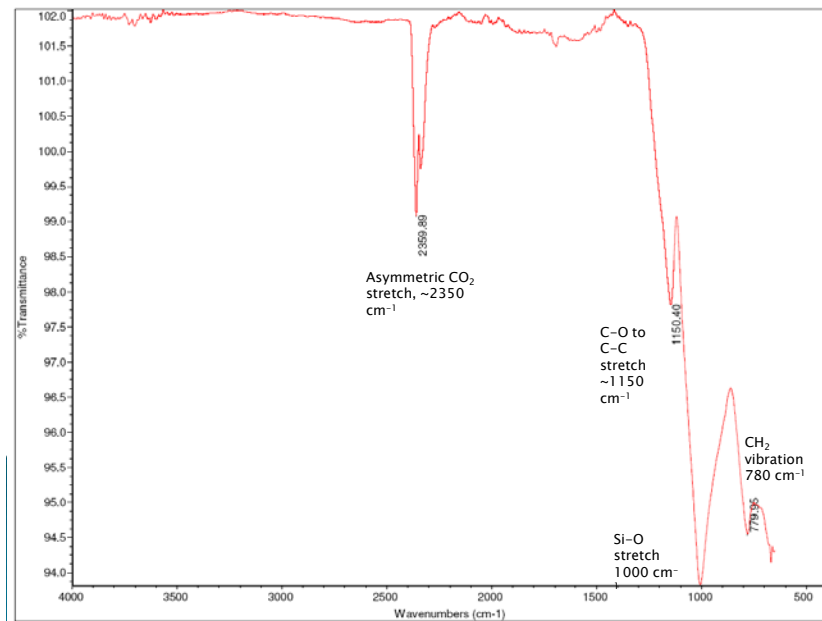
Figure 3-2 Microscopic image of gold interdigitated transducer electrode array.

3.1.2.1 FT-IR analysis of SAM-coated and EDC-NHS activated GID surfaces

The fabricated sensor platform was subjected to SAM formation with 3-Mercaptopropionic acid. The SAM coated sensor surface was then activated with an EDC-NHS mixture prior to the immobilization of anti-EGFR antibody. The activated sensor surface was scanned and the recorded FT-IR spectra were compared with the reference spectra [90] and all spectra were collected with 64 scans for the reference and the sample, with 4 cm^{-1} resolution in the reflection mode. FT-IR spectrum of SAM coated surface indicated the formation of a MPA layer on the gold surface by the disappearance of the S-H stretch at 2551.5 cm^{-1} , as well as the existence of CH_2 vibration (at 780 cm^{-1})

and C-C stretch ($\sim 1150\text{ cm}^{-1}$) that is present in MPA backbone [91] (Figure 3-3a). FT-IR spectra of the sensor after EDC-NHS application verified the activation of the surface through the additional bond on the spectra, representing the ester chemical group. The ester bond belonged to the NHS complex and it is expected between $1500\text{--}1700\text{ cm}^{-1}$ as in our FT-IR spectra (at 1698.15 cm^{-1}) [92]. The Si-O stretch in 1000 cm^{-1} peak came from the fabricated capacitive sensor, as gold was patterned on silicon dioxide wafer (Figure 3-3b).

a)



b)

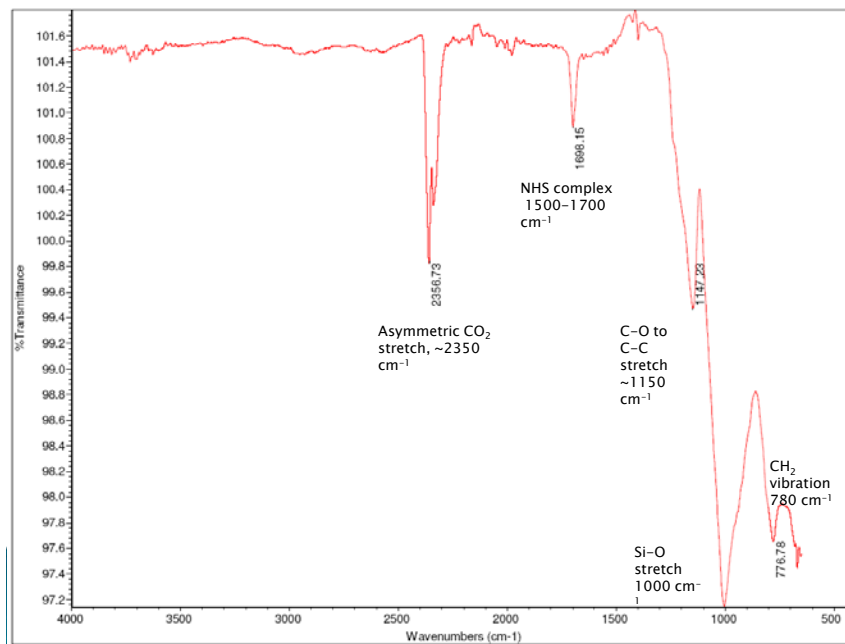


Figure 3-3 FT-IR spectra of SAM coated (a) and EDC-NHS activated (b) sensor surfaces.

Different concentrations of anti-hEGFR antibody were initially tested for immobilization and $50 \mu\text{g}\cdot\text{mL}^{-1}$ antibody concentration was determined as the optimum concentration for this study. Anti-hEGFR antibody ($50 \mu\text{g}\cdot\text{mL}^{-1}$ in a $2.5 \mu\text{L}$ volume) was immobilized on to each EDC-NHS activated capacitor sensor surface for 1 h and the non-reacted groups were blocked with ethanolamine, and later by BSA as a non-specific protein to prevent from any non-specific binding on the surface during the antigen detection steps.

3.1.2.2 Surface topology by atomic force microscopy (AFM) of the sensor surface

To confirm the antibody immobilization on the electrodes, the surface characterization was performed using tapping mode AFM [93]. The surface topographical AFM image of electrodes for blank and antibody immobilized surfaces were shown in Figure 3-4. AFM height image (Figure 3-4a and b) and the distance between the particles (Figure 3-4c and d) on blank and antibody immobilized surfaces were compared. When the distribution of the particles on the blank and immobilized surfaces were considered, the distance between two particles were determined to be $\sim 100 \text{ nm}$ and $\sim 175 \text{ nm}$, respectively. This difference could be attributed to the existence of different size molecules on the immobilized surface [71]. 3D-height map image of the blank and the immobilized surfaces showed varying heights within scanned $1 \times 1 \mu\text{m}^2$ electrode area. The surface roughness was measured as $345.9 \text{ nm}\cdot\mu\text{m}^{-1}$ and $486.0 \text{ nm}\cdot\mu\text{m}^{-1}$ for blank and antibody immobilized surfaces, respectively (Figure 3-4e and f). The increase on the surface roughness confirmed the immobilization of the antibody when compared to the blank surface [71].

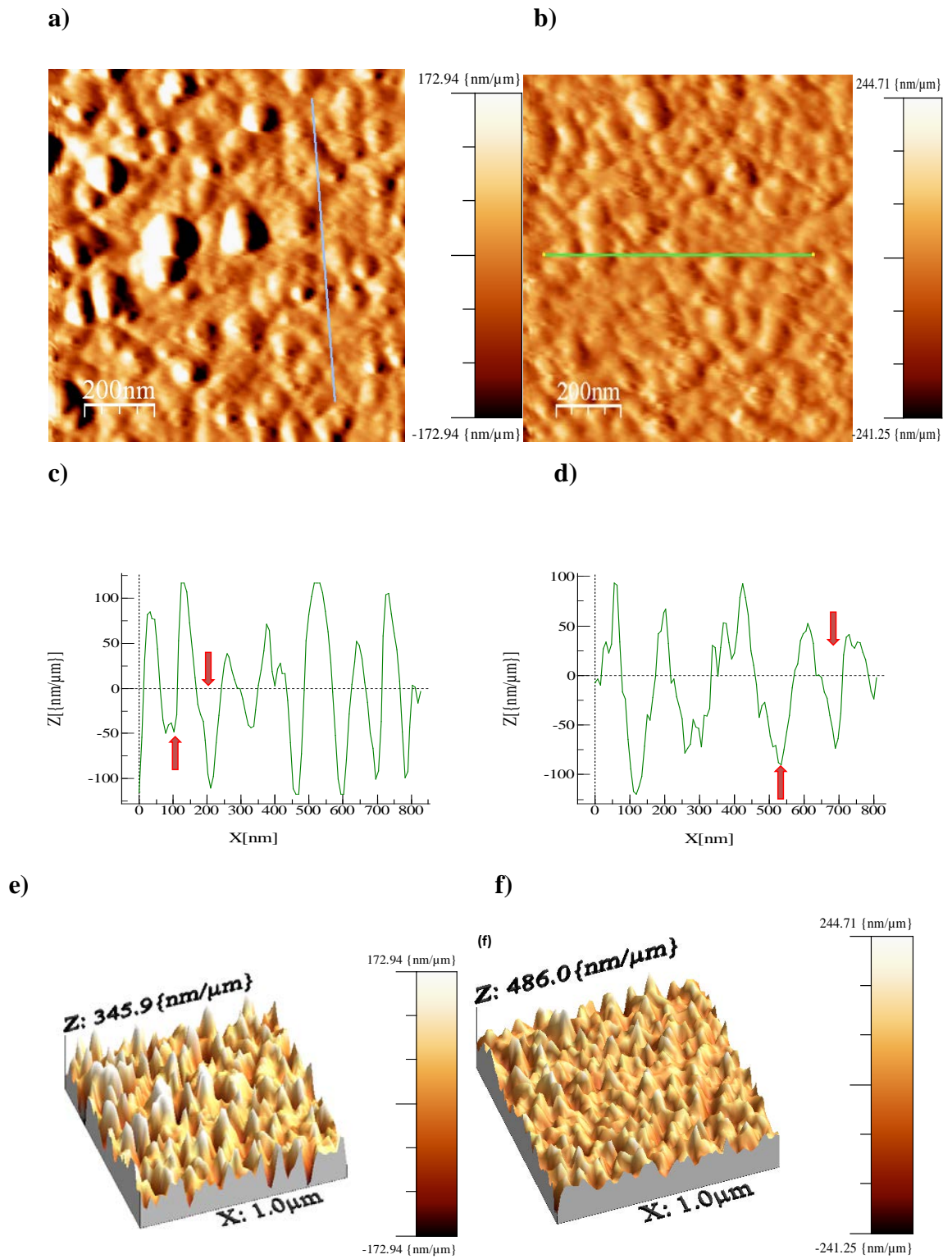


Figure 3-4 AFM analysis of blank and antibody immobilized surfaces. Height images (a, b), particle distribution on the surface (c, d) and surface roughness (e, f) of blank and antibody immobilized sensor platforms.

3.1.2.3 Determination of hEGFR using Network Analyzer

The sensor surfaces immobilized with anti-hEGFR antibodies were used for the determination of hEGFR antigens. For this, a Network Analyzer was employed to record the S11 parameters generated due to the immobilization of anti-hEGFR antibody on each GID capacitor. For the analysis, the capacitance was deduced from the S11 parameters. First, different concentrations of hEGFR antigen (0.5-256 ng.mL⁻¹) in a final 2.5 µl volume were incubated on each GID sensor surface in triplicates and bovine serum albumin (BSA, 50 ng.mL⁻¹) was used as a negative control. The specificity of the sensor to hEGFR was derived from the specific binding between the anti-hEGFR and hEGFR antigen as there was no binding with BSA non-specific protein. To observe the baseline response of the dilution buffer, 1 × HEPES buffer (no antigen) was also incubated on three GID electrodes as the blank control. The sensor platform was scanned in the frequency range of 50 MHz-1 GHz and inter-assay analysis was performed with three independent experiments. The deduced capacitance after antigen binding was subtracted from the values obtained for only antibody immobilization and the results were analysed as the normalized capacitance change (ΔC) according to the equation 3-8.

$$\text{Normalized } \Delta C = \frac{C_{\text{Antigen}} - C_{\text{Antibody}}}{C_{\text{Antibody}}} \quad \text{Equation 3-8}$$

A clear difference and the sensitivity in response to hEGFR antigen were evident under the applied frequency. The clear difference in sensor response with target antigen was probably dependent on the nature of protein and geometry of metal electrodes [94-95]. For the frequency range analysed, the antigen was clearly detected in the concentration range of 0.5-64 ng.mL⁻¹. Further, no response with BSA or with blank (1 × HEPES buffer) indicates the specificity of the bioassay (Figure 3-5). The logarithmic regression analysis with responses obtained at 800 MHz frequency was chosen that exhibited the dynamic detection range of 0.5-64 ng.mL⁻¹ with good correlation (R²=0.97) as shown in Figure 3-6. The saturation level of the immunoassay was achieved at 64 ng.mL⁻¹ hEGFR concentration.

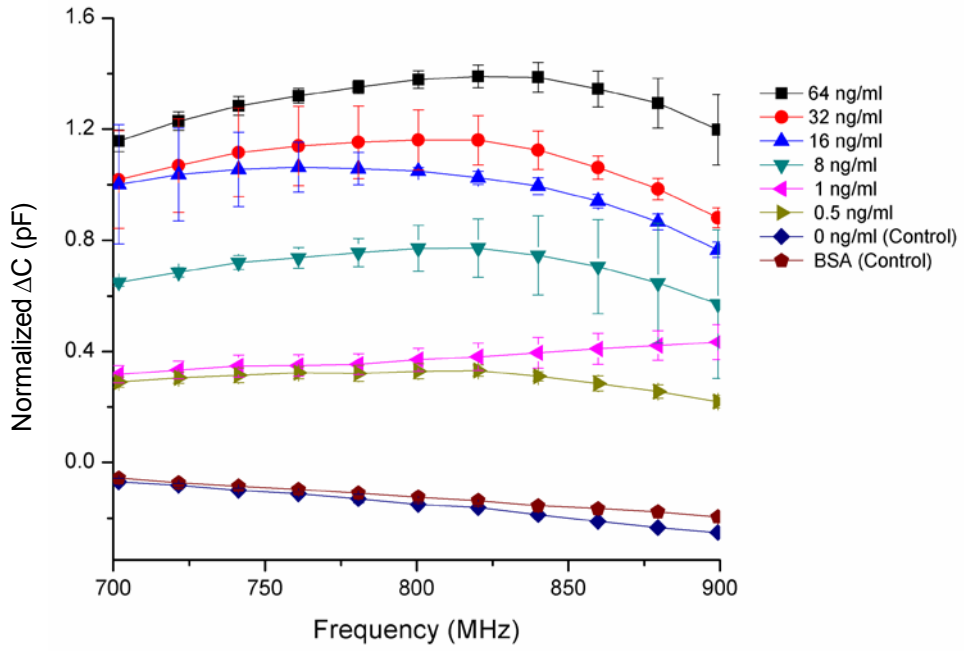


Figure 3-5 Changes in the capacitance depending on the different concentrations of hEGFR antigen in the frequency range of 700-850 MHz.

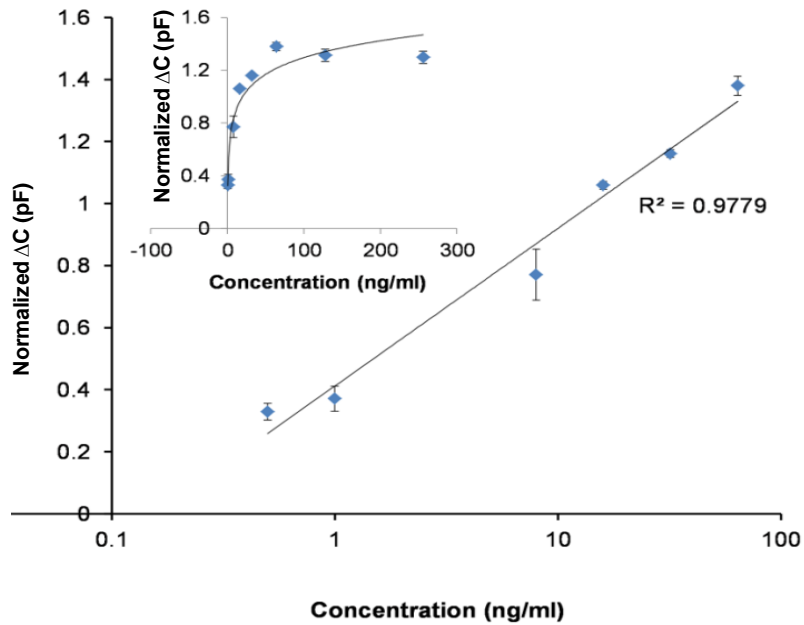


Figure 3-6 Logarithmic regression and correlation coefficient of the results obtained at 800 MHz frequency.

3.1.2.4 Kinetics of hEGFR binding on the sensor surface

The responses obtained at three different frequency points did not affect the capacitive signal significantly and a consistency was observed according to the concentrations tested in buffer conditions (Figure 3-7). The affinity of the anti-hEGFR antibody immobilized sensor surface against to hEGFR was calculated by assuming the Langmuir adsorption isotherm and the data fitted to non-linear regression analysis, and the dissociation constants (K_d) was determined [56, 96].

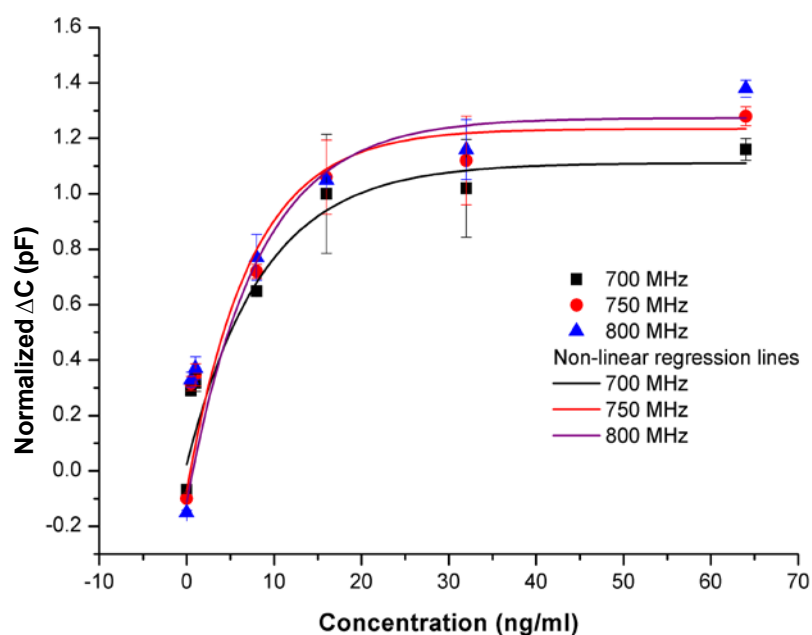


Figure 3-7 Kinetic analysis for the bioassay in dose and frequency dependent manner.

The K_d was calculated from the tested concentration range of 0.5-64 ng.mL⁻¹. The maximum responses at frequencies of 700, 750 and 800 MHz were calculated and the dissociation constants were found to be consistent to their capacitive signal with K_d values of 6.05, 5.6 and 5.7 ng.mL⁻¹, respectively (Table 3-1). These K_d values indicated the strong binding nanogram levels of hEGFR occurred in buffer, against a constant number of anti-hEGFR antibodies present on an area of 3×3 mm² with a defined geometry of sensor surface, under standard condition as described in experimental methods.

Table 3-1 Calculations of dissociation constants (K_d) and maximum responses (R_{max}) in the selected frequency points in the concentration range of 0.5-64 ng.mL⁻¹ antigen.

Frequency (MHz)	Max. response (R_{max}) (pF)	Dissociation constant (K_d) (ng mL ⁻¹)
700	1.139	6.05
750	1.272	5.65
800	1.354	5.69

3.1.2.5 Detection of hEGFR in real human serum samples

It was imperative to test the sensor platform for hEGFR detection in a complex real human serum to evaluate the potential applicability of the sensor assay for suspected serum samples. Therefore, different concentrations of hEGFR protein (0-10 ng.mL⁻¹) were spiked in real human serum. The sensor containing constant number of immobilized anti-hEGFR antibodies was incubated with serum containing different concentrations of hEGFR. The sensor showed sensitive capacitance responses to hEGFR with an extrapolated linear detection limit of 0.5-10 ng.mL⁻¹ in human serum (Figure 3-8). Normal serum samples without target marker spiked were used as the negative control. The capacitance response of the control showed only negligible background signal. This was probably because of washing the sensor surface with PBS buffer after incubating with serum, followed by blocking free and active functional groups and passivation by coating with BSA. Here, the sensor surface was normally dried before taking each capacitance measurement that may have also contributed to prevent large background signal. Therefore, we observed no interference of other serum molecules on the sensor surface, enabled measuring signal that was indeed coming from the binding of hEGFR on the sensor surface.

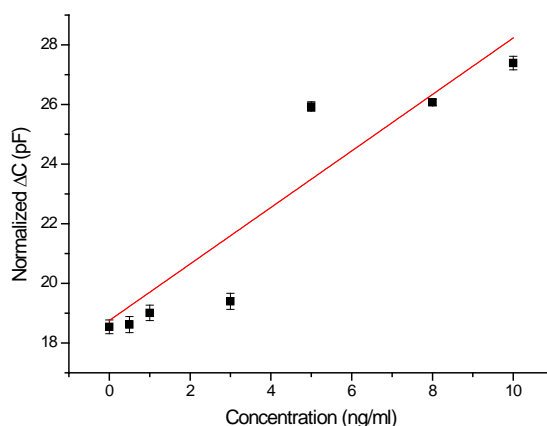


Figure 3-8 Test of hEGFR protein in real human serum in the concentration range of 0-10 ng.mL^{-1} .

The results demonstrated that use of GID capacitors has a great potential for early detection of the cancer and it is also a promising alternative platform where rapid detection, early diagnosis, lower cost are higher priorities. When compared with other sensor platforms (optical, piezoelectric, electrochemical sensors), the capacitive biosensor has provided a simpler instrumentation, possibility of miniaturization for point of care application, extreme sensitivity and less expensive that do not require qualified personnel to use the sensor. The miniaturization could provide usage of very little amount of sample and the nano-patterning of gold interdigitated fingers of capacitors would further increase the surface, and thus, increase the sensitivity of the recorded signal for biomarker detection.

Although the sensitivity of the sensor is good, it needs further improvement to detect the markers that have threshold levels at pg.mL^{-1} and extent the dynamic concentration range for the detection. With this aim, the capacitive sensor was developed using magnetic and gold particles with different methodologies for signal amplification (Chapter 4).

CHAPTER 4

4 DEVELOPMENT OF NANOPARTICLE-MODIFIED CAPACITIVE SENSOR PLATFORM

The SPR and QCM-based sensors were employed for the verification of the bioassays/surface chemistries and the methods were then transferred into an electrochemical-based capacitive sensing platform to enhance sensitivity while decrease the cost and the need for special qualification on the use of sensor. We initially tested this biosensor with standard methods and then we aimed to develop it using gold and magnetic particles for signal amplification. These nanoparticles were employed through performing different methodologies. In the section 4.1, Au-NP modified platform was described and the signal was increased via the enhancement of the surface for the binding of biological molecules. For this, the capacitive sensor platform was initially covered with a SAM layer and then modified with Au-NPs prior to the antibody immobilization. On the other hand, (section 4.2), magnetic beads were used for signal amplification at the end of the bioassays. For this, the appropriate magnetic bead amount and the frequency range for the marker quantification were determined. Magnetic beads were functionalized with a detector antibody using a specific method. The sensor was initially immobilized with surface antibody and then treated with target marker. The functionalized beads were injected to the sensor after antigen binding to improve the signal. This led to detect trace concentrations of the markers which could not be detected without using magnetic bead modification.

4.1 GOLD NANOPARTICLE MODIFIED SENSOR PLATFORM

Electrochemical biosensors created by coupling biological recognition elements with electrochemical transducers based on or modified with gold nanoparticles have played an increasingly important role in biosensor research over the last few years. The great promise of these bioelectroanalytical devices derive from the unique properties of gold nanoparticles [97-98]. Among them, their ability to provide a stable surface for the immobilization of biomolecules that retain their biological activities (probably due to enhanced orientational freedom) is extremely useful when preparing biosensors. Moreover, gold nanoparticles permit direct electron transfer between redox proteins and

bulk electrode materials, which allows electrochemical sensing to be performed without the need for electron-transfer mediators. Various characteristics of gold nanoparticles, such as their high surface-to-volume ratio, their high surface energy, their ability to decrease the distance between proteins and metal particles, and their ability to act as an electron-conducting pathway between prosthetic groups and the electrode surface, may facilitate electron transfer between redox proteins and the electrode surface [98].

Gold nanoparticle-modified electrode surfaces can be prepared in three ways: (a) by binding gold nanoparticles with functional groups of self-assembled monolayers (SAMs); (b) by direct deposition of nanoparticles onto the bulk electrode surface; (c) by incorporating colloidal gold into the electrode by mixing the gold with the other components in the composite electrode matrix. Biosensors can then be constructed by immobilizing the biomolecules by adsorbing them onto the nanoparticles, by cross-linking them with bifunctional agents such as glutaraldehyde, or by mixing them with the other components of composite electrodes [99]. In this work, the interdigitated capacitive transducer was modified with Au-NPs after SAM formation for signal amplification to detect trace amount of cancer biomarkers (Figure 4-1). This method allowed us to prevent from negative background signal that plays crucial role especially for the detection of serum or real patient samples. Thus, too small or low level of biomarker can be specifically detected in human body fluids without time-consuming, high-cost methodology.

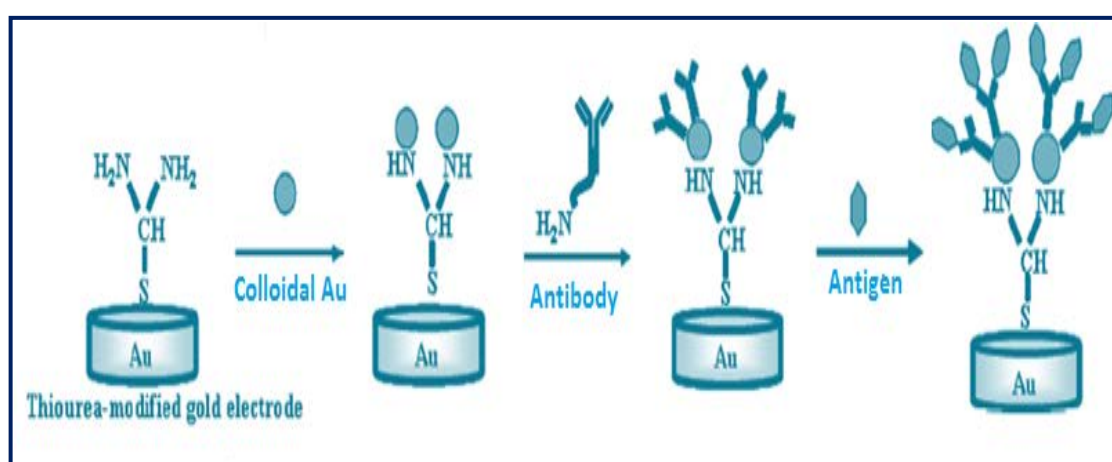


Figure 4-1 The principle of the bioassay on Au-NP modified capacitive sensing platform.

4.1.1 Materials and Methods

Phosphate buffered saline (PBS) and 2X HEPES buffer were purchased from PAN BIOTECH GmbH and Fluka, respectively. Ethanolamine (99%), bovine serum albumin (BSA), mouse monoclonal antibody to human IL-6, human IL-6 antigen, thiourea, N-(3-dimethylaminopropyl)-N-ethylcarbodiimide hydrochloride (EDC) and N-hydroxysuccinimide (N-hydroxy-2,5-pyrrolidinedione, NHS), sheep monoclonal antibody to human epidermal growth factor receptor (anti-hEGFR) and human epidermal growth factor receptor (hEGFR) were purchased from Sigma Aldrich (USA). CEA and CA15-3 antigens and their monoclonal antibodies were bought from Fitzgerald (USA). Gold nanoparticles were purchased from NanoComposix (San Diego, CA). Doubly distilled water was used throughout the experiments.

4.1.1.1 Preparation of Au-NP modified sensor platform

Gold interdigitated electrodes were fabricated and cleaned prior to do any application as described in section 3.1.1.2. The fabricated sensor chip was washed several times with ethanol and rinsed with sterile dH₂O. The cleaned surface was dried by nitrogen gun. The blank measurements were taken by Network Analyzer prior to any surface/bio-chemical treatment/application on the surface. The sensor surface was then coated with self-assembled monolayer (SAM) by immersing the sensor in 10 mM solution of thiourea which has two amine group during overnight incubation followed by rinsing with ethanol and Milli-Q water and then dried using nitrogen gas. The formation of SAM layer on the surface was confirmed by FT-IR. Au-NPs that have 5-nm size was prepared using the buffer solution in 27 $\mu\text{g}\cdot\text{mL}^{-1}$ concentration [100]. Au-NPs were then applied onto the GID electrodes for 8 hours to enhance the immobilization surface of the antibodies. The sensor platform was then washed with PBS and dH₂O. The capacitive response of Au-NP application was measured employing a Network Analyzer. To confirm the modification of the platform using Au-NPs; the surface topology, roughness and the distribution of the particles on Au-NP modified surface was tested through an Atomic Force Microscope (AFM, Nanoscope) and compared with non-modified surface.

4.1.1.2 Antibody immobilization

The Au-NP modified GID electrode surfaces of capacitors were immobilized by incubating 2.5 μL of 25 $\mu\text{g}\cdot\text{mL}^{-1}$ IL-6 antibody in PBS buffer for 1 h. The sensor wafer

was then washed with PBS and dried prior to the blocking step with ethanolamine. The non-reacted groups on the sensor surface were blocked by adding 5 μL of 100 mM ethanolamine on each GID electrode and incubated for 1 h. The sensor was then rinsed with PBS and sterile dH_2O , and dried with nitrogen gun prior to the measurements for antibody immobilization using a Network Analyzer. The analyzer was calibrated and triplicate measurements were then taken for each GID electrode for error analysis.

4.1.1.3 Protein detection

A series of IL-6 concentrations ($0.02\text{-}10\text{ ng}\cdot\text{mL}^{-1}$) were prepared in 1X PBS buffer and the same buffer was used as a blank control. Each concentration of the biomarker was tested on three independent GID capacitors for error analysis. The IL-6 samples prepared in the buffer were incubated for 1 h for the antigen detection step and the sensor was then carefully rinsed with PBS followed by dH_2O to remove traces of salts on the sensor surface. The sensor was quickly dried with nitrogen gas and each GID capacitor was measured for the detection of IL-6 marker. The specificity of the interaction between the target antibody (anti-IL6) and antigen (IL-6) was checked by applying $10\text{ ng}\cdot\text{mL}^{-1}$ of non-specific BSA protein on the anti-IL6 immobilized (GID) electrodes instead of the target protein marker. The average values of the change in capacitance were plotted and the standard deviations of the triplicate experiments were shown as error bars.

4.1.2 Results and Discussions

4.1.2.1 FT-IR and AFM analysis

The fabricated sensor platform was subjected to SAM formation with thiourea. Since thiourea was used for the first time by our research group, self assembled monolayer of thiourea was tested using FT-IR. The sensor surface was scanned and the recorded FT-IR spectra were compared with the reference spectra [90] and all spectra were collected with 64 scans for the reference and the sample, with 4 cm^{-1} resolution in the reflection mode. FT-IR spectrum of SAM coated surface indicated the formation of a thiourea layer on the gold surface by the disappearance of the S-H stretch at 2551.5 cm^{-1} , as well as the existence of NH vibration (at 779 cm^{-1}) and CH stretch (at 1150 cm^{-1}) [91]. The Si-O stretch in 1000 cm^{-1} peak came from the fabricated capacitive sensor, as gold was patterned on silicon dioxide wafer (Figure 4-2).

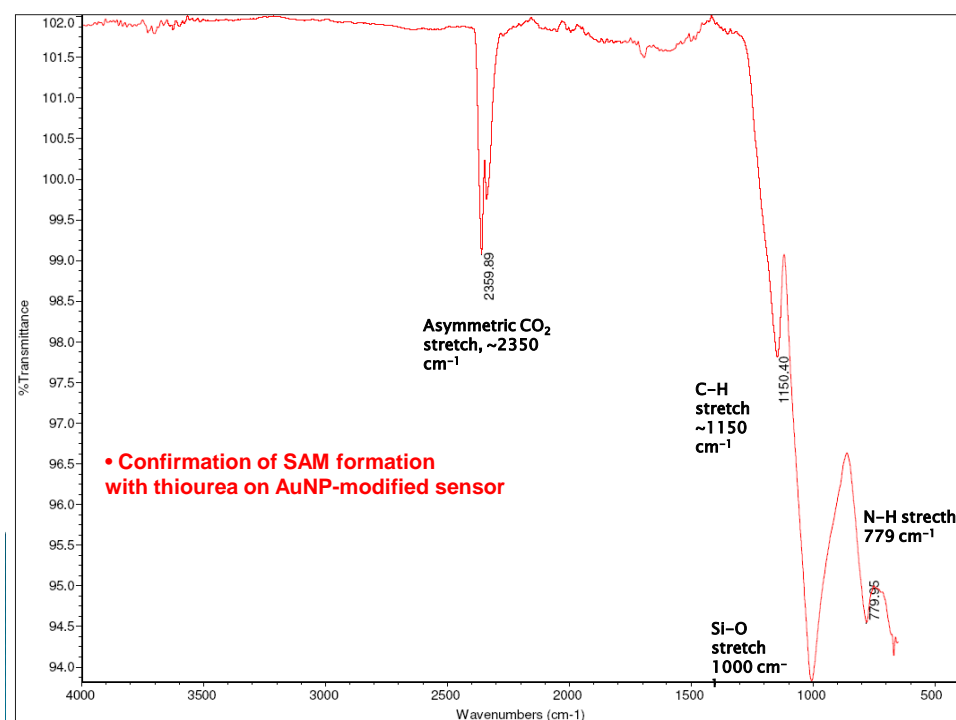


Figure 4-2 Confirmation of SAM formation with thiourea employing FT-IR prior to Au-NP modification.

To verify the modification of the capacitive transducer with Au-NPs, AFM was employed and height images, particle distribution on the surface were compared for Au-NP modified and non-modified sensor platforms. Attachment of Au-NPs on the surface verified the modification as seen in Figure 4-3. Surface roughness was observed as $509.61 \text{ nm} \cdot \mu\text{m}^{-1}$ for Au-NP modified sensor while it was recorded as $244 \text{ nm} \cdot \mu\text{m}^{-1}$ for non-modified sensor surface (Figure 4-3a and b). When the distribution of the particles on the Au-NP modified and non-modified sensor surfaces were considered, the distance between two particles were determined to be $\sim 50 \text{ nm}$ and $\sim 150 \text{ nm}$, respectively. This difference was attributed to the existence of Au-NPs on the surfaces that increase the surface and capture more biological molecule when compared with non-modified surface (Figure 4-3c and d). This may be due to their ability to provide a stable surface for the immobilization of biomolecules that retain their biological activities (probably due to enhanced orientational freedom) is extremely useful when preparing biosensors. Moreover, various characteristics of gold nanoparticles, such as their high surface-to-volume ratio, their high surface energy, their ability to decrease the distance between proteins and metal particles, and their ability to act as an electron-conducting pathway

between prosthetic groups and the electrode surface, may facilitate the binding of more antibody [101].

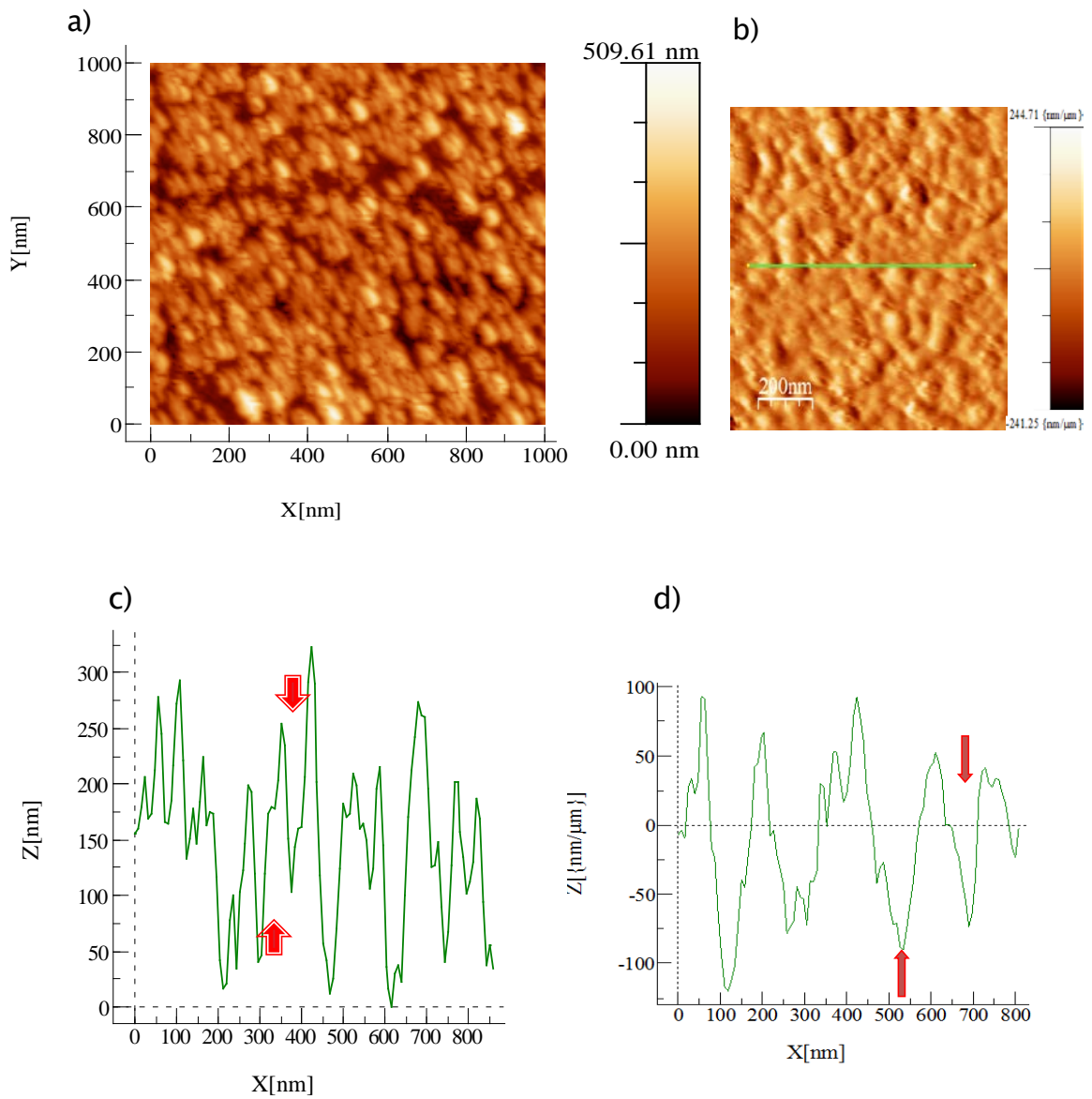


Figure 4-3 Confirmation of Au-NP modification on the sensor using AFM tool. Surface roughness of Au-NP modified (a) and non-modified (b) sensor platforms. Particle distribution on the Au-NP modified (c) and non-modified (d) sensor surfaces. (Red arrows show the distance between two particles).

4.1.2.2 Determination of IL-6 antigen

A Network Analyzer was employed to record the S11 parameters generated due to the SAM formation, Au-NP application and the detection of IL-6 antigen using IL-6 antibody on each GID capacitor. For the analysis, the capacitance was deduced from the S11

parameters. Capacitive response of SAM formation and Au-NP application were initially measured by Network Analyzer and validated for 5 separate electrodes. To prevent from a background capacitance prior to the antigen detection, it was expected that Au-NPs would not increase the capacitance. The comparison of the capacitive responses of SAM and Au-NP applications shows that Au-NP changed the dielectric permittivity and charge distribution of the medium and leads to a little decrease on capacitance prior to the antibody immobilization (Figure 4-4). The difference between capacitive response of SAM and Au-NP according to the IDTs was observed ~ 0.06 pF.

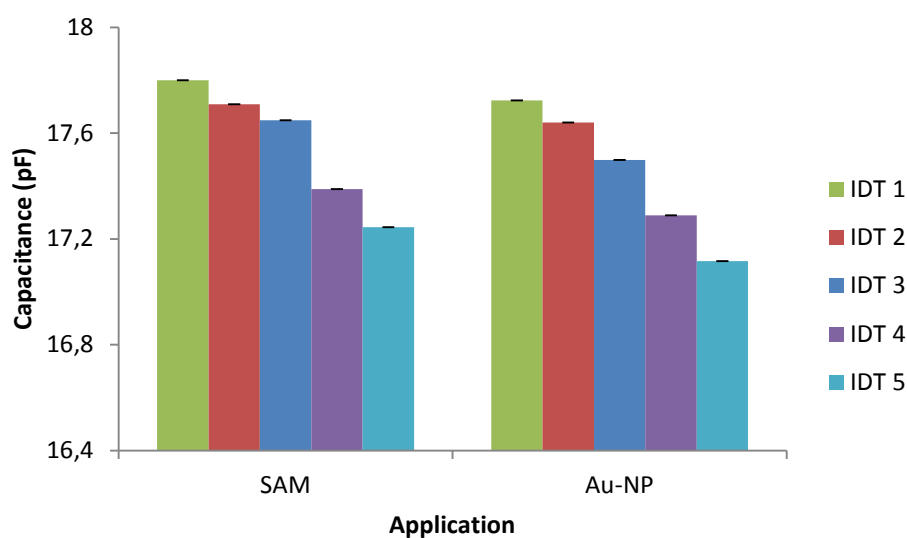


Figure 4-4 Capacitive responses of SAM-coated and Au-NP modified sensor surfaces for 5 electrode.

After Au-NP modification, $25 \mu\text{g.mL}^{-1}$ was immobilized to the sensor surface for the detection of IL-6 antigen. Different concentrations of IL-6 antigen (0.02 - 10 ng.mL^{-1}) in a final $2.5 \mu\text{l}$ volume were incubated on each GID sensor surface in triplicates and PBS buffer was used as a negative control. The optimal antibody concentration for the immobilization changes between 20 - $50 \mu\text{g.mL}^{-1}$ in different biosensor types. The various concentrations between this range for antibody immobilization were tested throughout the PhD thesis using SPR, QCM and capacitive sensor platforms. A preliminary test was also performed prior to this study and a $25 \mu\text{g.mL}^{-1}$ antibody concentration was chosen. The investigated antigen concentration was selected between 0.02 ng.mL^{-1} and 10 ng.mL^{-1} since we could detect 0.1 - 10 ng.mL^{-1} concentration of IL-6 using standard assay methodology in our previous works. The Au-NP modified sensor platform was initially

tested using IL-6 in the selected concentration range and the sensitivity level was then increased with lower concentrations according to the results obtained here.

The specificity of the sensor to IL-6 was derived from the specific binding between the anti-IL6 and IL-6 antigen as there was no binding with BSA non-specific protein. The sensor platform was scanned in the frequency range of 50 MHz-1 GHz and inter-assay analysis was performed with three independent experiments. The deduced capacitance after antigen binding was subtracted from the values obtained for only antibody immobilization and the results were analysed as the normalized capacitance change (ΔC). The normalized capacitance was calculated according to the equation 3.8. A clear difference and the sensitivity in response to IL-6 antigen were evident under the applied frequency. For the frequency range analysed, the antigen was clearly detected in the concentration range of 0.02-10 ng.mL⁻¹(Figure 4-5).

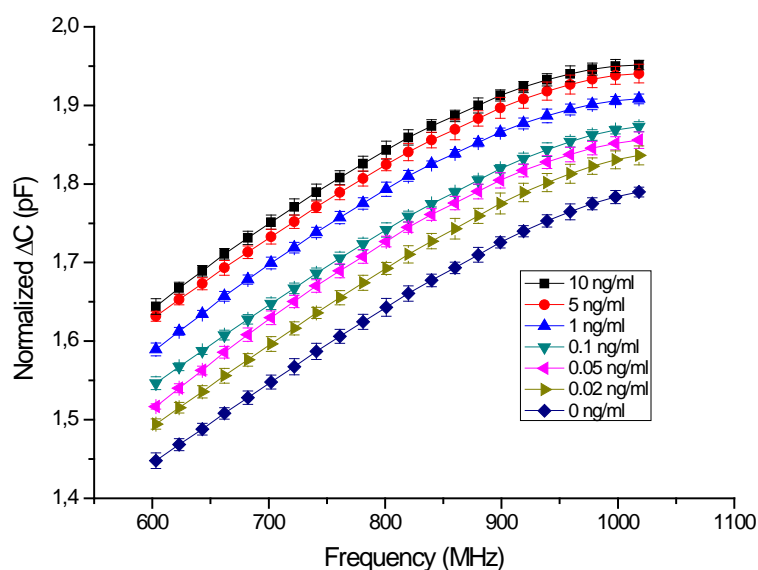


Figure 4-5 Capacitive detection of IL-6 marker with standard errors in the frequency range of 600-1000 MHz.

To determine the optimal frequency range of bioassay with Au-NPs, 6 frequency points between 600-1000 MHz were selected and validated and the capacitive response showed saturation after 800 MHz frequency point as seen in Figure 4-6. It was observed that

frequency range was fitted with our normal range for biological assays in the platform since the best results were usually obtained between the range of 600-850 MHz.

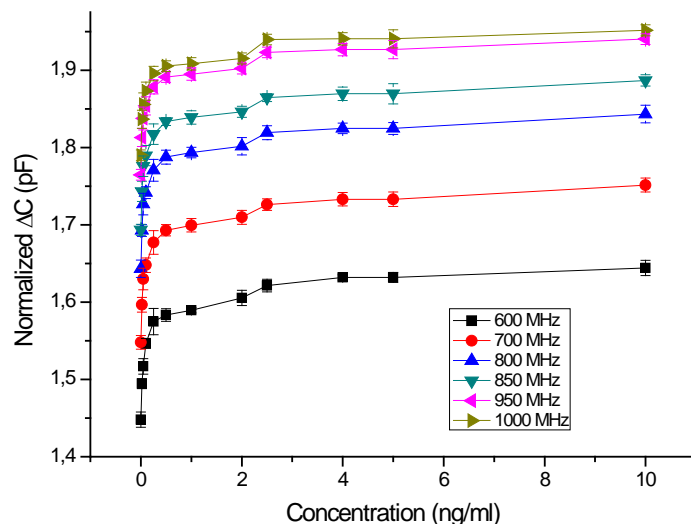


Figure 4-6 All investigated concentration range of IL-6 at selected 6 frequency points to determine the optimal frequency range for the bioassay.

Further, a constant frequency was chosen and the logarithmic regression analysis was performed in the dynamic detection range of 0.02-10 ng.mL⁻¹ with good correlation ($R^2=0.98$) as shown in Figure 4-7. Kinetic data analysis was also performed in the selected frequency points to determine the binding affinity between target antibody-antigen pair on the Au-NP modified sensor platform. Table 4-1 shows the dissociation constants (K_d) at particular frequencies with standard deviations.

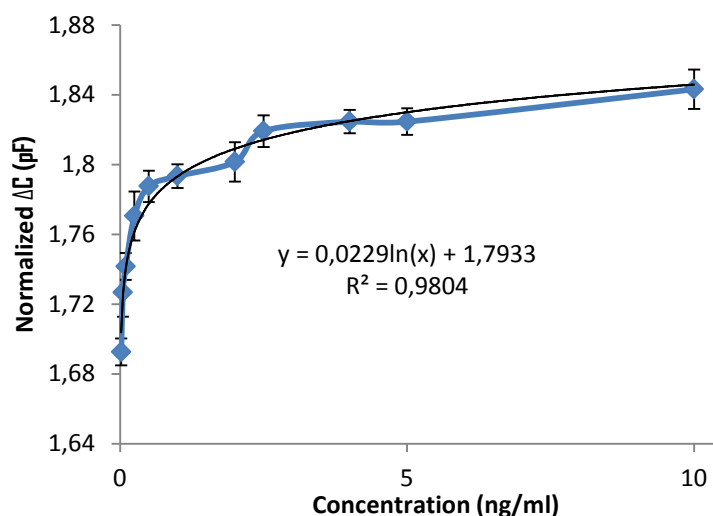


Figure 4-7 Logarithmic regression analysis for the bioassay at a constant frequency point (800 MHz).

Table 4-1 Kinetic data analysis at selected frequency points to determine the affinity between the target antigen-antibody pair (IL-6-anti-IL-6).

Frequency (MHz)	Dissociation constant (K_d)(ng. mL ⁻¹)	Std error
800	1.60	± 0.2
850	1.59	± 0.1
900	1.50	± 0.4
950	1.58	± 0.3
1000	1.59	± 0.1

We previously investigated IL-6 marker using standard assay methodology in the concentration range of 0.1-10 ng.mL⁻¹ and the obtained signal was much lower than the Au-NP modified sensor surfaces. The 10 ng.mL⁻¹ concentration of IL-6 gave ~0.35 pF and ~2 pF response with standard and modified sensor platforms, respectively. Moreover, 0.02 ng.mL⁻¹ ml IL-6 could be detected through Au-NP modified capacitors with 1.85 pF capacitance change whereas the detection limit of the standard assay for IL-6 was 0.1 ng.mL⁻¹. The detailed comparison can be shown in Table 4-2.

Table 4-2 Comparison of IL-6 detection for standard and Au-NP modified capacitive sensor platforms.

	Standard assay	Au-NP modification
Concentration range	0.1-10 ng.mL ⁻¹	0.02-10 ng.mL ⁻¹
R _{max} for 10 ng.mL ⁻¹ IL-6	0.35 pF	2 pF
R _{max} for lowest IL-6 concentrations	0.33 pF	1.85 pF
Detection limit	0.1 ng.mL ⁻¹	0.02 ng.mL ⁻¹
Signal increase	1 fold	~6 fold

The difference between the results of Au-NP modified and standard assays may be due to (a) ability of Au-NPs to provide a more stable surface for antibody immobilization that retain their biological activities, (b) capture of more antigen due to more antibody on

Au-NPs (c) enhancement of orientational freedom for antigen binding on Au-NP modified sensor, (d) high surface to volume ratio and surface energy of Au-NPs, (e) ability of Au-NPs to decrease the distance between proteins and metal particles [101].

4.2 DEVELOPMENT OF MAGNETIC BEAD MODIFIED CAPACITIVE SENSOR PLATFORM

In the previous section, Au-NP modified platform was described and the signal was increased via the enhancement of the surface for the binding of biological molecules. For this, the capacitive sensor platform was initially covered with a SAM layer and then modified with Au-NPs prior to the antibody immobilisation. Here, as an alternative approach, magnetic particles were used for signal amplification with different methodology. The beads were functionalized and injected to the sensor after antigen binding to improve the signal for the detection of trace marker concentrations which could not be detected without using magnetic bead modification.

Magnetic beads used in biomedical applications present usually a core/shell structure such as iron oxide, surrounded by an outer layer of shell wall that consists of long-chain organic ligands or inorganic/organic polymers [102]. The attachment of bioactive ligands to the surface of the outer shell is the crucial point in bioapplications of magnetic beads. The main immobilization procedures of bioactive species using magnetic microbeads are summarized in Table 4-3. Magnetic microbeads can be used in three biosensing systems include affinity biosensors, enzymatic biosensors and bio-bar codes [103].

Capacitive immunosensors are designed through the immobilization of the specific antibody on the surface of the electrochemical transducer. The main problem affecting immunosensors is reproducible regeneration of the sensing surface. The need of renewal of the sensing surface arises from the affinity constants derived from the strong antigen-antibody interaction. This renewal is a difficult task since the drastic procedures required alter immunoreagent bound to the surface of the transducer. This drawback makes immunosensors difficult to be integrated into automatic systems. An alternative approach avoiding regeneration consists of using disposable antibody-coated magnetic microbeads and building up *in situ* immunosensing surface by localizing the immunomagnetic beads on the electrode area with the aid of a magnet. Moreover, the use of immunomagnetic

beads is particularly evident in the detection of analytes contained in complex sample matrices that may exhibit either poor mass transport to immunosensor or physical blockage of immunosensor surface by non-specific adsorption.

The immunomagnetic bead is pinched magnetically on the electrode surface, exposed to the enzymatic substrate and the electroactive product is detected electrochemically. This type of immunomagnetic electrochemical assay was applied for different analytes with different transducer/enzyme combinations as seen in Table 4-3.

Table 4-3 Immunomagnetic electrochemical assays using different transducers and enzymatic labels.

Analyte	Transducer	Enzyme	Detection Limit	Dynamic range	Reference
Rabbit IgG	pH-ISFET	urease	8nM	0 – 2.07 μ M	[104]
Rabbit IgG	Graphite composite electrode	HR Peroxidase	9x10 ⁻⁶ μ g.l ⁻¹	0 – 0.26 μ M	[105]
<i>E. coli</i> 0157:H7	Graphite ink electrode	Alkaline Phosphatase	4.7x10 ³ cells.ml ⁻¹	0 – 10 ⁵ cells.ml ⁻¹	[106]
2,4-D herbicide	Nafion-SPE	Alkaline phosphatase	0.01 μ g.l ⁻¹	0.01 - 100 μ g.l ⁻¹	[103]
Human IgG	Carbon paste electrode	HR Peroxidase	0.18 μ g.ml ⁻¹	0.51 – 30.17 μ g.ml ⁻¹	[107]

The magnetic beads aim at interacting with the target molecule through biological recognition, namely DNA/DNA complementary sequence (hybridization) or antigene/antibody interaction. It gives to the sandwich structure magnetic properties allowing its separation from unreacted material and medium. Immobilisation of the monoclonal antibody is achieved by reaction of glutaraldehyde with the primary amine at the surface of the particle and with free amine of the antibody. In the case of oligonucleotide target complement, the particle is modified with surface maleimido groups using succinimidyl 4-(p-maleimidophenyl) butyrate (SMPB) or sulfosuccinimidyl 4-N-maleimidomethyl cyclohexane-1-carboxylate (sulfo-SMCC) [108]. The oligonucleotide is then immobilised through thiol addition to the double bound of the

maleimido group. The average number of DNA strand per particles is 3×10^5 . In the case of antibody immobilisation, the average number of immobilised molecules is 3500 (small) per MMB as estimated by optical density at 280 nm. Capping is accomplished with BSA or sulfo-NHS acetate [103]. Helali et al. developed an disposable immunomagnetic electrochemical sensor involving magnetic particles and employed the sensor for the detection of atrazine. The developed sensor was based on a magnetic monolayer of magnetic particles coated with streptavidin, formed on a gold electrode after application of a magnetic field. The experimental procedure was shown in Figure 4-8. The atrazine could be sensitively detected in the range of $10\text{-}600 \text{ ng}\cdot\text{mL}^{-1}$ and this study shows the promising usage of magnetic beads through impedimetric/capacitive sensors in biomedical applications with the aim of detection [109].

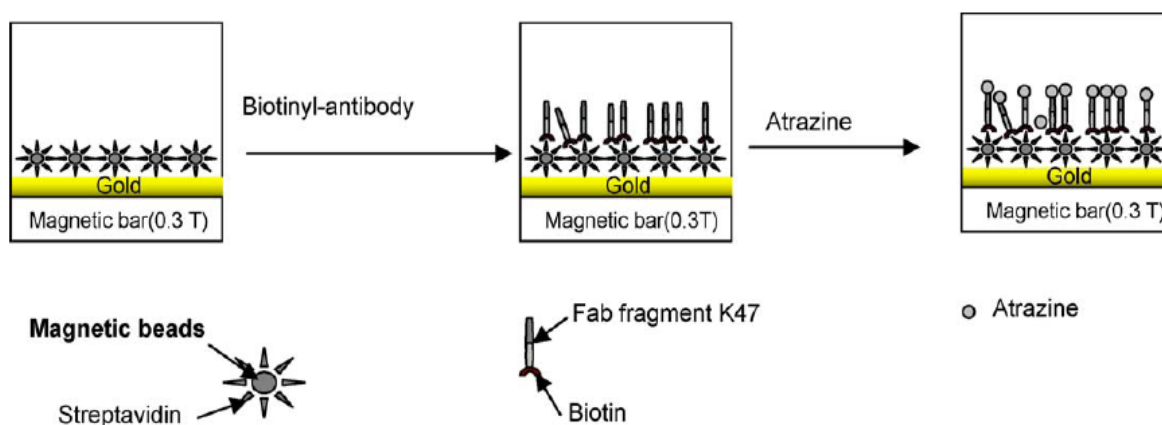


Figure 4-8 Experimental steps of atrazine detection using immunomagnetic electrochemical sensor.

4.2.1 Behaviour of magnetic beads on the platform

A stable dispersion of magnetic particles in a liquid medium plays critical role for the applications. Due to this, the characteristics of the particle surface have to be compatible with the medium used and the interaction between the particle and solvent must be strong to overcome Van der Waals attraction in the case of permanent magnetic moment of the particles. The behavior of the magnetic particles suspended in a fluid and the magnetic moment can be described with two different mechanisms. The first mechanism involves the bulk rotation of the particle within the fluid due to Brownian motion. This mechanism is usually used when the magnetic moments of the particles are fixed relative to the

crystal axes of the particles and the Brownian rotational diffusion time is defined by the equation 4-2.

$$\tau_B = \frac{4\pi\eta r^3}{kT} \quad (\text{Equation 4-1}) \quad [110]$$

Where r is the hydrodynamic radius of the particle, η is the dynamic viscosity of the fluid, k is Boltzmann's constant and T is the absolute temperature. When a particle is unblocked, the magnetic moment vector rotates, but the particle remains stationary. The response of the magnetisation of a magnetic bead solution that includes spherical particles to an alternating magnetic field can be modelled by Debye theory to explain the dielectric dispersion in dipolar fluids. The fluid magnetisation is related to the applied magnetic field due to the finite magnetisation change with time. In a small applied field, the magnetisation is a linear function of the field; therefore, the magnetisation response to an alternating field can be defined depending on the complex magnetic susceptibility.

When biological macromolecules bind to the particles, the hydrodynamic radius of it increases and this increase leads to decrease in the frequency. The higher the increase in the hydrodynamic radius, the higher will be the frequency shift [110]. Due to the big hydrodynamic radius of our magnetic beads, a frequency shift was expected when compared with our normal frequency range for standard bioassays and the obtained results of magnetic bead investigations supported all of these hypothesis.

As a part of PhD thesis, magnetic beads have been used to develop capacitive sensor platform to obtain more stable and sensitive surface with higher specificity for bioassays as an alternative to Au-NP modified sensor. The purchased MBs have an iron core with three positive charge and capsulated with glycodyle ether that has hydrophilic nature. The coat seals the iron oxide inside the beads, and the surface is activated with primary amino functionality on a short hydrophilic linkers. The MBs have neutral net charge due to the hydrophilic coat; however, the charge distribution on the sensor are changed due to the positive charge of the iron core since the positively charge layer of the bead induce the negative charge on the sensor layer due to the electric field. More charge increases the electric field and polarization, thus, the measured capacitance will increase. This can be theoretically explained with the equation 4-3 where the increase dipole moment (m) leads to decrease in impedance (Z); moreover, the capacitance (C) shows an increase in this case due to the reverse relationship between Z and C .

$$Z(\omega) = Z(o)\left\{1 - m \left[1 - \frac{1}{1+(j\omega\tau)}\right]\right\} \text{ Equation 4-2}$$

Charge distribution is the most crucial issue in capacitive sensor platform and it may be affected by electrical permittivity of the medium, nature of the biological molecule, dipole-dipole interaction between molecules, pH and the temperature of the used media in the assays. Since the charge distribution plays a direct role on capacitor, the sensor surface must be uniform and the clustering of the particles must be counteracted. The clustered particles may lead to short-circuiting; therefore, decrease in capacitance and/or collapsing of the capacitors on the sensor platform. When all of these issues are considered, it is clear that the concentration, manipulation, application type of MBs are very important in our research. For an instance, high concentration of MBs cause the clustering and short-circuiting or specific usage of the MBs is critical in bioassays. Bare-MBs were previously investigated on our IDE-based capacitive sensor to determine the effect of MBs on capacitance and the appropriate concentration of the MBs without observing any clustered particles on the surface.

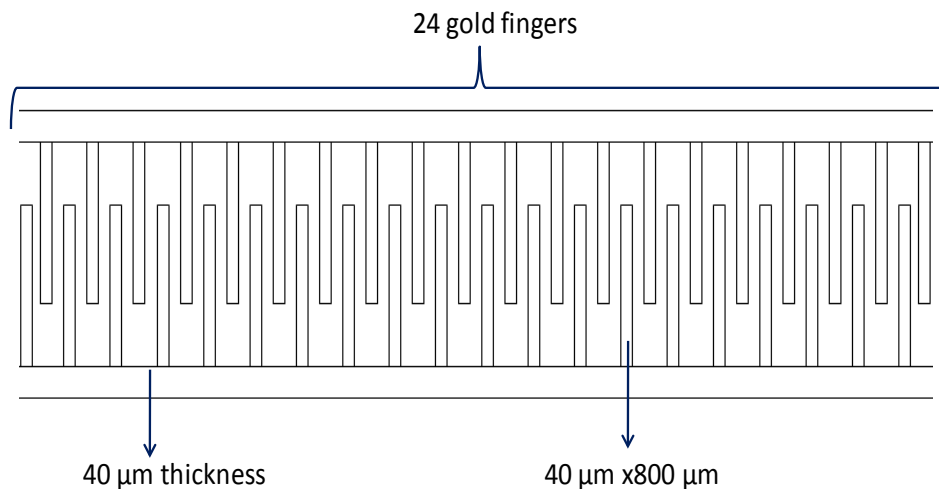


Figure 4-9 Schematic representation of gold interdigitated fingers of an IDE.

The sensor surface was calculated using the dimension of the gold area on the sensor (Figure 4-9). Total gold area was calculated as 918.400 μm and this result was divided to one magnetic bead area (a MB has 2.8 μm radius) to find the number of needed MB to coat all surface. It was found that 125.000 MBs were necessary to coat all surface (100% coverage) and the MB concentrations were prepared as a serie. Prior to the preparation of MB concentrations, 25% and 50% MB were examined on two IDE electrodes and the

surfaces were checked under the microscope to observe whether clusters occur or not. It was found that 50% MB caused an apparent agglomeration; therefore maximum concentration of MBs for preliminary testing was chosen as 25%. The tested concentrations were 25%, 20%, 17%, 12%, 10%, 6%, 5%, 3% and 0% (only PBS buffer that used for the dilution of MBs). The data analysis showed that higher concentration of MBs leads to decrease in capacitance and the evaluated capacitance was lower than the negative control except for 3% and 5%. The tested MB concentrations were measured by Network analyzer in the frequency range of 50 MHz-4 GHz as seen in Figure 4-10a. It was observed that capacitive response coming from MB application has shown a stabilisation after 1000 MHz and a clear response obtained between 500-1000 MHz (Figure 4-10b).

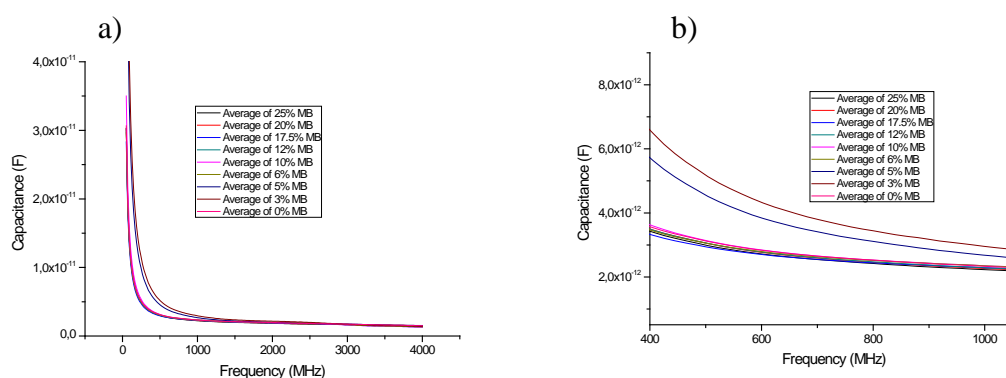


Figure 4-10 Bare-MB measurements according to the tested concentrations of MBs by Network Analyzer in a wide (50MHz-4 GHz) and zoomed (600-1000 MHz) frequency ranges.

Moreover, when the incubation time was extended, a weak agglomeration was also observed on IDE electrodes coated with 20% and 25% MBs. These findings indicate that the appropriate concentration of MBs for our sensor platform should be 5% or lower to obtain a uniform and stable surface without any problem on charge distribution, thus on capacitance. After obtaining these results from bare-MB study, 1% MB concentration was chosen to use in bioassays and this MB concentration was also tested on SAM coated sensor surface without any modification (no biological molecule or coating with secondary antibody). 1% MB was measured in the same frequency range with bare-MB study and similar results were recorded. It was shown that MB usage led to a shift in frequency up to 1000 MHz while our normal range for biological assays without particles

is between 600-900 MHz. Moreover, 1% MB concentration gave the higher capacitance change when compared with 3% MB tested in previous experiments and this was the expected output since the decrease concentration of MB leads to the increase in the capacitance. 3% and 1% MBs produced ~ 3 pF and ~ 3.5 pF capacitance, respectively. Figure 4-11 shows the result of 1% MB application on the SAM coated sensor surface and in a broad and zoomed frequency range. The capacitive response of 1% MB on SAM layer was scanned in the frequency range of 50 MHz- 4 GHz and a stabilization on the capacitance was observed at 1 GHz frequency point as in Figure 4-10. The results indicated that there is no change on the response after 1 GHz while working with magnetic beads. Due to this, the frequency range was determined up to 1 GHz for the assays.

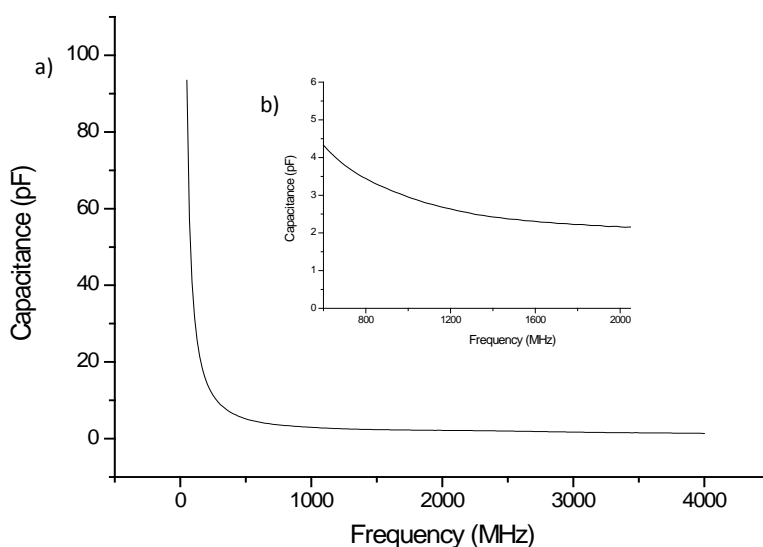


Figure 4-11 Capacitance measurements of 1% MB on SAM-coated sensor surface in a broad (a) and particular frequency ranges (b).

After the optimization of frequency range for MB application and the determination of MBs behavior on the capacitive sensor platform, real bioassays were conducted using CRP antibody-antigen pair in the frequency range of 50 MHz-1 GHz since this marker was previously investigated and successfully detected using standard assay approach through capacitive sensor platform in our research group. After the testing of the MB-modified sensor with CRP, the methodology was transferred into lung cancer biomarkers

for the detection. This section will continue with methodology of MB-modified platform in bioassays.

4.2.2 Methodology

4.2.2.1 The protocol of the applied bioassay using magnetic beads:

- 1) Self assembled monolayer was formed on the capacitive sensor surface using 10 mM thiourea prepared in analytical grade ethanol. Overnight incubation was applied under dark conditions at ambient temperature.
- 2) The sensor surface was activated with the mixture of EDC and NHS in 1:1 volume ratio using 0.1 M EDC and 0.05 M NHS during 3 hours incubation.
- 3) 25 $\mu\text{g.mL}^{-1}$ antibody was immobilized to the activated sensor surface for the antibody immobilization and the wafer was incubated for 2 hours.
- 4) To cap the antibody-free areas of the sensor surface, ethanolamine was applied to the sensor for 1 hour.
- 5) Different concentrations (10-500 pg.mL^{-1}) of CRP protein were prepared within PBS buffer and antigen was injected to the sensor for 2 hour incubation.
- 6) Sandwich assay was applied using secondary antibody immobilized-magnetic beads.

4.2.2.2 Preparation of secondary antibody immobilized-magnetic beads

Dynabeads M-270 Epoxy are uniform beads composed of crosslinked polystyrene with magnetic material precipitated in pores evenly distributed throughout the particles. The beads are further coated with glycidyl ether (epoxy) functional groups which seals the iron oxide inside the beads. The epoxy groups allow for binding of biological molecules such as proteins, peptides or other ligands, with covalent bond formation at neutral pH. The glycidyl ether coat of the beads has hydrophilic nature. The beads should be washed prior to coating with secondary antibody will be used in sandwich assay. The following steps are performed before the use of the beads in bioassay:

- 1) 0.1 M PBS buffer (pH 7.4) was added to the tube that includes the magnetic beads.
- 2) The tube was vortexed for 30 seconds and incubated with mixing for 10 minutes.

- 3) The tube was placed on a magnet for 2 minutes and carefully pipetted off the supernatant and the beads are left undisturbed.
- 4) The test tube was removed from the magnet and the beads are carefully resuspended in the same volume of the buffer. Vortex was used to mix the tube properly.
- 5) Third step was applied again.
- 6) The washed beads were resuspended in the same buffer.
- 7) Calculated concentration of the antibody ($5 \mu\text{g.mL}^{-1}$, $3 \mu\text{g.mL}^{-1}$ and $1 \mu\text{g.mL}^{-1}$) was added to the bead suspension. The tube was vortexed to ensure good mixing prior to the addition of the calculated ammonium sulfate-stock solution.
- 8) The test tubes include different concentrations of the antibody was incubated for 16-24 hours to make the covalent coupling faster and more efficient.
- 9) After incubation period, the tube was placed on the magnet for 4 minutes for magnetic separation and the supernatant was carefully removed.
- 10) The coated beads were washed for 4 times with PBS buffer. BSA was added to the last solution for blocking.
- 11) The prepared magnetic beads coated with secondary antibody was used in the 6. step of the bioassay in the current investigation. The principle of the applied bioassay is shown in Figure 4-12.

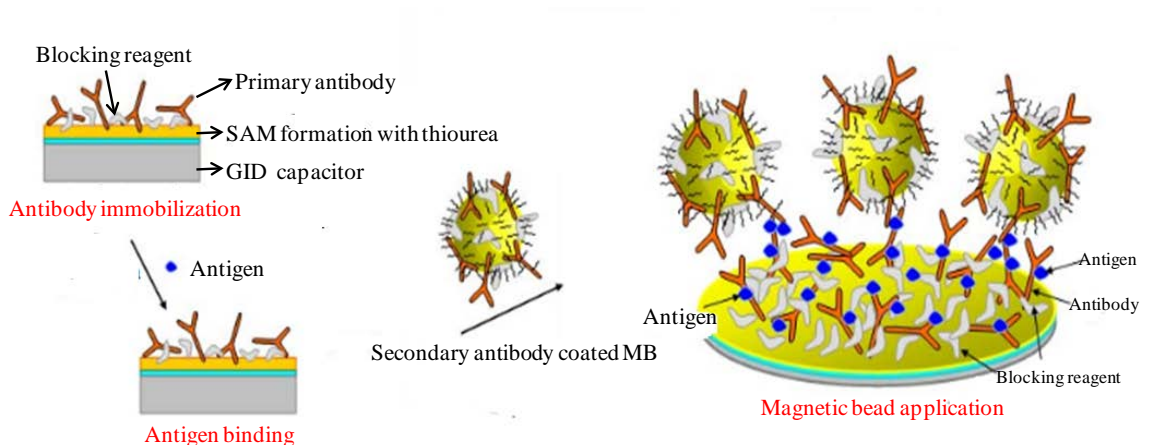


Figure 4-12 The principle of the applied bioassay using magnetic particles. (Adapted).

[111]

4.2.3 Results

Magnetic beads have much bigger size when compared with proteins. Due to this, a large number of antibody bind to only one magnetic beads and low concentration of magnetic beads are required in the current methodology that provides cheaper and easily applicable approach. For optimization of the assay parameters with magnetic beads, a well-known surface chemistry was applied using thiourea that has two amine group to catch more activation material when compared with other thiol molecules used in our previous works. 1% magnetic bead concentration was preferred to use in this study according to the preliminary testing of different bead concentrations. This concentration can be further decreased according to the concentration of the target marker or the size of the target antigen and antibody. When the investigated marker concentration is selected in lower levels such as ng.mL^{-1} or pg.mL^{-1} , the available marker number is more limited on the sensor surface that means the required secondary antibody or magnetic bead concentration will decrease. In the case of smaller size protein markers or antibody, the magnetic bead concentration should also be decreased even the secondary antibody concentration is increased to increase the probability of secondary antibody coated MB binding to the antigen injected sensor surface.

Here, two different secondary antibody concentrations ($3 \mu\text{g.mL}^{-1}$ and $5 \mu\text{g.mL}^{-1}$) were used to coat 1% magnetic beads and the solutions were applied for the antigen concentrations as two main parallels. (One parallel includes the detection range of 10-500 pg.mL^{-1} antigen and $3 \mu\text{g.mL}^{-1}$ secondary antibody coated magnetic beads application whereas the other includes the same antigen series with $5 \mu\text{g.mL}^{-1}$ secondary antibody coated magnetic beads.) Since $3 \mu\text{g.mL}^{-1}$ secondary antibody concentration gave better results, this concentration was chosen to use in bioassays for the modification of MBs.

4.2.3.1 Antigen binding on the surface

Here, CRP-anti-CRP pair was tested using magnetic bead-modified sensor platform. CRP has 224 aminoacid length and the size of it has been determined by Matrix-assisted laser desorption/ionization (MALDI) technique as 23026 Da. CRP exhibits several functions associated with host defense; for instances, it promotes agglutination, bacterial capsular swelling, phagocytosis and complement fixation through its calcium-dependent binding to phosphorylcholine. The protein can interact with DNA and histones and may

scavenge nuclear material released from damaged circulating cells. Due to its broad range effects in the cell, it has crucial roles in cancer, cardiovascular system diseases and some other complications.

To determine the efficiency of our capacitive sensor with magnetic bead modification, a detection range of 10-500 $\text{pg}\cdot\text{mL}^{-1}$ was selected as the marker concentration. The CRP protein could be clearly detected in the range of 10-500 $\text{pg}\cdot\text{mL}^{-1}$ and the negative control showed a background signal at ~ 0.17 pF level. The significant and stabile capacitance change was observed between 600-900 MHz. Figure 4-13 and Figure 4-14 shows the antigen detection responses in the whole and a constant frequency point, respectively. Linear regression analysis was performed at 800 MHz and R^2 value was calculated as 0,974.

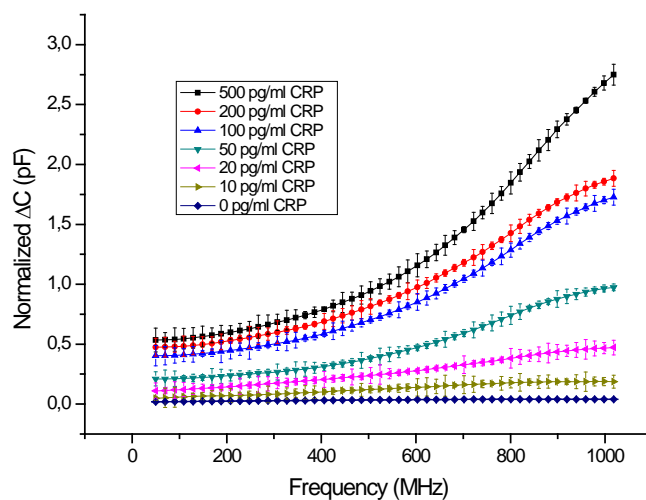


Figure 4-13 CRP antigen detection in the concentration range of 0-500 $\text{pg}\cdot\text{mL}^{-1}$ at all frequency range.

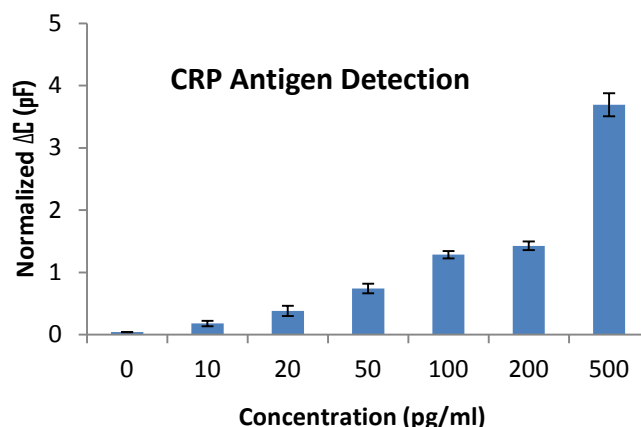


Figure 4-14 Capacitive detection of CRP antigen in the concentration range of 0-500 $\text{pg}\cdot\text{mL}^{-1}$ at a constant frequency.

4.2.3.2 Modified MB application on the surface

After the measurements of antigen binding, MB application was conducted using secondary antibody-coated magnetic particles. The prepared MB solution was applied to each sensor by a pipette using 3 μl volume per capacitor. Three capacitors were employed to obtain the negative control. For the control, the sensor was immobilized with anti-CRP antibody and PBS buffer was then injected to the sensor surface instead of the target antigen (CRP). After antigen binding step of the assay, these electrodes were treated with secondary antibody coated-MBs as in the positive samples. 3 h incubation was performed for MB application to all capacitors. Each electrode was then washed with a pipette using PBS and dH_2O for several times to prevent from outspreading. The sensor was then dried prior to take measurements by Network Analyzer.

The change in capacitance due to the MB application was calculated for each antigen bound electrode and standard deviations were obtained from each 3 electrodes that were treated with same antigen concentration at the antigen binding step. The capacitance change was calculated as the normalized capacitance according to the equation 4-3.

$$\text{Normalized } \Delta C = \frac{C_{\text{MB}} - C_{\text{Antigen}}}{C_{\text{Antigen}}} \quad \text{Equation 4-3}$$

Figure 4-15 shows capacitance change after MB application on the surface and the obtained responses represent an increase on the capacitance change depending on the

increase antigen concentration on the surface. A clear signal difference was observed due to the MB usage on the platform. Lowest antigen concentration (10 pg.mL^{-1} CRP) gave $\sim 0.17 \text{ pF}$ capacitance change at antigen binding stage, whereas the response on this surface increased to $\sim 2.1 \text{ pF}$ after secondary antibody-coated MB application.

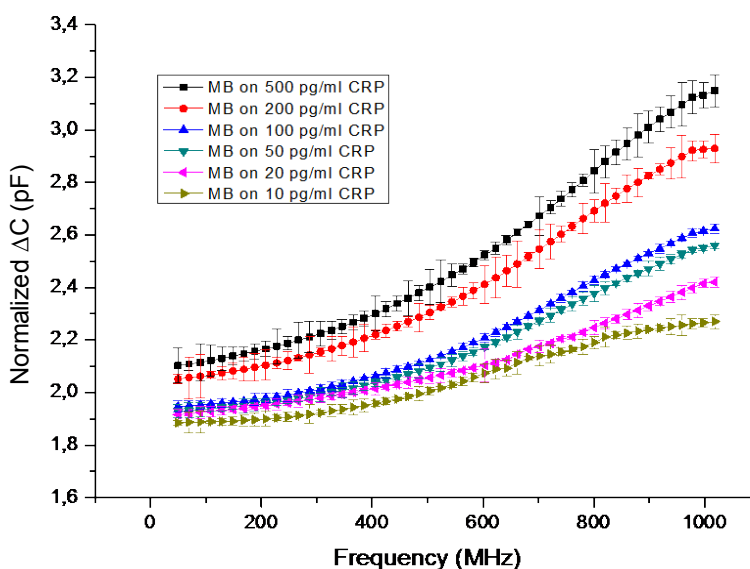


Figure 4-15 Capacitance change after secondary antibody-coated MB application on the antigen bound surfaces in all frequency range.

For the frequency range, the optimal range was found between 600-1000 MHz although the best output was obtained in the range of 800-900 MHz as seen in Figure 4-16a. Moreover, specificity of the assay was determined using a negative control; thus, MB application on the lowest antigen concentration and the antigen-free control were compared. MBs on the control surface produced $\sim 0.25 \text{ pF}$ capacitance change while it was $\sim 2.5 \text{ pF}$ on the antigen bound surface that has lowest concentration (10 pg.mL^{-1}) as shown in Figure 4-16b.

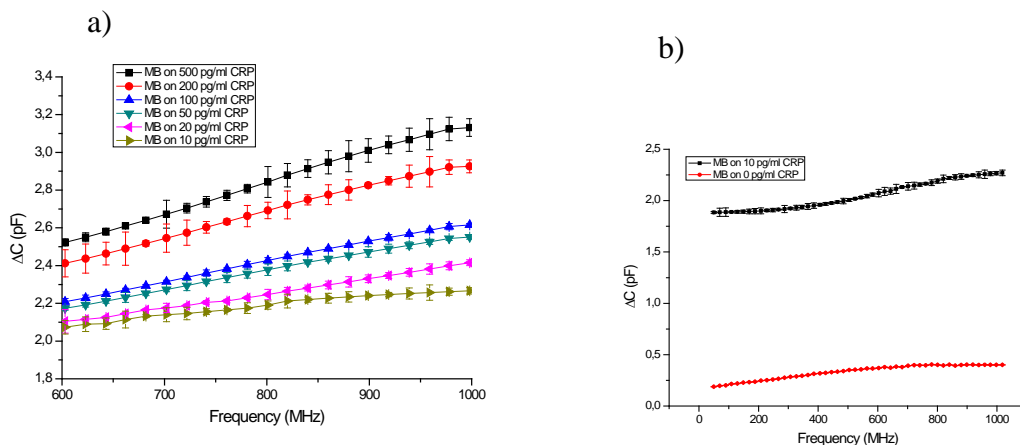


Figure 4-16 Capacitance change after secondary antibody-coated MB application on the antigen bound surfaces in the frequency range of 600-1000 MHz (a) and the difference between the control surface and the lowest antigen bound surface after MB application (b).

The development of MB-modified capacitive sensor platform indicated an alternative methodology for the detection of cancer biomarkers, especially for small size or low threshold level biomarkers. The bioassays conducted using CRP antigen-antibody pair with MB-application gave expected results and the platform was optimized to work with magnetic particles for the detection of disease markers. The MB-modified platform was also used for multiple marker detection to provide an alternative quantification approach to the Au-NP modified sensor platform for precise disease diagnostics.

4.3 MULTIPLE MARKER ASSAY FOR PRECISE DISEASE DETECTION

Label-free biosensors can detect disease markers to provide point-of-care diagnosis that is low-cost, rapid, specific and sensitive [112-125]. Biomarkers have emerged as potentially important diagnostic tools for cancer and many other diseases. Continuing discoveries of such biomarkers and their aggregation into molecular signatures suggests that multiple biomarkers will be necessary to precisely define disease states. Thus, parallel detection of biomarker arrays is essential for translation from benchtop discovery to clinical validation. Such a technique would enable rapid, point-of-care (POC) applications requiring immediate diagnosis from a physiological sample. Critically, such a system must also be capable of detecting very low levels of aberrant genes and proteins, as many biomarkers are present at minute concentrations during early disease phases

[115-118]. Due to this, multiple marker detection was investigated for lung cancer markers through employing nanoparticle modified electrochemical-based capacitive biosensors and the multiple detection of lung cancer protein markers (CEA, EGFR and CA 15-3) was investigated for the first time (Figure 4-17).

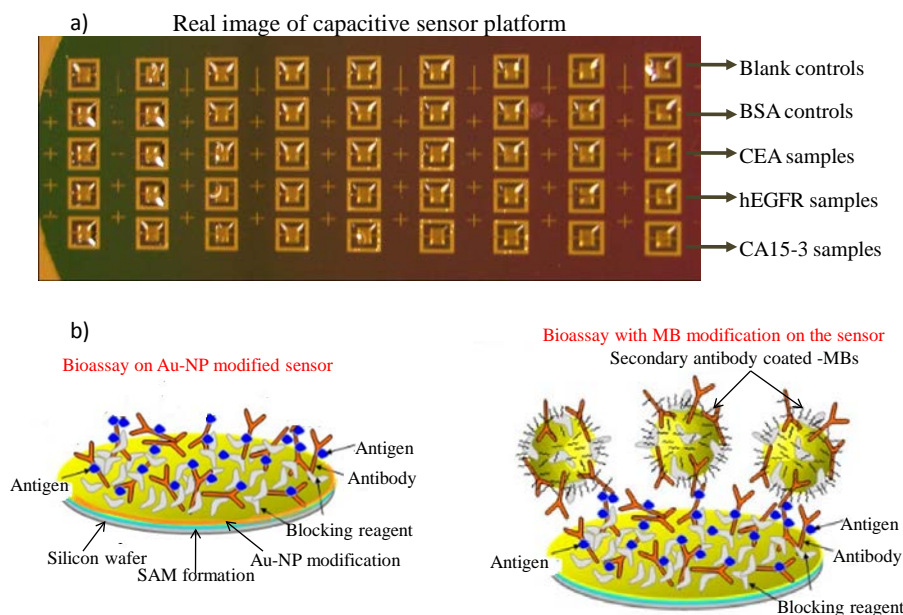


Figure 4-17 Schematic representation of capacitive biosensor chips (a) and bioassays applied with the particle modifications (b). (b part of the figure was adapted). [111]

4.3.1 Materials and Reagents

Monoclonal antibodies and purified antigens for CEA and CA15-3 were purchased from Fitzgerald (USA). Sheep monoclonal antibody to human epidermal growth factor receptor (anti-hEGFR) and human epidermal growth factor receptor (hEGFR) were bought from Sigma Aldrich (USA). All other reagents and solvents of analytical grade were purchased from the companies as mentioned in previous sections of the thesis.

4.3.2 Antibody immobilization (anti-CEA, anti-hEGFR and anti-CA15-3)

Antibody immobilization on Au-NP modified and magnetic particle modified sensor platforms was carried out as described in section 3.2.1.2 and 3.3.3, respectively. The GID electrode surfaces of capacitors were immobilized by incubating 2.5 μL of 25 $\mu\text{g}\cdot\text{mL}^{-1}$ anti-CEA, anti-hEGFR and anti-CA15-3 antibodies in PBS buffer for 1 h. The sensor

wafer was then washed with PBS and dried prior to the blocking step with ethanolamine. The non-reacted groups on the sensor surface were blocked by adding 5 μL of 100 mM ethanolamine on each GID electrode and incubated for 2 h. The sensors were then rinsed with PBS and sterile dH_2O , and dried with nitrogen gun prior to the measurements for antibody immobilization using a Network Analyzer. The analyzer was calibrated and triplicate measurements were then taken for each GID electrode for error analysis.

4.3.3 Detection of multiple cancer markers

A series of antigen concentrations in the range of 0-1 ng.mL^{-1} were initially prepared in PBS buffer on ice. The capacitors were then incubated for 2 h with different antigen concentrations in 2.5 μL volume for each biomarker. The capacitive measurements were taken before and after the antigen treatment. The capacitance was measured with (a) blank capacitor, (b) capacitor after SAM formation, (c) after Au-NP modification, (d) after antibody immobilization and compared the results with (e) capturing of different concentrations of antigens on the antibody immobilized capacitors. In the case of magnetic particle modified capacitive platform, secondary antibody-coated magnetic beads were applied on the antigen bound surface and the signal was measured instead of the measurement c. Network analyzer was calibrated using SOLT (short-open-load-through) method prior to the measurements. Capacitance change was calculated from the measurements of the sample capacitance and 3 individual electrodes were used for each antigen concentration to understand the repeatability and reliability of the assays. Capacitance change was calculated from the data measurements in the effective frequency range of 500-1000 MHz for plotting under standard assay conditions. Negative control assays were also performed using the buffer solution and BSA protein to check the specificity of the assays. Average values of ΔC obtained from triplicate experiments were plotted and the standard deviations were calculated that were shown as errors.

4.3.4 Results and Discussion

In this study, multiple markers of lung cancer were investigated using nanoparticle modified capacitive sensor platform for the first time. With this aim, three target protein markers (CEA, hEGFR and CA15-3) were selected due to their presence at elevated levels in human blood for the cancer cases and worked employing two different methodology of nanoparticle modification.

Au-NP modification was carried out after SAM formation with thiourea for signal enhancement via the increase of surface for the biological molecules. After the modification of the sensor surface with Au-NP during 8 h incubation, antibody immobilization was performed using three different target antibodies. Antigen binding step of the bioassay was then applied in the concentration range of 0-1 ng.mL⁻¹ for CEA and hEGFR while 0-100 U.mL⁻¹ for CA15-3. BSA was used as negative control to determine the specificity of the assays.

In the case of modification with magnetic particles, antibody immobilization and antigen binding steps of the experiments were conducted and the signal was then enhanced applying secondary antibody coated magnetic beads on the antigen bound surfaces. Same concentrations with Au-NP modified sensor were used here and the results were compared as capacitance change according to the target marker and the modification type with nanoparticles. The capacitance change of Au-NP modified sensors were calculated for CEA, hEGFR and CA15-3 cancer markers and successful detection was achieved in the concentration range from 5 pg.mL⁻¹ to 1 ng.mL⁻¹ for each marker. The specificity of the assays were checked using a non-specific protein (10 ng.mL⁻¹ BSA) and a clear difference was observed between the lowest concentration of the antigen and the controls. PBS buffer (0 pg.mL⁻¹ CEA, EGFR or CA15-3) was also tested as negative control on the antibody immobilized sensor surfaces (anti-CEA, anti-hEGFR and anti-CA15-3) to measure the baseline response of the solution used for the preparation of the samples. The capacitive responses of the sensors were plotted in the optimal frequency range for protein markers (Figure 4-18).

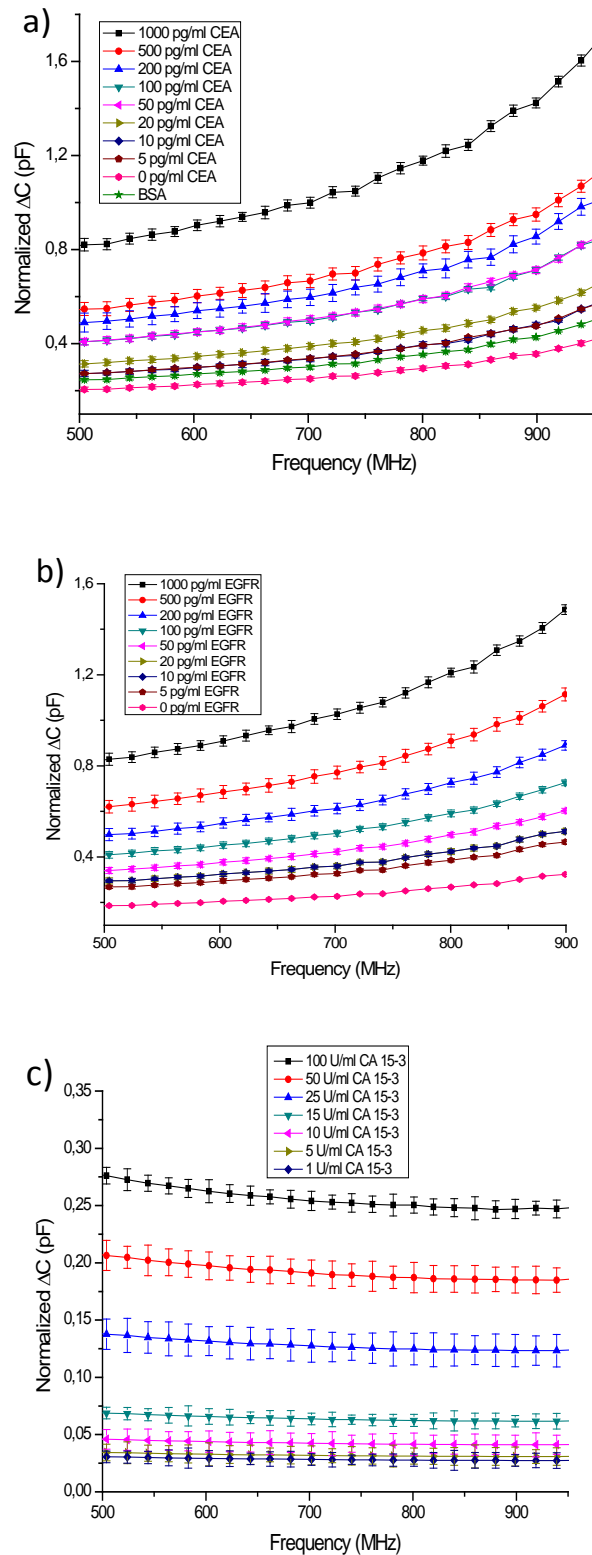


Figure 4-18 Capacitive detection of CEA, hEGFR and CA15-3 cancer markers with Au-NP modified capacitive sensor in the frequency range of 500-900 MHz. CEA and hEGFR detection in the concentration range of 5-1000 $\text{pg}\cdot\text{mL}^{-1}$ (a and b). CA15-3 marker detection in the concentration range from 1 $\text{U}\cdot\text{mL}^{-1}$ to 100 $\text{U}\cdot\text{mL}^{-1}$ (c).

Capacitance responses of the marker at a constant frequency were also compared in the concentration range of 5-1000 pg.mL^{-1} for CEA and hEGFR, and 1-100 U.mL^{-1} for CA15-3 proteins as shown in Figure 4-19 and the regression analysis was also performed for each marker and R^2 values were calculated as 0.99, 0.94 and 0.98 respectively (Figure 4-20). The results of CA15-3 detection were plotted separately due to the difference between concentration types. The normal range of CA15-3 marker in human blood is 50 U.mL^{-1} and the increased level of the marker plays a role as cancer indicator. The marker has not been tested with sensor technologies whereas ELISA tests have been conducted for clinical analysis and disease diagnostics. Moreover, this marker has been investigated as U.mL^{-1} instead of molar concentration due to its enzymatic behaviour and the detection limits of commercially available ELISA kits change between 5-10 U.mL^{-1} . The concentration of samples for CA15-3 marker was prepared according to the threshold level of the marker in human blood and ELISA tests and the concentration range of 1-100 U.mL^{-1} was successfully detected as shown in Figure 4-20.

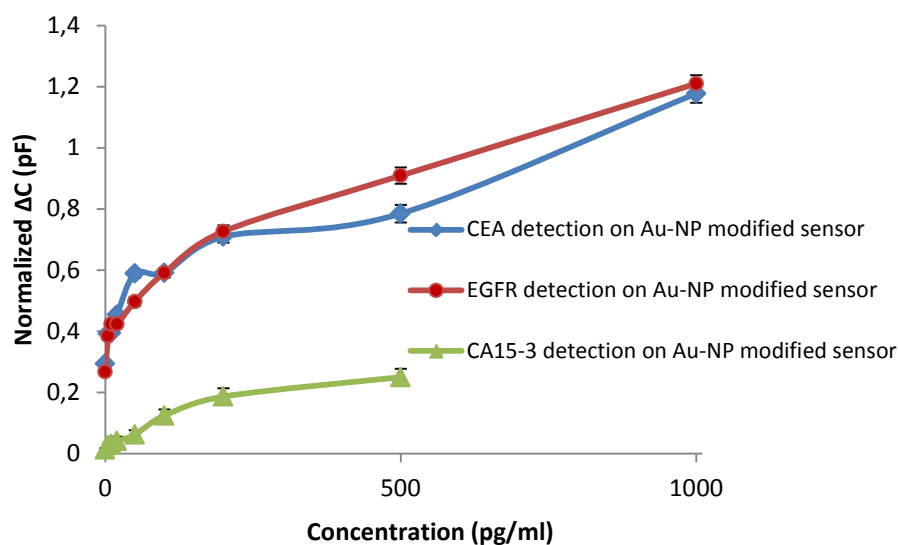


Figure 4-19 Multiple marker detection at a constant frequency (800 MHz) with Au-NP modified sensor platform. The concentration range of CEA and EGFR is 5-1000 pg.mL^{-1} while it is 1-100 U.mL^{-1} for CA15-3 protein marker.

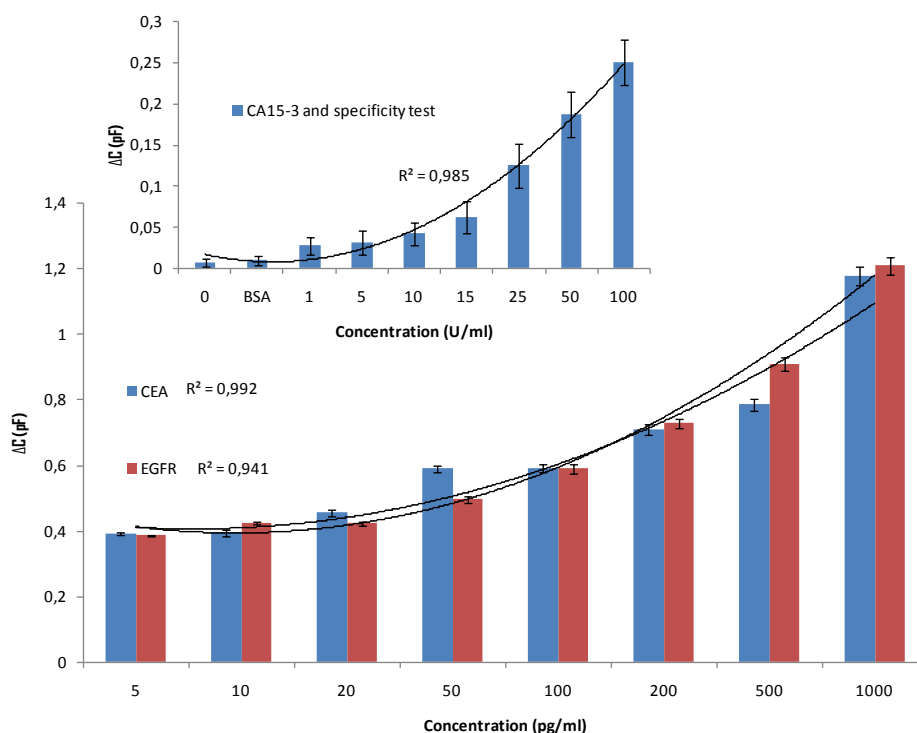


Figure 4-20 Regression analysis of the bioassays conducted with Au-NP modified sensor platform at a constant frequency. The specificity of the assays was tested using PBS buffer ($0 \text{ pg}\cdot\text{mL}^{-1}$ marker) and a non-specific protein ($10 \text{ ng}\cdot\text{mL}^{-1}$ BSA).

The results of CEA and EGFR detection according to the antigen concentration were found very similar while the obtained signal was quite different when compared with CA15-3 protein. The similarity of the results for CEA and EGFR may depend on the molecular weight of the markers that are very close to each other and the same concentration level of the prepared samples. The results of CA15-3 tests show difference due to the concentration type ($\text{U}\cdot\text{mL}^{-1}$ instead of $\text{pg}\cdot\text{mL}^{-1}$) when compared with the other markers and the sample concentrations of CA15-3 were in trace amount in this study. The marker could be successfully detected at $1 \text{ U}\cdot\text{mL}^{-1}$ concentration using Au-NP modified sensor platform which is much lower than the threshold level and ELISA kits.

Moreover, the efficiency of Au-NP modified capacitive sensor platform can also be compared with the previous hEGFR results in which a standard capacitive sensor was employed. For example, $1 \text{ ng}\cdot\text{mL}^{-1}$ concentration of hEGFR gave $\sim 0.3 \text{ pF}$ capacitance change with non-modified sensor whereas the same amount of the antigen produced ~ 1.6

pF capacitance change with Au-NP modified sensor platform and the modification led to detect much lower concentration such as 5 pg.mL^{-1} at high specificity.

Multiple markers of lung cancer for precise disease diagnosis were also investigated using magnetic bead modification. Here, the modification was applied after the antigen treatment on the sensing surface to enhance the signal. For this, the magnetic beads were initially functionalized with secondary antibodies (anti-CEA, anti-hEGFR or anti-CA15-3) and the solutions were then applied to the sensor after antigen binding during 2 h incubation at room temperature. The ΔC was calculated for antigen binding step at the selected concentration range. A clear capacitance change was observed depending on the marker concentration although the lowest concentrations of the markers gave little difference when compared with the negative protein control (10 ng.mL^{-1} BSA) as shown in Figure 4-21.

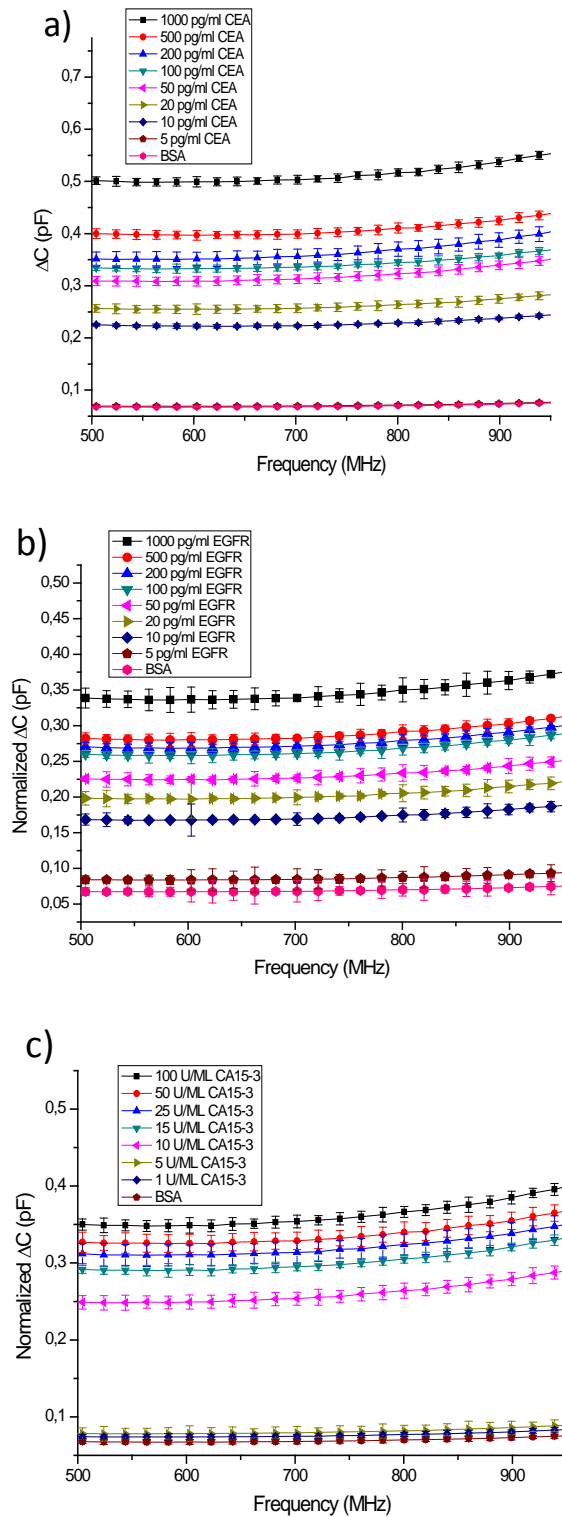


Figure 4-21 Capacitance change on the sensor due to the antigen binding at the effective frequency range prior to the magnetic bead modification. CEA and hEGFR marker detection in the concentration range of 5-1000 pg.mL⁻¹ (a, b). CA15-3 detection in the concentration range of 1-100 U.mL⁻¹ (c).

When we compared the antigen binding results of these assays with Au-NP sensor platform (the modification was carried out after SAM formation and the surface was enhanced for the binding of biological molecules), it was observed that all sample concentrations were clearly detected with a higher signal on Au-NP modified sensor platform whereas the lowest sample concentrations gave a weak response in these bioassays that cannot be meaningful in our sensor platform. Moreover, the highest concentrations of the markers produced much more capacitance change in the case of Au-NP modification. For instance, 1 ng.mL^{-1} CEA gave $\sim 1.6 \text{ pF } \Delta C$ with Au-NP modification while it led only $0.5 \text{ pF } \Delta C$ prior to the magnetic bead application to the sensor in these bioassays.

After the antigen detection stage of the bioassays, the sensor surface was modified with secondary antibody coated magnetic particles to enhance the signal and the results were evaluated as ΔC for each marker. The difference between the negative controls (PBS buffer and BSA protein) and the sample concentrations showed a change in capacitance drastically as seen in Figure 4-22. Moreover, the magnetic bead modification increases the signal ~ 5 fold and it led to a meaningful detection for the lower concentrations of the markers when compared with the controls. A significant signal increase was observed for the 5 pg.mL^{-1} , 1 U.mL^{-1} and 5 U.mL^{-1} concentrations of the markers against the negative control in the case of magnetic bead modification; therefore, this output indicates the importance of the particle usage in our platform for reliable detection of the cancer markers. The ΔC results of magnetic bead modification showed that there was trace amount of the marker bound on the antibody immobilized sensor surface although it could not give an observable change in capacitance prior to the particle modification. The magnetic particle modification increased the signal for 5 pg.mL^{-1} of CEA from $\sim 0.05 \text{ pF}$ to $\sim 1.6 \text{ pF}$ whereas the signal was change from ~ 0.05 to $\sim 0.07 \text{ pF}$ for the non-specific protein control.

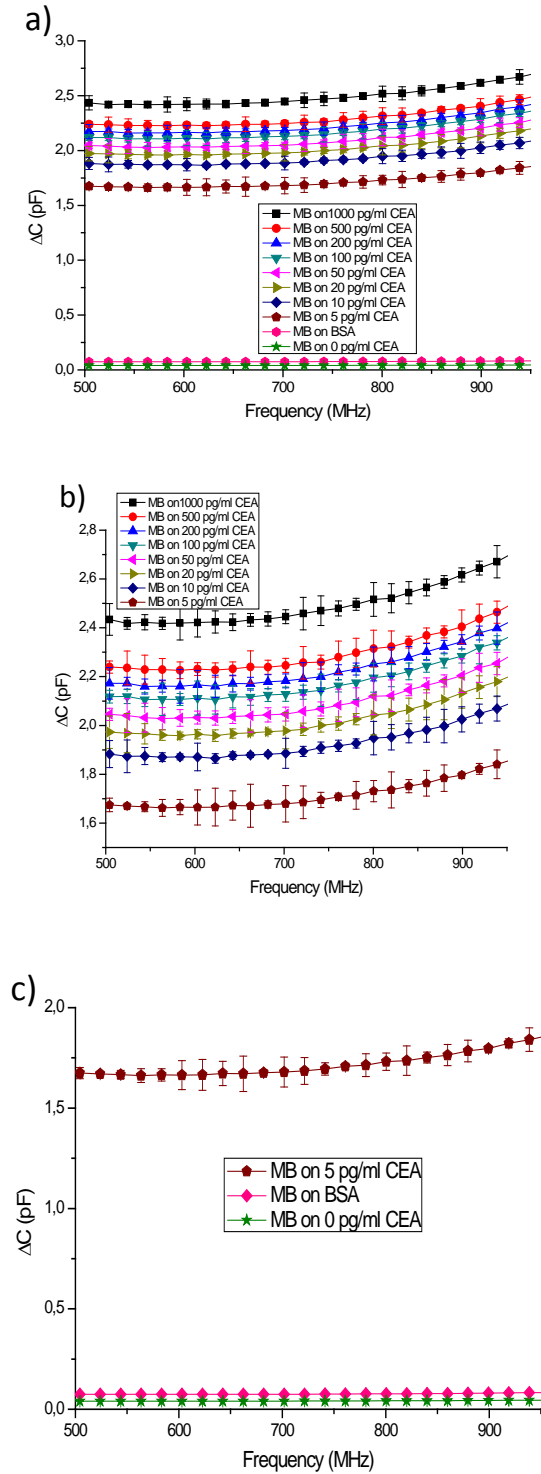


Figure 4-22 Signal enhancement with magnetic particles for the detection of CEA marker in the concentration range of 5-1000 pg.mL⁻¹ at the effective frequency range. Comparison of the sample responses with the negative controls after magnetic bead application (a). The results of constant magnetic bead solution application on the different CEA concentrations in the concentration range of 5-1000 pg.mL⁻¹ (b). Specificity test of the bioassays using the lowest amount of CEA sample and the negative controls (c).

As a part of multiple marker tests using magnetic bead modification in the capacitive sensor, the signal enhancement assay was also conducted for hEGFR and CA15-3 bound surfaces. The similar results were obtained for these markers and the particle application on all investigated antigen concentrations led to a significant signal increase whereas a difference was not observed for the control surfaces as seen in Figure 4-23.

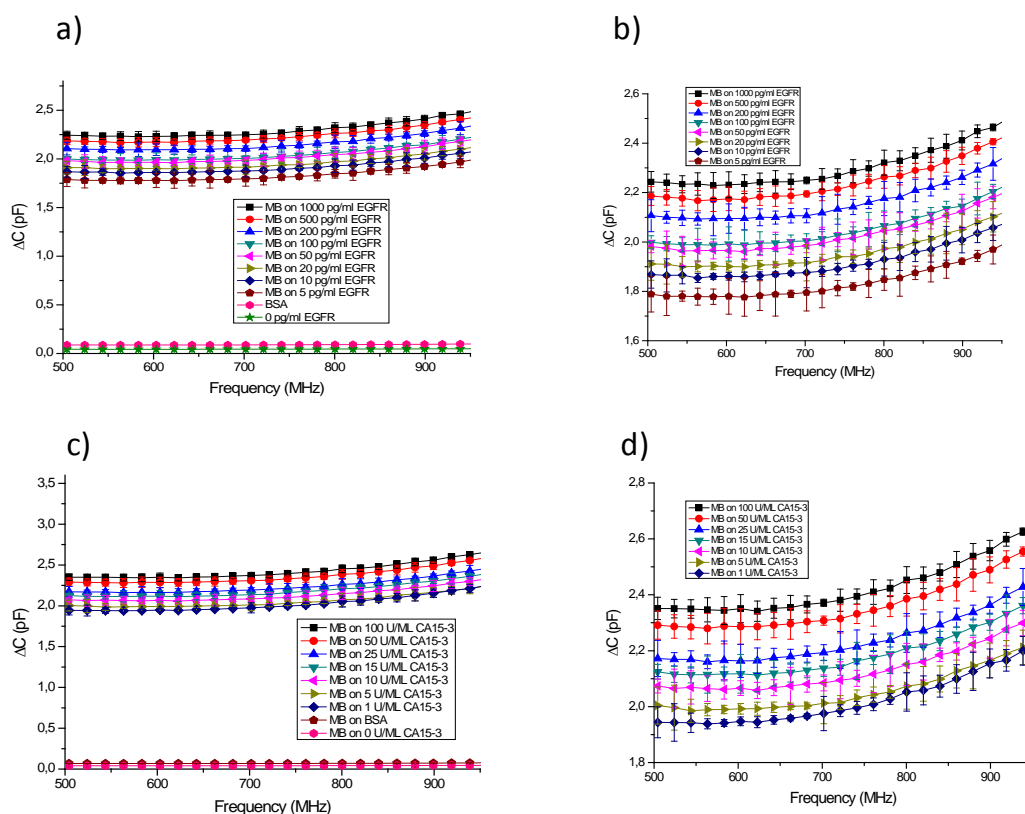


Figure 4-23 Signal enhancement with magnetic bead modification on the capacitive sensor platform for hEGFR and CA15-3 cancer markers at the effective frequency range. Capacitance change due to the magnetic bead application after antigen binding step of hEGFR bioassay with/out the negative controls (a, b). Capacitance change due to the magnetic bead application after antigen binding step of CA15-3 bioassay with/out the negative controls (c, d).

The results obtained during this PhD thesis have provided alternative approaches for cancer detection and quantification using biomarkers. The developed and improved methodologies/sensors can also be applied for the other diseases that have biomarkers in human body. A comparison of all sensor platforms used throughout the PhD process can be seen in Table 4-4.

Table 4-4 Comparison of all investigated sensor platforms in this PhD thesis.

	QCM/SPR sensors	Capacitive Sensor	Capacitive sensor with Au-NP modification	Capacitive sensor with MB modification
Concentration range	3-400 ng/ml	0.5-256 ng/ml	5 pg/ml-1 ng/ml	5 pg/ml-1 ng/ml
Detection limit	3 ng/ml	0.5 ng/ml	5 pg/ml	5 pg/ml
Signal amplification as detection limit	1 fold	6 fold	600 fold	600 fold
Signal amplification as ΔC	-	1 fold	~5 fold	~5 fold
Specificity	High (~0)	High (~under zero)	Good (~0,2 pF)	High (~0)

CHAPTER 5

5 SUMMARY, CONCLUSION AND FUTURE PROSPECTS

In this thesis, an electrochemical based, cost effective, highly sensitive capacitive biosensor was developed using different nanoparticles to promote lung cancer detection for the first time. SPR and QCM-based sensors were employed to develop the bioassays and the surface chemistries for the detection of biological molecules [56, 126]. The successful achievements of these research works were transferred into an electrochemical based-biosensor to decrease the cost, time and need to special skills on the usage of these sensors and increase the sensitivity, reliability of the assays for the quantification of the biological markers, especially small-sized and trace threshold level markers, with the aim of disease detection. The optimized sensor methods were conducted in the capacitive sensor using standard methodologies and the detection limits of the other sensors for the biomarker quantification were decreased efficiently without any signal amplification methodology. However, the signal enhancement plays crucial role in the quantification through biosensors due to the need for sensitive and reliable detection of some markers that have too low levels as the cancer indicators. For an instance, disease levels of many biomarkers are at ng.mL^{-1} ranges such as CEA [56], hEGFR [79], PSA [68] while some others have the level at pg.mL^{-1} ranges such as IL-6 [127].

Moreover, the binding affinity between the biosensing molecule and the target is one of the most crucial parameter in biosensor assays. In this study, kinetic data analysis was performed using 1:1 Langmuir binding model and the affinity between antibodies and the target antigens were increased when the bioassays were optimized. For an instance, the standard and the optimized assays were compared in SPR sensor and R_{max} were increase from 215 RU to 734 RU. The dissociation constant was also decreased from 8.8×10^{-9} M to 3.04×10^{-11} M in the case of optimization and this indicated the increment of affinity between the target pairs.

Last decades are the heyday of biosensor technology; however, there have been still some gaps to fulfil and important problems to solve such as cross-reactivity between biological molecules and sensitivity/specificity/accuracy of the sensor/sensor surface chemistry, etc. Another important issue about cancer detection by biomarkers is the availability of the antibody or probes with an excellent specificity against the target protein or genetic marker. Due to this fact, there is a need to use bioinformatics tools and compare the sequences of the selected human proteins and genes with many species such as goat, monkey, mouse and rabbit. The achievement of this kind of research can be evaluated to produce biosensing molecules under laboratory conditions. The successful results of the production can eliminate the need for commercial antibody or probes that are quite expensive and show an unacceptable specificity against targeted biomarkers. The production strategies may also provide fundamental methodologies and approaches for both the commercial markets and research facilities. Moreover, real patient samples and human serum include various biological molecules beside the target analyte; thus, make the detection difficult due to the non-specific responses and require the signal amplification using appropriate modification.

5.1 Novelty and Quality of the Work

Here, both Au-NPs and MBs were successfully implemented to the non-faradaic interdigitated capacitive sensor for the first time and 600-fold increment was achieved as the detection limit for the tests of lung cancer biomarkers. Multiple marker detection for the precise cancer definition employing the capacitive sensing platform was the other novelty of the research. The improved methodologies and the obtained results provide a very prospective alternative approach for the early diagnosis of the cancer cases without an invasive and painful tool such as biopsy. The achievements of the study can also be compared with the other non-invasive methods including SPR, QCM and capacitive sensors in the literature. Table 5-1 summarizes the different sensing platforms depending on the detection methods and the sensitivity; indicates the efficiency and priority of our research works. When we compared our work within itself, it is clear that the particle-modified sensor platforms have provided a significant superiority over the other sensors (SPR and QCM) and non-modified capacitive sensor platform. (The asterisk shows the samples prepared in the diluted serum.)

Table 5-1 Comparison of different sensor platforms for the marker detection with each other and our results in this thesis.

Method	Detectable range	Sensitivity	Signal enhancement methodology	Labelling	Reference
QCM	4.7-5000 ng.ml ⁻¹	4.7 ng.ml ⁻¹	-	-	[68]
QCM	2.3-150 ng.ml ⁻¹	2.3 ng.ml ⁻¹	yes	yes	[68]
QCM	0.29-150 ng.ml ⁻¹	0.29 ng.ml ⁻¹	yes	-	[68]
QCM	0.001-100 µg. dl ⁻¹	0.001 µg. dl ⁻¹	yes	yes	[128]
SPR	10.2-18.1 ng.ml ⁻¹	10.2 ng.ml ⁻¹	yes	yes	[129]
SPR	20.7-47.5 ng.ml ⁻¹	20.7 ng.ml ⁻¹	-	-	[129]
Capacitance biochip	10-1000 times diluted human serum	2.43 µg.ml	-	-	[54]
Capacitive sensor	1-75 ng.ml ⁻¹	1 ng.ml ⁻¹	-	-	[130]
Capacitive sensor	0.05-75 ng.ml ⁻¹	0.05 ng.ml ⁻¹	yes	-	[130]
SPR in this work	3-400 ng.ml ⁻¹	3 ng.ml ⁻¹	-	yes	[56]
QCM in this work	3-400 ng.ml ⁻¹	6 ng.ml ⁻¹	-	yes	[56]
Capacitive sensor in this work	0.5-256 ng.ml ⁻¹	0.5 ng.ml ⁻¹	-	-	
Au-NP modified capacitive sensor in this work	5-1000 pg.ml ⁻¹	5 pg.ml ⁻¹	yes	-	
MB modified capacitive sensor in this work	5-1000 pg.ml ⁻¹	5 pg.ml ⁻¹	yes	-	

5.2 Future Prospects

This work has shown that biosensor technology provides the alternative and reliable detection/quantification approaches using biomarkers for the early detection of lung cancer that has the highest mortality rate in all cancer types due to the short survival time and quick invasion of the malign tumors. The markers of the disease can be used to define the cancer cases with a non-invasive technology; however, only one marker may not be

enough for the precise detection. Due to this, as one of the most important aspects of this PhD thesis, multiple marker quantification has crucial role and increases the reliability of the biosensors in disease detection. The normal ranges of many biomarkers are at ng.mL^{-1} and it is possible to detect these amounts using appropriate surface chemistries/ bioassays/ biosensors. However, there are some challenges about the determination of the disease markers through biosensors including (a) affinity between the sensing molecule (antibody, probe, aptamer) and the target (protein or gene marker), (b) small size of the target (a few kD, 24 kD), (c) trace amount of the marker in human body in disease cases, (d) possibility of high non-specific binding in the case of serum or real patient samples, (e) the effect of the microfluidics systems or the open system of the sensors during the quantification/ measurement processes. All of these issues will form the subjects of subsequent research projects and challenges.

6 REFERENCES

1. Yılmaz, H.H., et al., *Cancer trends and incidence and mortality patterns in Turkey*. Japanese journal of clinical oncology, 2011. **41**(1): p. 10.
2. Boice Jr, J.D., et al., *Frequent chest X-ray fluoroscopy and breast cancer incidence among tuberculosis patients in Massachusetts*. Radiation research, 1991. **125**(2): p. 214-222.
3. de González, A.B. and S. Darby, *Risk of cancer from diagnostic X-rays: estimates for the UK and 14 other countries*. The Lancet, 2004. **363**(9406): p. 345-351.
4. Watt, I., et al., *Laparoscopy, ultrasound and computed tomography in cancer of the oesophagus and gastric cardia: A prospective comparison for detecting intra-abdominal metastases*. British journal of surgery, 1989. **76**(10): p. 1036-1039.
5. Lardinois, D., et al., *Staging of non-small-cell lung cancer with integrated positron-emission tomography and computed tomography*. New England Journal of Medicine, 2003. **348**(25): p. 2500-2507.
6. Leach, M.O., et al., *Screening with magnetic resonance imaging and mammography of a UK population at high familial risk of breast cancer: a prospective multicentre cohort study (MARIBS)*. Lancet, 2005. **365**(9473): p. 1769.
7. Beets-Tan, R., et al., *Accuracy of magnetic resonance imaging in prediction of tumour-free resection margin in rectal cancer surgery*. The Lancet, 2001. **357**(9255): p. 497-504.
8. Ollinger, J.M. and J.A. Fessler, *Positron-emission tomography*. Signal Processing Magazine, IEEE, 1997. **14**(1): p. 43-55.

9. Ter-Pogossian, M.M., M.E. Raichle, and B.E. Sobel, *Positron-emission tomography*. Scientific American, 1980. **243**(4): p. 170.
10. Mao, L., et al., *Detection of oncogene mutations in sputum precedes diagnosis of lung cancer*. Cancer research, 1994. **54**(7): p. 1634.
11. Palmisano, W.A., et al., *Predicting lung cancer by detecting aberrant promoter methylation in sputum*. Cancer research, 2000. **60**(21): p. 5954.
12. Woolner, L.B. and J.R. McDonald, *Biopsy in Cancer Diagnosis*. Plastic and Reconstructive Surgery, 1952. **9**(4): p. 388.
13. Kronz, J.D., et al., *Predicting cancer following a diagnosis of high-grade prostatic intraepithelial neoplasia on needle biopsy: data on men with more than one follow-up biopsy*. The American journal of surgical pathology, 2001. **25**(8): p. 1079.
14. Gajra, A., et al., *The predictive value of neuroendocrine markers and p53 for response to chemotherapy and survival in patients with advanced non-small cell lung cancer*. Lung cancer, 2002. **36**(2): p. 159-165.
15. Barlési, F., et al., *Prognostic value of combination of Cyfra 21-1, CEA and NSE in patients with advanced non-small cell lung cancer*. Respiratory medicine, 2004. **98**(4): p. 357-362.
16. Matsuoka, K., et al., *Prognostic value of carcinoembryonic antigen and CYFRA21-1 in patients with pathological stage I non-small cell lung cancer*. European journal of cardio-thoracic surgery, 2007. **32**(3): p. 435-439.
17. Alataş, F., et al., *Diagnostic value of CEA, CA 15-3, CA 19-9, CYFRA 21-1, NSE and TSA assay in pleural effusions*. Lung cancer, 2001. **31**(1): p. 9-16.

18. Molina, R., et al., *Mucins CA 125, CA 19.9, CA 15.3 and TAG-72.3 as tumor markers in patients with lung cancer: comparison with CYFRA 21-1, CEA, SCC and NSE*. *Tumour Biol*, 2008. **29**(6): p. 371.
19. Seemann, M.D., et al., *An evaluation of the tumour markers, carcinoembryonic antigen (CEA), cytokeratin marker (CYFRA 21-1) and neuron-specific enolase (NSE) in the differentiation of malignant from benign solitary pulmonary lesions*. *Lung cancer*, 1999. **26**(3): p. 149-155.
20. Zhou, J., et al., *Expression of early lung cancer detection marker: hnRNP-A2/B1 and its relation to microsatellite alteration in non-small cell lung cancer*. *Lung cancer*, 2001. **34**(3): p. 341-350.
21. Grossi, F., et al., *Prognostic significance of K-ras, p53, bcl-2, PCNA, CD34 in radically resected non-small cell lung cancers*. *European Journal of Cancer*, 2003. **39**(9): p. 1242-1250.
22. Kristiansen, G., et al., *Overexpression of c-erbB2 protein correlates with disease-stage and chromosomal gain at the c-erbB2 locus in non-small cell lung cancer*. *European Journal of Cancer*, 2001. **37**(9): p. 1089-1095.
23. Woenckhaus, M., et al., *Prognostic value of FHIT, CTNNB1, and MUC1 expression in non—small cell lung cancer*. *Human pathology*, 2008. **39**(1): p. 126-136.
24. Gautschi, O., et al., *Origin and prognostic value of circulating KRAS mutations in lung cancer patients*. *Cancer letters*, 2007. **254**(2): p. 265-273.
25. Andriani, F., et al., *Detecting lung cancer in plasma with the use of multiple genetic markers*. *International journal of cancer*, 2004. **108**(1): p. 91-96.
26. Jang, J.S., et al., *Telomere length and the risk of lung cancer*. *Cancer science*, 2008. **99**(7): p. 1385-1389.

27. Carcereny, E., et al., *Blood-based CHRNA3 single nucleotide polymorphism and outcome in advanced non-small-cell lung cancer patients*. Lung cancer, 2010. **68**(3): p. 491-497.
28. Hosgood, H.D., et al., *Genetic variation in telomere maintenance genes, telomere length, and lung cancer susceptibility*. Lung cancer, 2009. **66**(2): p. 157-161.
29. Xie, Y., et al., *Altered miRNA expression in sputum for diagnosis of non-small cell lung cancer*. Lung cancer, 2010. **67**(2): p. 170-176.
30. Romanowska, M., et al., *DNA damage, superoxide, and mutant K-ras in human lung adenocarcinoma cells*. Free Radical Biology and Medicine, 2007. **43**(8): p. 1145-1155.
31. Camps, C., et al., *Is there a prognostic role of K-ras point mutations in the serum of patients with advanced non-small cell lung cancer?* Lung cancer, 2005. **50**(3): p. 339-346.
32. Tsao, D.A., et al., *A fast and convenient new technique to detect the therapeutic target, K-ras mutant, from peripheral blood in non-small cell lung cancer patients*. Lung cancer, 2010. **68**(1): p. 51-57.
33. Kondo, K., et al., *The reduced expression and aberrant methylation of p16INK4a in chromate workers with lung cancer*. Lung cancer, 2006. **53**(3): p. 295-302.
34. Belinsky, S.A., et al., *Aberrant methylation of p16INK4a is an early event in lung cancer and a potential biomarker for early diagnosis*. Proceedings of the National Academy of Sciences, 1998. **95**(20): p. 11891.
35. Sasaki, H., et al., *Expression of the cdc25B gene as a prognosis marker in non-small cell lung cancer*. Cancer letters, 2001. **173**(2): p. 187-192.
36. Spinola, M., et al., *Genome-wide single nucleotide polymorphism analysis of lung cancer risk detects the KLF6 gene*. Cancer letters, 2007. **251**(2): p. 311-316.

37. Lee, W.K., et al., *Polymorphisms in the Caspase7 gene and the risk of lung cancer*. Lung cancer, 2009. **65**(1): p. 19-24.
38. Jang, J.S., et al., *Polymorphisms in the survivin gene and the risk of lung cancer*. Lung cancer, 2008. **60**(1): p. 31-39.
39. Cheng, Y.L., et al., *Prognostic prediction of the immunohistochemical expression of p53 and p16 in resected non-small cell lung cancer*. European journal of cardio-thoracic surgery, 2003. **23**(2): p. 221-228.
40. Belinsky, S.A., et al., *Plutonium targets the p16 gene for inactivation by promoter hypermethylation in human lung adenocarcinoma*. Carcinogenesis, 2004. **25**(6): p. 1063.
41. An, Q., et al., *Detection of p16 hypermethylation in circulating plasma DNA of non-small cell lung cancer patients*. Cancer letters, 2002. **188**(1-2): p. 109-114.
42. Planque, C., et al., *KLK5 and KLK7, two members of the human tissue kallikrein family, are differentially expressed in lung cancer*. Biochemical and biophysical research communications, 2005. **329**(4): p. 1260-1266.
43. Feng, J., et al., *Polymorphisms of the ribonucleotide reductase M1 gene and sensitivity to platin-based chemotherapy in non-small cell lung cancer*. Lung cancer, 2009. **66**(3): p. 344-349.
44. Yanagawa, N., et al., *Promoter hypermethylation of RASSF1A and RUNX3 genes as an independent prognostic prediction marker in surgically resected non-small cell lung cancers*. Lung cancer, 2007. **58**(1): p. 131-138.
45. Gresner, P., et al., *Expression of selenoprotein-coding genes SEPP1, SEP15 and hGPX1 in non-small cell lung cancer*. Lung cancer, 2009. **65**(1): p. 34-40.

46. Paci, M., et al., *Circulating plasma DNA as diagnostic biomarker in non-small cell lung cancer*. Lung cancer, 2009. **64**(1): p. 92-97.
47. van der Vaart, M. and P.J. Pretorius, *Is the role of circulating DNA as a biomarker of cancer being prematurely overrated?* Clinical biochemistry, 2010. **43**(1-2): p. 26-36.
48. Brimelow, C.J.B., *Instrumentation and sensors for the food industry*. 2001: Woodhead Publishing.
49. Mulaa, F.J. and P.M. Krämer, *13 Biosensors*. Handbook of Food Safety Engineering, 2011: p. 313.
50. Tothill, I.E. *Biosensors for cancer markers diagnosis*. 2009: Elsevier.
51. Homola, J., *Present and future of surface plasmon resonance biosensors*. Analytical and bioanalytical chemistry, 2003. **377**(3): p. 528-539.
52. Laschitsch, A. and D. Johannsmann, *High frequency tribological investigations on quartz resonator surfaces*. Journal of applied physics, 1999. **85**: p. 3759.
53. Cooper, M.A. and V.T. Singleton, *A survey of the 2001 to 2005 quartz crystal microbalance biosensor literature: applications of acoustic physics to the analysis of biomolecular interactions*. Journal of Molecular Recognition, 2007. **20**(3): p. 154-184.
54. Carrara, S., et al., *Label-free cancer markers detection by capacitance biochip*. Sensors and Actuators B: Chemical, 2009. **136**(1): p. 163-172.
55. Berggren, C., B. Bjarnason, and G. Johansson, *Capacitive biosensors*. Electroanalysis, 2001. **13**(3): p. 173-180.
56. Altintas, Z., et al., *Surface Plasmon Resonance based Immunosensor for the Detection of the Cancer biomarker Carcinoembryonic Antigen*. Talanta, 2011.

57. Carney, W.P., *Circulating oncoproteins HER2/neu, EGFR and CAIX (MN) as novel cancer biomarkers*. Expert review of molecular diagnostics, 2007. **7**(3): p. 309-319.
58. Kimura, Y., et al., *Serum CA125 level is a good prognostic indicator in lung cancer*. British journal of cancer, 1990. **62**(4): p. 676.
59. Manukyan, G., et al., *Cytokine profile of Armenian patients with Familial Mediterranean fever*. Clinical biochemistry, 2008. **41**(10-11): p. 920-922.
60. Singer, B.B., et al., *Carcinoembryonic antigen-related cell adhesion molecule 1 expression and signaling in human, mouse, and rat leukocytes: evidence for replacement of the short cytoplasmic domain isoform by glycosylphosphatidylinositol-linked proteins in human leukocytes*. The Journal of Immunology, 2002. **168**(10): p. 5139.
61. Gold, P. and S.O. Freedman, *Demonstration of tumor-specific antigens in human colonic carcinomata by immunological tolerance and absorption techniques*. The Journal of experimental medicine, 1965. **121**(3): p. 439-462.
62. Laboria, N., et al., *Amperometric immunosensor for carcinoembryonic antigen in colon cancer samples based on monolayers of dendritic bipodal scaffolds*. Analytical chemistry, 2010. **82**(5): p. 1712-1719.
63. Limbut, W., et al., *A reusable capacitive immunosensor for carcinoembryonic antigen (CEA) detection using thiourea modified gold electrode*. Analytica chimica acta, 2006. **561**(1-2): p. 55-61.
64. Macdonald, J.S. *Carcinoembryonic antigen screening: pros and cons*. 1999.
65. Sakao, Y., et al., *Carcinoembryonic antigen as a predictive factor for postoperative tumor relapse in early-stage lung adenocarcinoma*. European journal of cardio-thoracic surgery, 2004. **25**(4): p. 520-522.

66. Jang, H.S., et al., *Optical fiber SPR biosensor with sandwich assay for the detection of prostate specific antigen*. *Optics Communications*, 2009. **282**(14): p. 2827-2830.
67. Healy, D.A., et al., *Biosensor developments: application to prostate-specific antigen detection*. *TRENDS in Biotechnology*, 2007. **25**(3): p. 125-131.
68. Uludağ, Y. and I.E. Tothill, *Development of a sensitive detection method of cancer biomarkers in human serum (75%) using a quartz crystal microbalance sensor and nanoparticles amplification system*. *Talanta*, 2010. **82**(1): p. 277-282.
69. Rich, R.L. and D.G. Myszka, *Grading the commercial optical biosensor literature—Class of 2008: ‘The Mighty Binders’*. *Journal of Molecular Recognition*, 2010. **23**(1): p. 1-64.
70. Daniels, J.S. and N. Pourmand, *Label-Free Impedance Biosensors: Opportunities and Challenges*. *Electroanalysis*, 2007. **19**(12): p. 1239-1257.
71. Qureshi, A., et al., *Review on carbon-derived, solid-state, micro and nano sensors for electrochemical sensing applications*. *Diamond and Related Materials*, 2009. **18**(12): p. 1401-1420.
72. Debye, P., *Polar Molecules (Chemical Catalog Company, New York, 1929)*, Chap.
73. Cole, K.S. and R.H. Cole, *Dispersion and absorption in dielectrics I. Alternating current characteristics*. *The Journal of Chemical Physics*, 1941. **9**: p. 341.
74. Antonyak, M.A., D.K. Moscatello, and A.J. Wong, *Constitutive activation of c-Jun N-terminal kinase by a mutant epidermal growth factor receptor*. *Journal of Biological Chemistry*, 1998. **273**(5): p. 2817.

75. Blume-Jensen, P. and T. Hunter, *Oncogenic kinase signalling*. Nature, 2001. **411**(6835): p. 355-365.
76. Cohen, P., *The role of protein phosphorylation in human health and disease*. European Journal of Biochemistry, 2001. **268**(19): p. 5001-5010.
77. Cohen, S., *Purification of the receptor for epidermal growth factor from A-431 cells: its function as a tyrosyl kinase*. Methods in Enzymology, 1983. **99**: p. 379-387.
78. Huang, H.J.S., et al., *The enhanced tumorigenic activity of a mutant epidermal growth factor receptor common in human cancers is mediated by threshold levels of constitutive tyrosine phosphorylation and unattenuated signaling*. Journal of Biological Chemistry, 1997. **272**(5): p. 2927.
79. Jorissen, R.N., et al., *Epidermal growth factor receptor: mechanisms of activation and signalling*. Experimental cell research, 2003. **284**(1): p. 31-53.
80. Wells, A., *Molecules in focus-EGF receptor*. International Journal of Biochemistry and Cell Biology, 1999. **31**(6): p. 637-644.
81. Marchetti, A., et al., *EGFR mutations in non-small-cell lung cancer: Analysis of a large series of cases and development of a rapid and sensitive method for diagnostic screening with potential implications on pharmacologic treatment*. Journal of Clinical Oncology, 2005. **23**(4): p. 857.
82. Castaldo, G., et al., *Carcinoembryonic antigen mRNA analysis detects micrometastatic cells in blood from lung cancer patients*. European Respiratory Journal, 2003. **22**(3): p. 418.
83. Clarke, L.E., et al., *Epidermal growth factor receptor mRNA in peripheral blood of patients with pancreatic, lung, and colon carcinomas detected by RT-PCR*. International journal of oncology, 2003. **22**(2): p. 425-430.

84. Jacot, W., et al., *Serum EGF-receptor and HER-2 extracellular domains and prognosis of non-small-cell lung cancer*. British journal of cancer, 2004. **91**(3): p. 430-433.
85. Kopreski, M.S., F.A. BENKO, and C.D. GOCKE, *Circulating RNA as a Tumor Marker*. Annals of the New York Academy of Sciences, 2001. **945**(1): p. 172-178.
86. Miura, N., et al., *Sensitive detection of human telomerase reverse transcriptase mRNA in the serum of patients with hepatocellular carcinoma*. Oncology, 2000. **64**(4): p. 430-434.
87. El-Sayed, I.H., X. Huang, and M.A. El-Sayed, *Selective laser photo-thermal therapy of epithelial carcinoma using anti-EGFR antibody conjugated gold nanoparticles*. Cancer letters, 2006. **239**(1): p. 129-135.
88. Aaron, J., et al., *Polarization microscopy with stellated gold nanoparticles for robust monitoring of molecular assemblies and single biomolecules*. Optics express, 2008. **16**(3): p. 2153-2167.
89. Choi, J.H., et al., *Detection of epidermal growth factor receptor in the serum of gastric carcinoma patients*. Cancer, 1997. **79**(10): p. 1879-1883.
90. Smith, B.C., *Fundamentals of Fourier transform infrared spectroscopy*. 2009: CRC.
91. Morales-Cruz, A.L., et al., *Atomic force measurements of 16-mercaptohexadecanoic acid and its salt with CH₃, OH, and CONHCH₃ functionalized self-assembled monolayers*. Applied surface science, 2005. **241**(3-4): p. 371-383.
92. Sam, S., et al., *Semiquantitative study of the EDC/NHS activation of acid terminal groups at modified porous silicon surfaces*. Langmuir, 2009. **26**(2): p. 809-814.

93. Horcas, I., et al., *WSXM: A software for scanning probe microscopy and a tool for nanotechnology*. Review of Scientific Instruments, 2007. **78**: p. 013705.
94. Dobrikova, A., et al., *Protein-coated [beta]-ferric hydrous oxide particles:: An electrokinetic and electrooptic study*. Colloids and Surfaces B: Biointerfaces, 2007. **56**(1-2): p. 114-120.
95. Song, X., *An inhomogeneous model of protein dielectric properties: Intrinsic polarizabilities of amino acids*. The Journal of Chemical Physics, 2002. **116**: p. 9359.
96. Rich, R.L. and D.G. Myszka, *Survey of the 2009 commercial optical biosensor literature*. Journal of Molecular Recognition, 2011. **24**(6): p. 892-914.
97. Shlyahovsky, B., et al., *Optical and Electrochemical Detection of NADH and of NAD+ Dependent Biocatalyzed Processes by the Catalytic Deposition of Copper on Gold Nanoparticles*. Small, 2005. **1**(2): p. 213-216.
98. Katz, E., I. Willner, and J. Wang, *Electroanalytical and bioelectroanalytical systems based on metal and semiconductor nanoparticles*. Electroanalysis, 2004. **16**(1 2): p. 19-44.
99. Yanez-Sedeno, P. and J. Pingarron, *Gold nanoparticle-based electrochemical biosensors*. Analytical and bioanalytical chemistry, 2005. **382**(4): p. 884-886.
100. Loyprasert, S., et al., *Label-free capacitive immunosensor for microcystin-LR using self-assembled thiourea monolayer incorporated with Ag nanoparticles on gold electrode*. Biosensors and Bioelectronics, 2008. **24**(1): p. 78-86.
101. Katz, E., I. Willner, and J. Wang, *Electroanalytical and bioelectroanalytical systems based on metal and semiconductor nanoparticles*. Electroanalysis, 2004. **16**(1-2): p. 19-44.

102. Haun, J.B., et al., *Magnetic nanoparticle biosensors*. Wiley Interdisciplinary Reviews: Nanomedicine and Nanobiotechnology, 2010. **2**(3): p. 291-304.
103. Jaffrezic-Renault, N., et al., *Biosensors and bio-bar code assays based on biofunctionalized magnetic microbeads*. Sensors, 2007. **7**(4): p. 589-614.
104. Solé, S., et al., *Flow injection immunoanalysis based on a magnetoimmunosensor system*. Analytical chemistry, 1998. **70**(8): p. 1462-1467.
105. Santandreu, M., et al., *Development of electrochemical immunosensing systems with renewable surfaces*. Biosensors and Bioelectronics, 1998. **13**(1): p. 7-17.
106. Gehring, A.G., et al., *1-Naphthyl phosphate as an enzymatic substrate for enzyme-linked immunomagnetic electrochemistry*. Journal of Electroanalytical Chemistry, 1999. **469**(1): p. 27-33.
107. Liu, Z.M., et al., *Core-shell magnetic nanoparticles applied for immobilization of antibody on carbon paste electrode and amperometric immunosensing*. Sensors and Actuators B: Chemical, 2006. **113**(2): p. 956-962.
108. Nam, J.M., S.I. Stoeva, and C.A. Mirkin, *Bio-bar-code-based DNA detection with PCR-like sensitivity*. Journal of the American Chemical Society, 2004. **126**(19): p. 5932-5933.
109. Helali, S., et al., *A disposable immunomagnetic electrochemical sensor based on functionalised magnetic beads on gold surface for the detection of atrazine*. Electrochimica acta, 2006. **51**(24): p. 5182-5186.
110. Connolly, J. and T.G. St Pierre, *Proposed biosensors based on time-dependent properties of magnetic fluids*. Journal of magnetism and magnetic materials, 2001. **225**(1): p. 156-160.
111. Vidotti, M., et al., *Biosensors based on gold nanostructures*. Journal of the Brazilian Chemical Society, 2011. **22**(1): p. 3-20.

112. Bunimovich, Y.L., et al., *Quantitative real-time measurements of DNA hybridization with alkylated nonoxidized silicon nanowires in electrolyte solution*. Journal of the American Chemical Society, 2006. **128**(50): p. 16323-16331.
113. Sander, C., *Genomic medicine and the future of health care*. Science, 2000. **287**(5460): p. 1977.
114. Jemal, A., et al., *Cancer statistics, 2008*. CA: a cancer journal for clinicians, 2008. **58**(2): p. 71.
115. Etzioni, R., et al., *The case for early detection*. Nature Reviews Cancer, 2003. **3**(4): p. 243-252.
116. Liang, S.L. and D.W. Chan, *Enzymes and related proteins as cancer biomarkers: a proteomic approach*. Clinica chimica acta, 2007. **381**(1): p. 93-97.
117. Fan, R., et al., *Integrated barcode chips for rapid, multiplexed analysis of proteins in microliter quantities of blood*. Nature biotechnology, 2008. **26**(12): p. 1373-1378.
118. Zheng, G., et al., *Multiplexed electrical detection of cancer markers with nanowire sensor arrays*. Nature biotechnology, 2005. **23**(10): p. 1294-1301.
119. Cui, Y., et al., *Nanowire nanosensors for highly sensitive and selective detection of biological and chemical species*. Science, 2001. **293**(5533): p. 1289.
120. Jain, K.K., *Nanotechnology in clinical laboratory diagnostics*. Clinica chimica acta, 2005. **358**(1-2): p. 37-54.
121. Burg, T.P., et al., *Weighing of biomolecules, single cells and single nanoparticles in fluid*. Nature, 2007. **446**(7139): p. 1066-1069.

122. Kim, A., et al., *Ultrasensitive, label-free, and real-time immunodetection using silicon field-effect transistors*. Applied Physics Letters, 2007. **91**: p. 103901.
123. Stern, E., et al., *Label-free immunodetection with CMOS-compatible semiconducting nanowires*. Nature, 2007. **445**(7127): p. 519-522.
124. Stern, E., et al., *Label-free biomarker detection from whole blood*. Nature nanotechnology, 2009. **5**(2): p. 138-142.
125. Stern, E., A. Vacic, and M.A. Reed, *Semiconducting nanowire field-effect transistor biomolecular sensors*. Electron Devices, IEEE Transactions on, 2008. **55**(11): p. 3119-3130.
126. Altintas, Z., et al., *Development of Surface Chemistry for SPR based Sensors for the Detection of Proteins and DNA molecules*. Analytica chimica acta, 2011.
127. Davas, E., et al., *Serum IL-6, TNF α , p55 srTNF α , p75 srTNF α , srIL-2 α Levels and Disease Acitivity in Systemic Lupus Erythematosus*. Clinical rheumatology, 1999. **18**(1): p. 17-22.
128. Kurosawa, S., et al., *Evaluation of a high-affinity QCM immunosensor using antibody fragmentation and 2-methacryloyloxyethyl phosphorylcholine (MPC) polymer*. Biosensors and Bioelectronics, 2004. **20**(6): p. 1134-1139.
129. Cao, C., et al., *A strategy for sensitivity and specificity enhancements in prostate specific antigen-[alpha] 1-antichymotrypsin detection based on surface plasmon resonance*. Biosensors and Bioelectronics, 2006. **21**(11): p. 2106-2113.
130. Yin, T., et al., *A novel capacitive immunosensor for transferrin detection based on ultrathin alumina sol-gel-derived films and gold nanoparticles*. Sensors and Actuators B: Chemical, 2006. **117**(1): p. 286-294.

APPENDIX

Journal Papers:

1. **Z. Altintas**, Y. Uludag, Y. Gurbuz, I. E.Tothill, “Surface Plasmon Resonance based Immunosensor for the Detection of the Cancer biomarker Carcinoembryonic Antigen” *Talanta*, Vol.86, October 2011, 377-383 (SCI).
2. **Z. Altintas**, Y. Uludag, Y. Gurbuz, I. Tothill, “Development of the immobilization surfaces in SPR biosensor for the detection of protein and DNA molecules”, *Analytica Chimica Acta*, Vol.712, January 2012, 138-144 (SCI).
3. **Z. Altintas** and I.E. Tothill, “Detection of TP53 point mutation using SPR and QCM biosensor platforms”, (Under the revision of *Sensors and Actuators B*).
4. S. Kallempudi, **Z. Altintas**, J. Kolkar, Y. Gurbuz, “A new microfluidics system with a hand-operated, on-chip actuator for immunosensor applications”, *Sensors and Actuators B*, Vol. 163, March 2012, 194-201 (SCI).
5. **Z. Altintas**, S.S. Kallempudi, Y. Gurbuz, U. Sezerman, J. Kolkar, “A capacitive biosensor for the detection of human-Epidermal Growth Factor Receptor – a cancer biomarker” (Submitted to *Talanta*).
6. **Z. Altintas**, U. Sezerman, Y. Gurbuz, , “Au-NP modified capacitive sensor platform for disease diagnostics”, Under preparation
7. **Z. Altintas**, U. Sezerman, Y. Gurbuz, , “Novel magnetic material modified electrochemical sensor for immunosensor applications”, Under preparation
8. **Z. Altintas**, U. Sezerman, Y. Gurbuz, “Multiple marker detection for the precise diagnosis of lung cancer”, Under preparation

Conference Papers:

1. **Z. Altintas**, Y. Gurbuz, I. Tohill, “Rapid and Sensitive Diagnostic Approach for Lung Cancer through Biosensing Technology”, poster presentation, the 7th annual Screening Europe conference (Barcelona, Spain), 11-12 February 2010
2. Y. Uludag, S.S. Kallempudi, **Z. Altintas**, I.E. Tohill, Y. Gurbuz, “Novel label-free capacitive sensor based on interdigitated electrode arrays for multiplex point-of-care testing”, poster presentation, Biosensors 2010 (Glasgow, UK) conference, 26-27.05.2010.
3. **Z. Altintas**, I.E. Tohill, “Diagnosis of lung cancer using biosensor technologies”, poster presentation, EBI-Wellcome Trust Summer School in Bioinformatics (Cambridge, UK) 14-18 June 2010.
4. **Z. Altintas**, S. S. Kallempudi, Y. Gurbuz, U. Sezerman, J. Kolkar, "A Capacitive Biosensor for the Detection of Human-Epidermal Growth Factor Receptor for Cancer Diagnosis", Poster presentation, the 2nd International Conference on Bio-Sensing Technology, (Amsterdam, The Netherlands), 10-12 October 2011
5. E. Sahin, **Z. Altintas**, U. Sezerman, Y. Gurbuz, “Magnetic Bead Modified Signal Enhancement for Capacitive Detection of Tau”, Oral Presentation, The International Conference on Enzyme Science and Technology, ICEST 2011, 31 October-4 November 2011, (Kuşadası, Turkey).